# Blood Cell Count On-a-Chip

Thesis by

**Wendian Shi**

In Partial Fulfillment of the Requirements

for the Degree of

Doctor of Philosophy

California Institute of Technology

Pasadena, California

2013

# Acknowledgements

This thesis is a product summarizing five years' work in searching and researching. The process of delivering this product, however, was beyond the data and the plots. At beginning, I was excited about the idea, to develop a blood test that people can use at home. During the process, however, I enjoyed a good bit of confusions and doubts because the complexity of this idea.

It was all the supports I received that guided me through this journey. For those priceless helps, I owe gratitude to many people.

First of all, I would like to thank my advisor, Professor Yu-Chong Tai. It was Dr. Tai who entrusted me with the blood test project. Later on, he encouraged me to explore freely ahead of the project, from academic findings to social impacts. What I received from him is beyond guidance and support. The lessons I learned from him, such as how to keep calm in difficult times, how to express myself, and how to think, will continue to inspire me in my future journey.

I would also like to thank my collaborator, Dr. Harvey Kasdan. Harvey worked with me on the blood test project for four years. His experiences and insights helped me to focus on new possibilities. He was also very supportive, when I participated in competition prizes and looked for start-up opportunities.

Thanks to all my colleagues in the Caltech Micromachining Lab, Siyang Zheng, Po-Jui Chen, Jason Shi, Nick Lo, Wen Li, Ray Huang, Quoc Quach, Mike Liu, Chun-Hui Lin, Mandheerej Nandra, Justin Kim, Penvipha Satsanarukkit, Bo Lu, Yu Zhao, Charles DeBoer, Luke Guo, Han-Chien Chang, Dongyang Kang, Zhao Liu, Nick Scianmarello,

Shell Zhang, Yang Liu, John Chen, Jogson Hu, Agnes Tong, Christine Garske, and Trevor Roper.  Siyang trained me extensively in my first year here. Luke Guo worked with me for a busy summer. Mike guided me on the algae project. Charles exchanged with me lots of helpful discussions. Christine and Trevor kept the lab running smoothly.

I would also like to thank Prof. Haixia Zhang and Prof. Zhihong Li for introducing me into the micro-fabrication field, and their continuously supporting me.

Thanks to my friends at Caltech, Wendy Chen, Xi Zhang, Tong Chen, Chengshan Zhou, Yu Zhao and many others. They have been so supportive of my work, and I never hesitated to ask for help from them. Thanks to Chenghao Chien and Hongchao Zhou. It was fun working with them on the Dr. Algae project. Thanks to my friends Jun Ying, Xiaofeng Wang, Xia Lou, Dake Wu, Le Liu, Peng Dai, Hao Fang, Jian Wang, Ang Chen, Yun Wang, Jia Xia, Suguo Wang, Huihui Chen, and so many others that I couldn't list them all. Thanks them for supporting me even when I was thousands of miles away, and welcoming me whenever I visited. Thanks to the wonderful life all of them have shared with me, so that I could focus on my research and on my path.

Thanks Wendy, Charles, Dongyang and Yu Zhao for proof reading this thesis. Thanks to my thesis committee Prof. Yu-Chong Tai, Prof. Changhuei Yang, Prof. Hyuck Choo, Prof. Joel Burdick and Prof. John Dabiri for reviewing this thesis.

Finally, I would like to thank my parents. I learned from them before I attended any school. They have always been there for me, allowing me to fly freely. This thesis is for you

III

# Abstract

White blood cell (WBC) count is one of the most frequently ordered clinical tests in hospitals. There are five types of WBCs in the circulating blood, including lymphocyte, monocyte, neutrophil, eosinophil and basophil. The WBC count test enumerates not only the total number of WBCs in per volume blood, but also the percentage of each WBC type. A portable instrument for the WBC count test is currently in demand by the NASA human spaceflight, and also by the on-earth telemedicine application. However, the commercially available tests do not meet the requirement of the portable applications, because of their large instrument size and the large reagent volume consumed per test.

This study describes the development of a WBC count technology optimized for portable applications. First, a sheathless microfluidic cytometer is developed for WBC count. This technology consumes only a small amount of blood (5 μL) and a minimal volume of reagents (50 μL). Second, fluorescent dye assays are developed for the WBC differential count by measuring fluorescent emissions on the microfluidic cytometer. Based on this technology, a portable instrument is built with high test accuracy (maximum error less than 10%).

Furthermore, this study explores two key components for future integrating this technology into a self-contained chip. First, a microvalve actuated by thermal blood clogging is developed. This valve has a simple structure suitable for on-chip integration. Second, a micromixer is used to demonstrate the staining of blood with dye assays, and the following fluorescent detection of WBCs on the cytometer.

IV

# TABLE OF CONTENTS

# LIST OF FIGURES

# LIST OF TABLES

# Chapter 1 : Introduction to Blood Cell Count

## 1.1 Blood Cell Count and Its Clinical Significance

Blood is a body fluid that is vital to maintain life [1]. On average, a normal adult has 6 to 7 liters of blood in total. Approximately 45% of the blood is composed of cell elements, and the remaining 55% is the fluid portion, termed plasma. Remarkably, blood constantly circulates throughout the body and carries out a wide variety of important functions [2]. For example, it transports oxygen and nutrients to various organs and transfers substances such as messaging hormones to other tissues for use. At the same time, metabolic waste products from tissues are picked up and carried away by blood circulation. It is appreciated in modern hematology that many diseases cause changes in the composition of blood, and therefore, the analysis of blood is important in clinical diagnosis [3-5].

The cellular components of blood consist mainly of three types of cell, erythrocyte (red blood cell, RBC), leukocyte (white blood cell, WBC) and thrombocyte (platelet) [1]. The RBCs contain the protein hemoglobin, which is responsible for the transportation of oxygen and carbon dioxide. The WBCs play key roles in the immune system, defending the body against foreign pathogens such as virus, bacteria and parasites. The platelets are primarily in charge of stopping of the bleeding. In addition, the WBCs can be further classified into five major types: lymphocytes, monocytes, neutrophils, eosinophils and basophils, and each type serves distinct functions [2, 5].

Numerous tests have been developed for the blood cell analysis, and one of the most widely used tests in clinical medicine is the complete blood count (CBC) [3, 5, 6]. The CBC test determines the quantities of the blood cells that present in blood, including WBCs, RBCs, and platelets. Particularly, the measurement of WBCs consists of the WBC count (the total number of WBC in per volume of blood) and the WBC differential count (the absolute numbers or percentages of different types of WBCs). The measurement of RBCs consists of the RBC count (the total number of RBCs in per volume of blood), hemoglobin (total amount of hemoglobin protein in per volume of blood), hematocrit (the volume ratio of RBCs in blood) and other RBC indices. Modern instruments for CBC tests can measure over 20 parameters. Table 1.1 and Table 1.2 summarize the most common parameters for the CBC test and the recommended normal ranges [3, 7, 8]. The commercial instruments dedicated for automatic CBC tests are normally referred as the Hematology Analyzer.

Table 1.1. Complete blood count and the normal ranges of the test parameter

|  | Male | Female |
| --- | --- | --- |
| WBC Count ( $\times 10^3/\mu l$ ) | 3.7–9.5 | 3.9–11.1 |
| WBC Differential Count | See Table 1.2 | |
| RBC Count ( $\times 10^6/\mu\lambda$ ) | 4.3–5.7 | 3.9–5.0 |
| Hemoglobin ( g/dl ) | 13.3–18.0 | 11.8–16.5 |
| Hematocrit ( l/l ) | 0.39–0.51 | 0.36–0.48 |
| Platelet Count ( $\times 10^3/\mu l$ ) | 140–330 | 140–350 |

Table 1.2. White blood cell differential count and the normal ranges

| WBC Type | Absolute ($\times 10^3/\mu l$) | Percentage (%) |
|---|---|---|
| Total WBC | 3.7 – 11.1 | 100 |
| Granulocyte | | |
| Neutrophil | 1.7 – 7.5 | 40 – 80 |
| Eosinophil | 0.03 – 0.46 | 0 – 7 |
| Basophil | 0.02 – 0.09 | 0 – 1 |
| Nongranulocyte | | |
| Lymphocyte | 1.0 –3.2 | 15- 40 |
| Monocyte | 0.2 – 0.6 | 3 – 12 |

The clinical usefulness of the CBC test has been addressed elsewhere extensively [7-10]. It is worthwhile to emphasize the importance of the WBC count and the WBC differential count in the CBC test [10]. The test results of the WBC count and the WBC differential count are greatly useful in diagnosis of the presence and severity of many diseases including leukemia, infections (virus, bacteria, parasite, fungi, etc.), inflammations, various allergies, immunodeficiency, etc. [3, 5, 7, 9]. In addition, it is used to reflect the body's ability to fight disease, and also utilized in monitoring the adverse effects of medicines, e.g., in cancer chemotherapies [5, 7, 11-14]. From a technology perspective, the tasks of counting WBCs and identifying all the WBC types with high accuracy are still among the most challenging issues of the modern CBC test [15].

## 1.2 Development of Blood Cell Count Technology

Until 1950s, the clinical tests of the blood cell count relied mainly on the observation of blood film smear under an optical microscope [16]. The manual preparation of the blood smear and the following efforts to visually identify and enumerate the blood cells were laborious and time consuming. The test required a trained hematologist, and the results were subject to numerous sources of imprecision [5]. Therefore, there was strong push to develop automated blood cell count technologies [16]. Since the 1980s, the use of automated blood cell count instrument had become common in large clinical laboratories, which could carry out large quantities of tests every day thanks to the high throughput of the automated test procedure [17].

Nowadays there are three major types of detection principles used in automated blood counters including image analysis, Coulter principle and flow cytometry [16], as summarized in Table 1.3. The image analysis method counts blood cells by first taking optical images of the cells, and then extracting cellular feature information (cell size, nucleus shape, etc.) from the images. Blood samples are normally treated with staining reagents beforehand to enhance the discrimination of different cell types. The image analysis method is no longer popular in modern automated blood counters due to the limited counting throughput and accuracy [16, 18, 19]. For example, the ambiguity of classifying WBCs by image information alone could introduce substantial inaccuracy to the WBC differential count result [2, 5, 16].

Table 1.3. Summary of the blood cell counting principles, image analysis, Coulter principle, and flow cytometry

| | | Image Analysis | Coulter Principle | Flow Cytometer |
|---|---|---|---|---|
| **Detection Principle** | **Detection Target** | Optical Image | Electrical Impedance | Optical Intensity • scattering • absorption • fluorescence |
| | **Sample Labeling** | Needed | Label free | Label free: • scattering Label needed: • absorption • fluorescence |
| **Capability** | **CBC** | Yes | Yes | Yes |
| | **WBC Differential** | 5-part | 3-part | 5-part + WBC subtypes |
| **Accuracy** | | Low | High | High |
| **Throughput** | | Low | High | High |

The Coulter principle detects the electrical impedance of blood cells, by flowing the sample through a narrow aperture to ensure the measurement of individual cells. This method can evaluate the cell properties such as cell size (direct current impedance) and the

cell electrical opacity (Alternating Current impedance). It is able to deliver a 3-part WBC differential (lymphocyte, monocyte, and granulocyte), and still widely used in the automatic blood counters because of the merits of low reagent cost and label-free detection. However, the Coulter principle alone is not sufficient to distinguish all five major types of WBCs (lymphocyte, monocyte, neutrophil, eosinophil and basophil) [16]. Therefore, it is often used in parallel with other detection methods, such as light-scattering detection, to extend the capability of distinguishing WBC types [20-25].

The flow cytometry principle is a general platform technology where single cells could be accurately quantified in suspension with high throughput, and the quantitative methods mainly involve optical detections such as light scattering, light absorption and fluorescence detection [16]. It is widely appreciated as a powerful technique which has a significant impact on various fields of biology and medicine [26-30]. However, most flow cytometers are quite complex to operate and need careful calibration. Some relatively simplified versions have been developed for the specific purpose of blood analysis [20, 31-38]. For measurement by the flow cytometer, blood samples usually need to be treated with labeling reagents (fluorescent dyes, fluorescent conjugated antibody assay, etc.) beforehand to introduce the cell labels for the optical detections.

Above all, the state-of-the-art instruments for the automatic blood cell counting are mostly based on the Coulter principle, the flow cytometry principle, or a combination of both methods [20-25, 31-38]. During the last two decades, the automated blood cell counter has undergone a formidable technological evolution owing to the introduction of new physical principles for cellular analysis and the progressive evolution of software [15]. The results have been significant improvement in both the test throughput, over 100 tests per

hour achievable on state-of-the-art instruments, and the increase of test parameters provided. For some parameters, such as WBC and RBC count, hemoglobin concentration, or RBC indices (e.g., mean corpuscular volume), the analytical performance of the automated counter is generally excellent. For others, in particular, the WBC differential count, the test performance is still less than satisfactory [15].

## 1.3 Needs of Portable Blood Cell Count Technology

In recent years, there are many newly emerging applications which require portable, easy-to-use blood cell count technologies [6, 39-41]. For example, the NASA human spaceflight program is actively searching for a portable and space-usable blood cell count technology, particularly for the tests of the WBC count and the WBC differential. It has been well-known since early Gemini and Apollo mission that various medical events happened repeatedly to astronauts in space, and the Space Shuttle Program alone reported 1867 medical events from 1981 to 1998 including the viral and bacterial infections [42]. However, there is currently a gap of medical feasibilities to provide the in-flight diagnostic information for these medical events. A portable blood cell count technology could provide an important first step to bridge this gap [43]. In addition, a portable blood cell count, particularly the test of WBC count can be a powerful technique to monitor the radiation effects on human body, one of the most important biomedical issues for long-term human space flight. Furthermore, such a portable blood analysis technology is also very useful for on-earth, point-of-care applications such as telemedicine, bedside healthcare, and medical care in remote rural areas [44-46].

The requirements for the portable, easy-to-use blood count technology have been discussed elsewhere [6, 47, 48], and some of the most important considerations include a

portable instrument size (e.g., handheld), easy-to-use test procedure (with minimal training), minimized sample volume (both blood sample and consumable reagents), and favorably a long shelf life. The requirement of long shelf life is particularly critical for NASA space applications, as a long-term flight mission could last from 6 months to 2 years.

However, the state-of-the-art blood cell counters are not optimal to meet the emerging needs of portable instruments. First of all, the modern blood cell counters have been evolving into cumbersome machines with large volume and heavy weight [40]. As the consequence, the CBC test is mostly carried out in central clinical laboratories, but not available for point-of-care sites such as physician offices, emergency room and other near-patient settings. Secondly, a large volume of reagent (dilution buffer, sheath buffer, etc.) is normally consumed to perform the test, and the necessary storage volume impedes the miniaturization of instruments. In addition, the blood sample needed for testing on the automated blood cell counters usually requires the collection by vein blood drawing, which is not favorable in portable applications [25].

Therefore, an increasing amount of attentions has been drawn to the development of the portable, easy-to-use blood count technologies [40]. Engineering efforts have been made to shrink the size of the instruments in the diagnostic companies [49-52]. Table 1.4 compares a few of those examples with a state-of-the-art instrument (Coulter LH750) [25, 49, 51, 52]. The size of these instruments are considerably compact, however, not satisfactory for the portable applications (favorably handheld system). Besides, the test performances are also limited. For example, the Sysmex pocH-100i system provides a 3-part WBC differential count (lymphocyte, monocyte and granulocyte), which is less

competent compared to the 5-part WBC differential count (lymphocyte, monocyte, neutrophil, eosinophil and basophil) provided in the central laboratories.

Table 1.4. Comparison of the compact-sized blood cell counters with a state-of-the-art blood cell counter (Coulter LH750)

| Model | | Coulter LH750 | Sysmex pocH-100i | Chempaq XDM70 | HemoCue WBC |
|---|---|---|---|---|---|
| Instrument Size (cm × cm × cm) | | 89 × 102 × 61 | 19 × 35 × 46 | 25 × 36 × 27 | 14 × 12 × 19 |
| Weight (kg) | | 93 | 14 | 4 | 1 |
| Power Consumption (W) | | 2080 | 150 | 100 | Battery |
| Blood Collection | | Venipuncture | Venipuncture | Finger-prick | Finger-prick |
| Performance | CBC Count | Full | Full | Full | Part |
| | WBC Differential | 5-Part | 3-Part | 3-Part | N/A |
| Throughput (minute/ test) | | 0.5 | 3 | 3 | 3 |

## 1.4 Microfluidics for Blood Cell Counting

Microfluidics is a field that deals with technology and phenomena of fluidic behavior in the submillimeter length scale [53, 54]. The term of microfluidic device is often used

interchangeably with lab-on-a-chip (LOC) and micro-total-analysis-system (µTAS). The development of the microfluidic system started around 1980s, and progressed rapidly in the last two decades as a promising alternative in improving modern biology and chemistry laboratory processes. In 1979, Terry et. al. developed a gas chromatography device on silicon, marking the invention of the first microfluidic devices [55]. In the mid-1990s, the field of microfluidic stepped into a booming stage, which was shown by the dramatic increase in the number of patents related to microfluidics from 1994 to 2004 [56]. The history of microfluidics development and the challenges for wide acceptance of microfluidic devices in practical applications have been discussed extensively elsewhere [53, 57-61].

Microfluidic devices provide various unique advantages over their macro counterparts [53, 54, 57-64]. One important advantage that was recognized early on is the minimized dimension of these devices. With the reduced length scale, physical processes such as molecular diffusion and thermal energy transfer can reach balance in a significantly shorter period of time [60]. In addition, the small size also makes microfluidic devices optimal for portable applications such as point-of-care clinical diagnosis and on-field testing [39, 41]. Another merit of the microfluidic devices is their capability to handle liquid precisely in a very small volume, e.g., in nanoliter range [58, 60]. As a consequence, a small amount of reagent is sufficient to run multiple tests in the microfluidic devices, multiple functions could be integrated on a single chip [58], and more experiments could be run in parallel to increase test throughput [65-68]. One more example of the advantages is the low cost of the microfluidic devices and their application as disposable devices [56, 69].

Because of these merits, microfluidic devices are considered great tools for miniaturizing medical diagnostics, and a great amount of microfluidic-based biomedical sensing technologies has been developed in the last decade [39-41, 70]. To name a few examples, i-State successfully commercialized the technology of using microfluidic integrated sensor for blood gas analysis [71]; recently Pipper et al. developed a complete microfluidic platform to detect the avian influenza virus H5N1 [72]; extensive efforts have been also devoted to developing microfluidic-based, point-of-care diagnosis and monitoring of infectious diseases such as HIV/AIDS, malaria and tuberculosis for developing countries [73]. The recent advances of microfluidics in the biomedical sensing field, including development of new fabrication materials, device architecture for fluidic manipulation on-chip, sensor integration with microfluidics, have been discussed in detail elsewhere [70].

Accurate and affordable analysis of the cellular component of blood is of prime interest to medical diagnostics. Therefore, microfluidic devices that could bring laboratory blood analysis to the near-patient settings are extremely attractive for reshaping the delivery of healthcare [41]. For example, Altendorf et al. first reported counting blood cells in a silicon microfluidic channel by the light scattering measurement [74]. Later Kummrow et al. reported the count of WBC, RBC and platelet on a microfluidic cytometer, using measurement of the intrinsic light scattering and the extrinsic fluorescence introduced by a immuno-assay staining [75]. Meanwhile, Holmes et al. [76, 77] reported the counting of blood cells on a microchip measuring electrical impedances, and Seo et al. developed a lensless microscope for blood cell imaging and analysis [78]. In addition to the CBC analysis, other types of blood cell analysis have been also demonstrated in microfluidic

devices, such as the evaluation of protein expression on WBCs [79], and the enumeration of two WBC subtypes (CD4+ lymphocyte cells and CD8+ lymphocyte cells) in HIV diagnosis [80, 81]. Reference [40] provides a good review of the recent progress of using microfluidic device for blood cell analysis.

## 1.5 Needs of Future Development

Nevertheless, there is still a lack of the microfluidic technologies that bridge the gap between the need of high-performance blood count and the strict requirement of portable applications. The feasibility of total WBC count and a 3-part WBC differential have been demonstrated in the Coulter approach [77] and the flow cytometry approach in microfluidics [82]. However, it is still limited compared with the 5-part WBC differential count provided by the modern laboratory blood counters. In addition, the immuno-assays used in the previous approaches [75, 80-82] suffer the limitations of low storage (e.g., 4°C) and short shelf life, while requirements of long shelf life and room temperature storage are important concerns for point-of-care applications.

Besides, a portable instrument delivering the WBC count and WBC differential alone could serve as a useful clinical test for point-of-care applications. For example, it could be used to monitor astronaut's exposure to space radiation during the space flight [43]. For another example, the WBC count with differential could be used in physician offices, as a screening test for discriminating bacterial and viral infections. For all these reasons, it is still of great importance to develop portable blood cell count technologies with improved performances, with emphasized need for the WBC count and the WBC differential count.

# Chapter 2 : Microfluidic Cytometer for White Blood Cell Count

## 2.1 Introduction

### 2.1.1 Flow Cytometry Principle

Cytometry is a process for measuring the physical and chemical characteristics of biological cells. In flow cytometer, the measurements are made as cells flow through the instrument in a liquid stream. Figure 2.1 illustrates the basic configuration of a flow cytometer, where a narrow stream of fluidic sample containing the cells passes through the center region of a laminar sheath flow. This setting is referred as hydrodynamic focusing, and the result is the passage of physically separated individual cells through the interrogation area. Two major principles have been widely used for cell detection including optical measurement and electrical impedance measurement. The electrical impedance measurement is derived from the Coulter principle, and adopted in flow cytometers mainly for the purpose of blood cell analysis. The optical measurement is more commonly used, and the parameters measurable include light scattering, light extinction, light absorption, and fluorescence, etc.

One important consideration in implementing flow cytometry for blood analysis is the ability to classify different types of blood cell, especially the WBCs. Flow cytometry is currently considered as the gold standard for WBC differential count in clinical laboratories [30] because of its ability to simultaneously deliver accurate measurements of versatile cellular characteristics. Table 2.1 summarizes the cellular characteristics that are measurable in the flow cytometry.
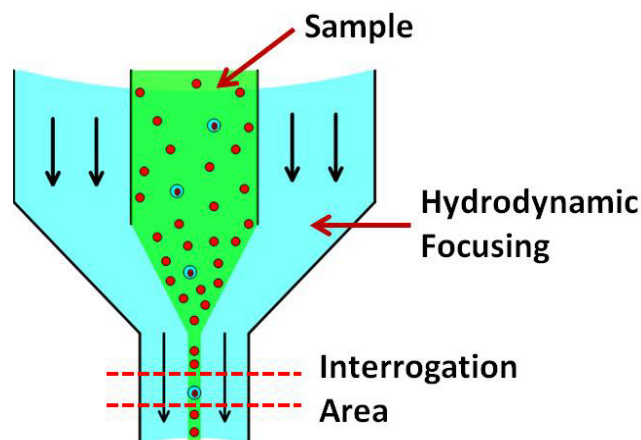
Figure 2.1. Illustration of the basic principle of flow cytometry.

Two major types of cellular characteristics can be measured, including the intrinsic cellular characteristics and the extrinsic cellular characteristics. The intrinsic cellular characteristics, such as cell size and cytoplasmic granularity, are sufficient to classify blood cells into WBCs, RBCs and platelets, but not different types of WBCs. In general, a 3-part WBC differential count (lymphocyte, monocyte and granulocyte) can be achieved by these cellular characteristics alone. The major methods for measurements include electrical impedance and light scattering signal. In recent years, progress has been made on these two measurement methods. For example, it has been demonstrated that the simultaneous measurement of the polarized orthogonal and the depolarized orthogonal light scattering signals is able to identify eosinophil cells in addition to the 3-part differential, thus achieving a 4-part WBC differential (lymphocyte, monocyte, neutrophil, eosinophil) [83]. Besides, Beckman Coulter Inc. developed a method which simultaneously measured the electrical DC impedance, AC impedance and light scattering signals, which is able to report a 5-part WBC differential (lymphocyte, monocyte, neutrophil, eosinophil and basophil). However, the accuracy of the basophil count in this technology is still questionable [15].

Table 2.1. Summary of cellular characteristics measurable by the flow cytometry

principle

| Cellular Characteristics | Measurement parameter (and probe if used) |
|---|---|
| Intrinsic Structural Characteristics (no probe) | |
| Cell size | Small angel light scattering; Electronic (DC) impedance |
| Cell shape | Pulse shape analysis; Image analysis |
| Cytoplasmic granularity | Large angel light scattering; Electronic (AC) impedance |
| Extrinsic structural Characteristics (probe required) | |
| DNA content | Fluorescence (e.g., propidium) |
| DNA base ratio | Fluorescence (e.g., Hoechst33258) |
| RNA content | Fluorescence (e.g., pyronin Y) |
| Total protein | Fluorescence (e.g., covalent-bonded acid dyes) |
| Basic protein | Fluorescence (e.g., acid dyes at high pH) |
| Surface/Intracellular antigens | Fluorescence, scattering (e.g., labeled antibodies) |
| Extrinsic Functional Parameters (probe required) | |
| Surface/Intracellular receptors | Fluorescence (e.g., labeled ligands) |
| Membrane integrity | Fluorescence (e.g., propidium) |
| Membrane permeability | Fluorescence (e.g., rhodamine 123) |
| Enzyme activity | Fluorescence, absorption (e.g., fluorogenic substrates) |
| Intracellular pH | Fluorescence (e.g., SNARF-1) |

The extrinsic cellular characteristics, on the other hand, provide a wider spectrum of measurement for blood cell analysis. For example, the measurement of protein antigens, including the surface antigens and the intracellular antigens, can deliver not only the complete 5-part WBC differential, but also measurement of abnormal and immature WBCs, and hundreds of WBC subtypes (e.g., CD4+, CD8+, etc.). The detection of the extrinsic characteristics is normally carried out by fluorescence measurement, and the cells need to be prelabeled by fluorescent probes to introduce the signal. Two major types of fluorescent probes have been developed: fluorescent dyes and fluorescent-conjugated proteins. The fluorescent dyes are used to measure the cellular contents such as nucleic acid, esterase, etc. The fluorescence-conjugated proteins are used to measure the antigen proteins, thus most powerful for WBC differential. In modern flow cytometry, multiple channels of fluorescence signals (e.g., 16 channels) can be detected simultaneously to provide comprehensive cell analysis.

## 2.1.2 Problem of Implementing Flow Cytometry in Portable Analysis

Despite the virtues discussed above, there are several drawbacks impeding the implementation of flow cytometry in point-of-care blood analysis:

(1) Non-portable instrument size;

(2) Large volume of blood sample;

(3) Large volume of consumable reagents.

First, the modern flow cytometer instruments are big and heavy [40]. Therefore, they are mostly used in central clinical laboratories, and optimized for high throughput measurement. These instruments are not suitable for on-field use. In addition, the flow cytometry operation normally required complicated test procedure including sample

preparation, optical calibration, etc. Trained technicians are needed to carry out these operations. For point-of-care applications, the instruments would be used in near patient settings, such as physician offices and emergency rooms, and the end users would be physicians, nurses or even patients themselves. A portable instrument size and easy-to-use test procedure are necessary.

Secondly, the volume of the blood sample needed for flow cytometer analysis is not optimal for point-of-care applications [39-41]. For example, a modern cytometry based blood counter (e.g., Coulter LH750) consumes a sample volume of 100 to 400 μl. To provide this amount of blood, venipuncture procedure is necessary for the sample collection. An alternative procedure of fingerprick for sample collection (e.g., 1-5 drops of blood) is more favorable for point-of-care applications.

Thirdly, the need of large volume of consumable reagents further impedes the use of flow cytometry [39, 40]. Two major sources of the consumables include the dilution buffer for sample preparation and the sheath buffer in hydrodynamic focusing. For example, in the commercial cytometry-based blood counter (e.g., Coulter Act-5diff), a 100× dilution is used for the WBC count test. In addition, a sheath buffer of 250 to 1,000 ml is needed for hydrodynamic focusing of every 1 ml of sample in the flow cytometer [84]. The storage of these consumable reagents constrains the miniaturization of the flow cytometer.

Above all, the development of a portable, cost-effective and easy-to-use cytometry technology is still urgently needed for the application of portable blood analysis.

## 2.1.3 Microfluidic Cytometer Technology

To address the drawbacks of the conventional flow cytometer, microfluidic-based flow cytometer, also referred to as microfluidic cytometer, has emerged as a promising

alternative [39, 40, 62, 64, 70, 73]. In microfluidic cytometer, chip-based fluidic system is used to replace the conventional fluidic system. In addition, optical components such as lens, filter and waveguide for light detection could also be integrated into the same chip. By nature, microfluidic cytometer offers the potential of substantially reducing the instrument footprint and consuming much less amount of samples. In addition, microfluidic cytometer chips allow for parallel, cost-effective fabrication, suitable for disposable applications.

The recent development of microfluidic cytometer have been reviewed elsewhere [62, 63, 70]. The current efforts have been directed mainly towards two areas, the miniaturization of the fluid handling components (e.g., pump, valve, etc.) and the optimization of the hydrodynamic focusing in microfluidics. Particularly, various approaches for hydrodynamic focusing have been investigated, including active focusing (e.g., one dimensional flow focusing, two-dimensional flow focusing, dielectrophoretic particle focusing, etc.), and passive focusing (e.g., groove generated sheath flow, no sheath flow, etc.). However, much less efforts have been devoted to the development of assays, which are optimal for microfluidic applications.

## 2.1.4 Previous Art of Microfluidic Cytometer for Blood Analysis

Altendorf et al. first reported implementing a silicon-based microfluidic cytometer for blood cell counting [74]. They used wet etching to micro-fabricate a V-groove shaped fluidic channel on a silicon substrate, and then pumped the blood samples through the channel for optical detection. Light scattering measurement was carried out and detection of RBCs and WBCs was demonstrated in this approach.

More recently, Kummrow et al. [75] and Frankowski et al. [82] developed a microfluidic cytometer with plastic substrate, and used immunological assays for WBC

count. The microfluidic device was built by hot embossing of thermoplastic material (polycarbonate), and the obtained structures were used to provide a two-dimensional hydrodynamic focusing. Blood samples were pretreated with fluorescent-conjugated immune-assays and the optical detections including light scattering and fluorescence measurement were carried out on a microscope-modified system. They were able to demonstrate the 3-part WBC differential (lymphocyte, monocyte and granulocyte) and the count of lymphocyte subtypes.

Meanwhile, Holmes et al. reported the counting of blood cells on a microchip by measuring electrical impedances [76, 77]. The microchip was fabricated by whole wafer bonding of two glass substrates with polyimide structures to define the microfluidic channels, and metal electrodes were prepatterned electrodes on the substrates. When pretreated blood sample flow through the microfluidic device, electrical impedance changes caused by individual cells were measured at multiple AC frequencies. With this method, they were able to demonstrate the count the WBCs, RBCs and platelets, as well as the feasibility of the 3-part WBC differential count.

Besides, there were also reports of using microfluidic cytometry approaches to carry out other blood cell analysis, such as the evaluation of protein expressions on WBC surface [79], and the enumeration of two WBC subtypes (CD4+ lymphocyte cells and CD8+ lymphocyte cells) in HIV diagnosis [80, 81], etc.

Nevertheless, there are still drawbacks in the above approaches, impeding their practical use. First of all, the capability of the WBC different count is still limited (3-part differential) comparing to the state-of-the-art blood counters (5-part differential). The remaining two types of WBCs, eosinophil and basophil, are important diagnostics for

diseases such as parasite infection and allergy [5], and could be very useful in point-of-care applications [85]. Second, most efforts have been devoted to the improving the microfluidic design, but few efforts have been taken to optimize the detection assays for the portable applications. For example, the immunological assays used in microfluidic cytometers discussed above, are developed for use in the conventional flow cytometer. There are several drawbacks to use these immunological assays for point-of-care applications, including limited shelf life, low-temperature storage and high assay cost. These drawbacks create extra barriers for implementation in resource-limited areas. Thirdly, the reagent volumes needed in these approaches are still high. For example, hydrodynamic focusing with sheath flow was used in the previous approaches, which significantly increased reagent volume needed. The two dimensional sheath focusing used by Kummrow et al. and Frankowski et al. [75, 82], consumed a sheath buffer of more than 1200μl for testing each 10μl blood sample. The consumption of the buffer reagents remained a significant size limitation.

## 2.2 Sheathless, Fluorescent Microfluidic Cytometer for WBC Count

### 2.2.1 Basic Principle

To address the problems discussed above, we propose a sheathless microfluidic cytometer and dye-based assays for fluorescent detection of WBCs. The principle of this approach is illustrated in Figure 2.2. The key component of the cytometer is a transparent, sheathless microfluidic channel for fluorescent sensing. The sheathless channel confines the blood sample into a narrow stream, ensuring the passages of WBCs one by one. Meanwhile, the fluorescence emissions are measured continuously as the sample flows

through the interrogation area, until finishing the measurement of the whole sample. Dye-based assays are utilized in this approach to introduce the fluorescence signals of WBCs. Before measurement, blood sample is pretreated with a dye assay, which selectively stains WBCs in the blood. Therefore, as the sample flows through the sheathless channel, WBCs can be detected by their fluorescent emissions. Furthermore, the measured fluorescence intensities are used to identify different WBC types.
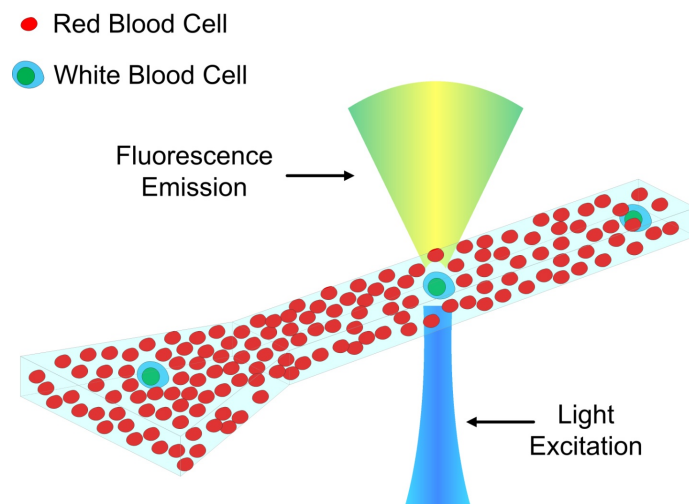


Figure 2.2. Illustration of the principle of the sheathless microfluidic cytometer for fluorescent detection of white blood cells in blood. The detection is carried out as the sample continuously flows through the sheathless channel.

Figure 2.3 compares the sheathless microfluidic cytometer to the conventional flow cytometry. There are two major differences. First, the use of the sheathless fluidic design, and second, the use of the dye-based assay.
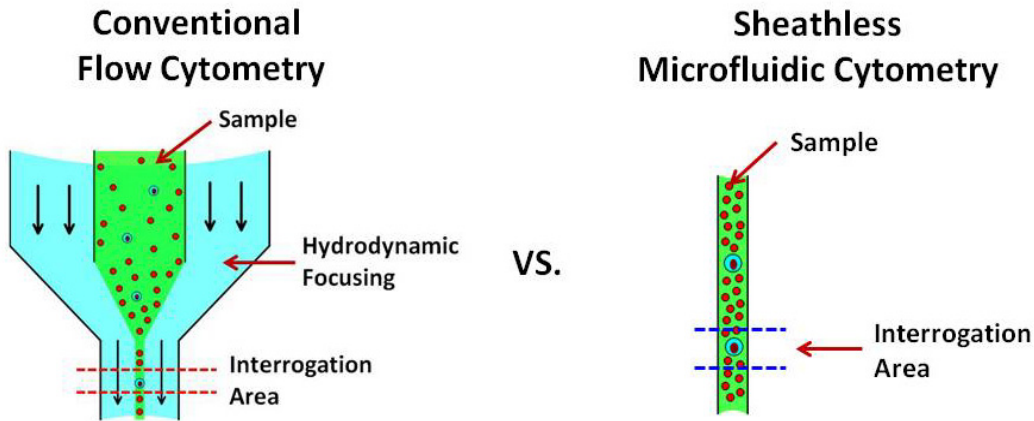
Figure 2.3. Comparison of the fluidic designs of conventional flow cytometer with the sheathless microfluidic cytometer. The sheathless microfluidic cytometer uses the fluidic channel to confine the sample into a narrow stream for detection, whereas the conventional cytometer uses hydrodynamic focusing.

In the conventional cytometry, the sample is confined into a narrow stream by using the sheath focusing. The prices paid included a more sophisticated fluidic design, and the consumption of extra sheath buffer. In the sheathless microfluidic cytometer, on the other hand, the sample is confined into the narrow stream by the sidewalls of the micro-fabricated channel, without using sheath flow. The sheathless design is considered as optimal for portable applications for two reasons. First, the fluidic design and control the cytometer are largely simplified, suitable for microfluidic devices. Second, the use of sheath buffer is eliminated, minimizing the sample volume. Besides, the dye-based fluorescent assays were investigated for the WBC detection in this study, because of their long shelf life, room temperature storage, and low cost. These three features meet the unique requirements of the portable applications.

Three major considerations of this approach, including the design of the sheathless channel, the development of the dye-based assay, and the optical detection system, are discussed in the following sections.

## 2.2.2 Design of Sheathless Cytometer Channel

There are two major considerations in designing the sheathless detection channel. On one hand, the channel has to be large enough so that human blood cells could freely flow through the channel. Considering the normal range of the blood cells in circulating blood, e.g., WBC 10-20μm, RBC 6-8μm, platelet 1.5-3μm in diameter [3], the cross section of the channel should be at least larger than 20μm×20μm. On the other hand, a larger detection channel would increase the possibility that multiple WBCs flowing through the interrogation area together and being measured as one cell, as illustrated in Figure 2.4. This possibility is referred as the coincidence error [16].
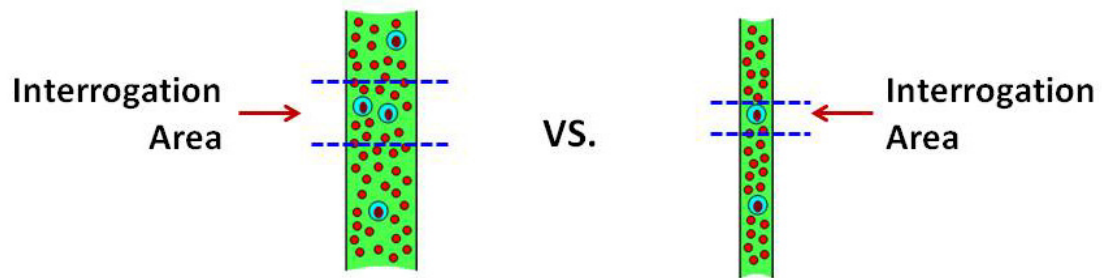


Figure 2.4. Comparison of two sheathless channel designs. (Left) Design with larger channel versus (Right) design with smaller channel (cross section area). In the larger channel design, the possibility is higher that multiple cells of interest would pass through the interrogation area together.

The relationship between the coincidence error and the channel dimension can be approximated by a Poisson Process [86]. Considering the volume of the interrogation zone (one portion of the sheathless channel, length of which is defined by the light illumination) is *V*, the average concentration of WBCs in blood is *c*, then the possibility of *n* WBCs flowing through the interrogation area together can be estimated as a Poisson Distribution [86]:

$$P(n) = (c \cdot V)^n \, e^{-c \cdot V} / n!$$

(1)

The coincidence error *P*, which is the possibility of two or more WBCs flowing through the interrogation area together, can be expressed as [86]:

$$P = 1 - (1 + c \cdot \Delta V) e^{-c \cdot \Delta V}$$

(2)
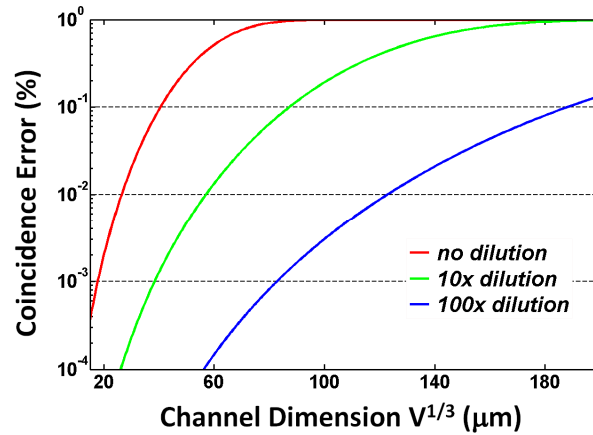


Figure 2.5. The estimated coincidence error versus the interrogation channel dimension. *V* is the volume of the interrogation area. In this plot, a WBC concentration of 10,000 cell/μl is considered. Different levels of sample dilution are also compared.

According to Equation (2), the coincidence error can be calculated as a function of the volume of the interrogation channel, as illustrated in Figure 2.5. In this example, the WBC concentration in blood is assumed to be 10,000 WBCs/μl, which is a normal value for a healthy adult [3]. The coincidence error decreases rapidly when the volume of the interrogation zone is reduced. For a given volume of the interrogation zone, the dilution of the sample (e.g., 10×dilution), which equivalent to a reduced WBC concentration, also reduces the coincidence error.

Table 2.2. Comparison of coincidence error vs. WBC concentration ranges in two designs of interrogation channel

| Interrogation Channel (height × width × length) | WBC Concentration (cells/μl) | Dilution | Maximum Coincidence Error |
|---|---|---|---|
| 150μm × 150μm × 150μm | 0 – 10,000 | N/A | 99% |
| | 0 – 10,000 | 10× | 85% |
| | 0 – 10,000 | 66× | 10% |
| 28μm × 32μm × 50μm | 0 – 10,000 | N/A | 8% |
| | 10,000 – 30,000 | | 40% |
| | 0 – 10,000 | 10x | <0.1% |
| | 10,000 – 30,000 | | <0.1% |

The coincidence errors of two interrogation channel designs are compared in Table 2.2. For a WBC concentration of 10,000 WBCs/μl, the larger interrogation channel design (150μm×150μm×150μm) requires a 66× dilution to reduce the coincidence error less than 10%. On the other hand, the smaller interrogation channel design (28μm×32μm×50μm) needs no dilution to achieve a less than 10% coincidence error. The 10% error is chosen for comparison here as it is the maximum tolerance for the WBC count accuracy in the standard of point-of-care applications. The difference demonstrates the advantage of using a smaller channel as the interrogation area. With a 10× dilution, the coincidence error in the second design is less than 1% even for the abnormal high range of WBC concentration (10,000 to 30,000 WBCs/μl).

Table 2.3. Comparison of coincidence error of the proposed microfluidic cytometer design with specification of a state-of-the-art counter (Coulter LH750). The cytometer channel has a dimension of 28μm × 32μm × 50μm.

| WBC Concentration (cells/μl) | Microfluidic Cytometer | | Commercial Blood Counter | |
|---|---|---|---|---|
| | Reagent Consumption | Coincidence Error | Reagent Consumption | Mean Error Specification |
| 0 – 10,000 | No sheath buffer | <0.1% | Sheath buffer | 3.5% |
| 10,000 – 30,000 | 10x dilution | <0.1% | ~100x dilution | 9.0% |

Table 2.3 compares the proposed sheathless microfluidic cytometer design with a state-of-the-art blood counter instrument (Coulter LH750) for their needs of consumable reagent in the WBC Count test [25]. The coincidence error of the microfluidic cytometer is tolerable comparing to the error tolerance range of the commercial instrument. In addition, the reagent consumption of the microfluidic cytometer is much less than the commercial instrument, and therefore, optimal for miniaturizing the WBC count.

## 2.2.3 Dye-Based Assay and Fluorescent Detection of WBCs

Dye-based assays are used in the proposed microfluidic cytometer for selective staining of the WBCs in blood sample. Human blood consists of a mixed population of three types of cells, WBCs, RBCs and platelets. In order to detect the WBCs, selective staining is used here to introduce fluorescence to WBCs for measurement. One feature that distinguishes WBCs from the RBCs and platelets is the cellular nucleus (mature RBCs and platelets have no nucleus). By using a dye with high binging affinity for the nucleus, such as nucleic acid dye, the WBCs can be selectively stained in the whole blood sample.

In this chapter, we investigated the nucleic acid dye, Acridine Orange (AO), to demonstrate the selective staining. AO has high affinity binding to the DNA contents in the WBC nucleus, introducing a green fluorescence (emission peak 525nm), as shown in Figure 2.6 (a). Meanwhile, it will also bind to the RNA content in the cytoplasm and introduce a red fluorescence (emission peak 650nm), as shown in Figure 2.6 (b). Upon incubation of the dye assay with the whole blood sample, the WBCs show high fluorescence intensities, as shown in Figure 2.6 (c), whereas the other blood cells have minimal fluorescence. Therefore, WBCs can be detected in the microfluidic cytometer by their fluorescence emissions.

One major benefit of the fluorescent detection of WBCs is the minimal sample volume. In normal human blood, the concentrations of RBCs ($4\text{-}6\times10^6$ cell/µl) and platelet ($150\text{-}400\times10^3$ cell/µl) are much higher than WBCs ($4\text{-}10\times10^3$ cell/µl). Therefore, when each WBC flows through the sheathless detection channel, it is actually companioned by many RBCs and platelets. In the detection methods such as impedance or light scattering measurement, large sample dilution (~100× dilution) is usually needed to minimize this interference, particularly the interference of RBCs. In the fluorescent detection, on the other hand, no or minimal dilution is needed, because RBCs and platelets have negligible fluorescence. Therefore, the sample volume needed is minimized.
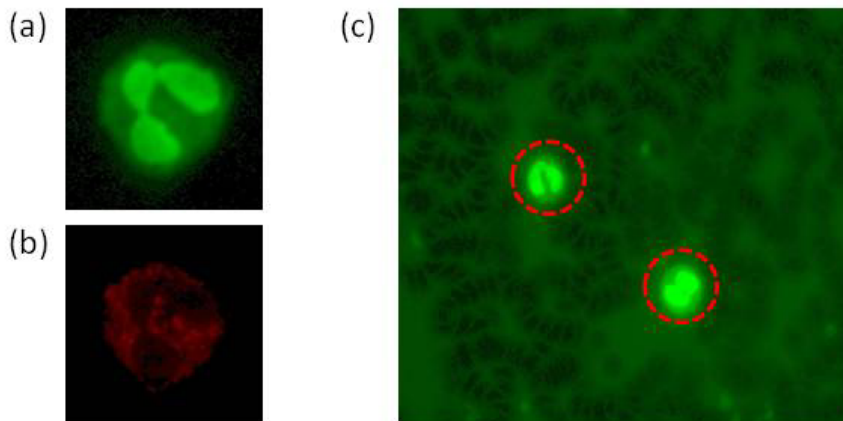


Figure 2.6. The fluorescent microscope images of white blood cells (WBCs) with Acridine Orange staining. (a) Green emission (510-550nm) fluorescence image of a WBC, where the nucleus shows a high intensity of fluorescence; (b) red emission (580-640nm) fluorescence image of the same WBC; (c) fluorescence image (510-550nm) of whole blood sample, where the WBCs are distinguished from other cells by their high intensity of fluorescence. RBCs appear as the dark shadows in the picture (c).

## 2.3 Experiment and Material

### 2.3.1 Device Layout

Fig. 2.7 shows the layout design and dimensions of the sheathless microfluidic channel. The fluidic channel consists of a sample inlet, a convergent channel, a straight channel to provide the sheathless interrogation zone, and a sample outlet. The inlet and the outlet are round holes with a diameter of 800μm. The width of the sheathless channel was design to be 30μm in the layout, and the total length was designed to be 3mm.
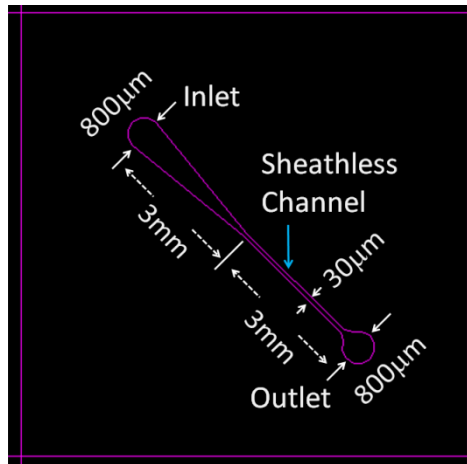


Figure 2.7. Layout design of the microfluidic channels for the sheathless cytometer.

### 2.3.2 Device Fabrication

The standard soft lithography process of polydimethylsiloxane (PDMS) was used to build the microfluidic device. The fabricated process, as shown in Fig. 2.8, is briefly described here. First, the master (mold) was made by deep reactive ion etching (DRIE) of a silicon wafer, after a lithography step to define the fluidic patterns. After etching, the silicon mold had an interrogation channel of 32μm in width and 28 μm in height, as

measured by a surface profiler (P15 Surface Profiler). Second, two parts of the PDMS

prepolymers (Sylgard 184, Dow Corning, MI, USA) were mixed in a 10:1 ratio. After

degassing in vacuum for 30 minute, the mixture was poured on top of the silicon mold, and

cured in a preheated convection oven at 80˚C for 30 minutes to partially solidify the

PDMS. After thermal curing, the PDMS was peeled off the mold and cut into individual

devices. The fluidic via (i.e., inlet and outlet) were punched through the PDMS block with

a stainless steel hypodermic needle (gauge 19, out diameter ~1.1mm). Afterwards, the

PDMS block was left cleaning in an ultrasonic water bath for 5 minute, rinsed first with

acetone and then isopropyl alcohol, and blow dried with compressed air. The devices were

left to dry up in air for 20 minutes. Finally, the PDMS blocks were bonded to a clean glass

slide (Plain Micro Slides, 25×75mm, VWR, USA) and cured in oven at 100˚C for 30

minutes to form the final device.
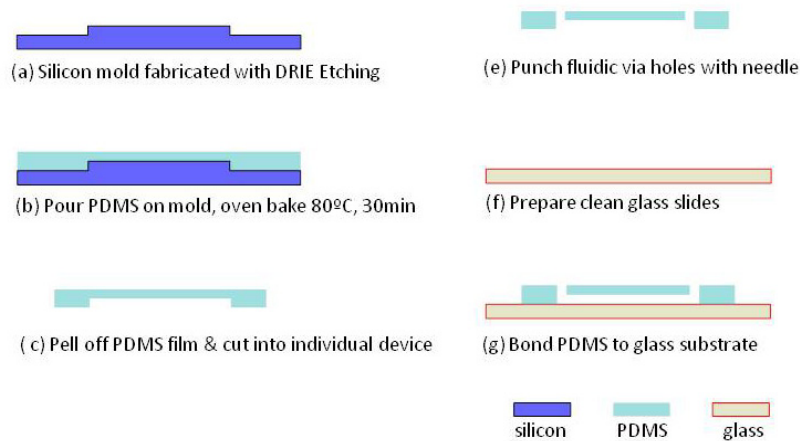


Figure 2.8. Illustration of the fabrication process flow of the PDMS devices.

Figure 2.9 shows the fabricated device and a zoomed-in picture of the fluidic

channel. The dimension of the interrogation zone in the sheathless channel, as determined

by the dimension of the silicon mold, is approximately 32μm in width and 28μm in height. The PDMS soft lithography process is chosen here for two major reasons. First, PDMS soft lithography is a standard microfabrication technique, which has the merits of easy and robust fabrication process. Second, PDMS and the glass substrate have excellent optical transparency in the wavelength range of this study (460nm to 700nm), therefore are suitable for the optical measurement.
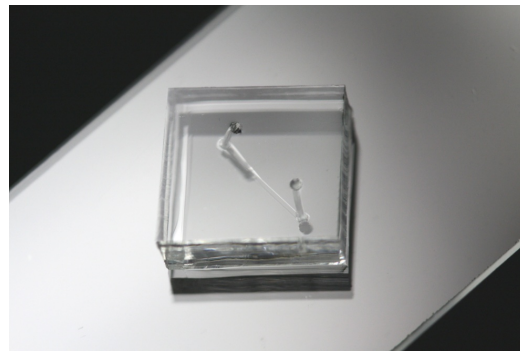


(a)



(b)

Figure 2.9. Photos of (a) the fabricated microfluidic device and (b) a zoomed-in photo of the fluidic channel.

### 2.3.3 Blood Sample

Blood samples were purchased from HemaCare Corp., CA, USA. Venous blood (4ml) was drawn from healthy donors and collected into Vacutainer$^{TM}$ tubes (K$_2$EDTA, 7.2mg, Becton Dickinson, USA). The samples were kept in a 4°C refrigerator for storage,

and all experiments were carried out within 24 hour after the blood drawing. For each sample, one extra vial of blood was collected and sent to a clinical laboratory (USC Clinical Reference Laboratory, USA) for independent blood count analysis on a hematology analyzer LH750 (Beckman Coulter, USA), and the CBC report with the WBC differential count was provided as reference data.

## 2.3.4 Fluorescent Dye Assay

The fluorescent dye, AO, was purchased from Sigma-Aldrich, USA (concentration 10mg/ml in water solution). The purchased dye solution was kept in room temperature for storage and shielded away from direct light illumination. The AO stock solutions used in the experiments were prepared by diluting the purchased AO solution (10mg/ml) with the phosphate buffer saline (PBS) solution (Invitrogen, USA) to the final concentrations needed.

## 2.3.5 Optical Configuration for Fluorescent Detection

A two-color fluorescence detection scheme was developed for the measurement of the blood sample. Figure 2.10 shows the optical configuration of the detection scheme. Excitation light was focused onto the microfluidic interrogation channel, and the fluorescence emission from the sample was simultaneously measured in two wavelength ranges, red (>590nm) and green (510-560nm). The measured fluorescence wavelength ranges were chosen to capture the fluorescence emission of AO-dye stained blood sample (DNA staining emission peak 525nm, RNA staining emission peak 650nm).
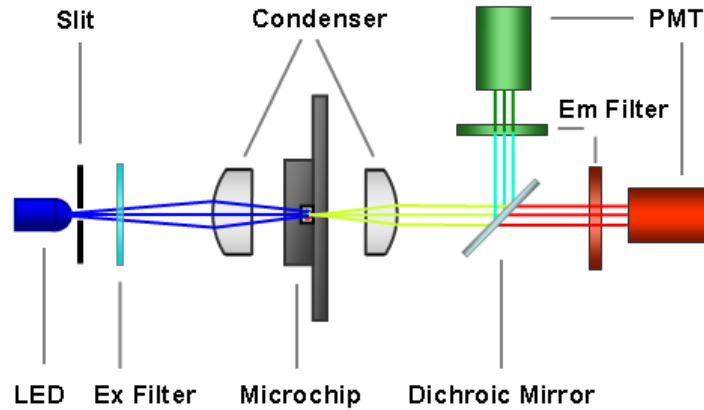
Figure 2.10. The optical configuration of the two color fluorescence detection scheme.

A prototype system was built with commercial, off-shelf components. A blue light-emitting diode (Royal blue Lumileds LED, Philips, 700mw, central wavelength 455nm) was used as the light excitation source. The emitted light was first passed through an optical slit (aperture width 50μm), and then focused onto the microfluidic interrogation channel by an optical condenser. The orientation of the slit was perpendicular to the orientation of the fluidic channel. The length of the interrogation area, as defined by the light illumination spot on the microfluidic channel, was controlled by the width of the slit. An excitation filter (band-pass filter, 440-480nm) was used in front of the slit to purify the light illumination wavelength.

The fluorescence emission from the sample, approximately a point source, was collected by the second condenser and converted into parallel light. Then the collected light was passed through a Dichroic mirror (Long pass, cut off wavelength 565nm). The portion of the collected light with a wavelength longer than 565nm was transmitted through the mirror, and measured in the red fluorescence channel. The portion with a wavelength shorter than 565nm was reflected by the mirror and measured in the green fluorescence

channel. A high-pass filter (cut-off wavelength 590nm) was placed in front of the red fluorescence channel to purify the measured red fluorescence wavelength range. A band-pass filter (510-560nm) was placed in the green fluorescence channel to remove the residual excitation light and to purify the measured green fluorescence wavelength range. The intensities of the green fluorescence and red fluorescence were finally measured by two photon-multiplier tubes (PMT, Hamamatsu H5784).
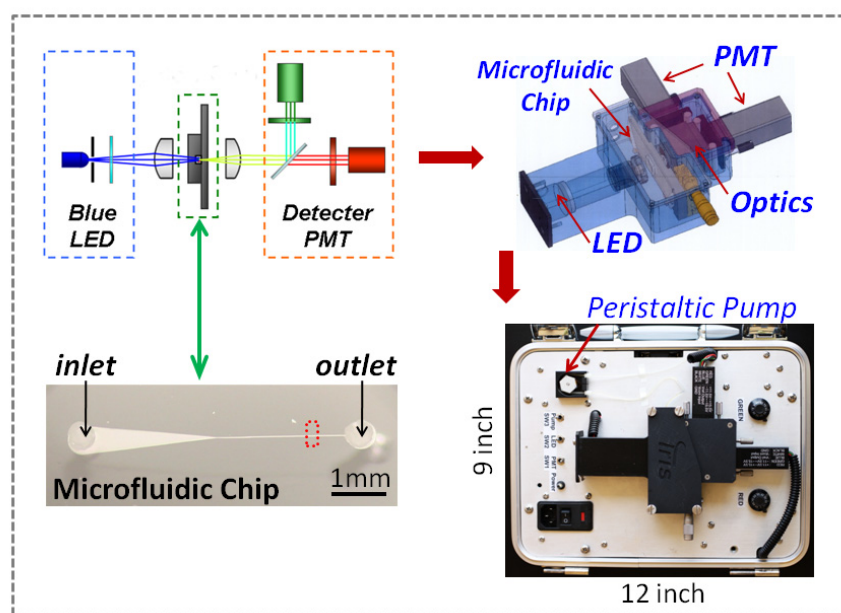


Figure 2.11. The configuration of the prototype system for two-color fluorescence measurement.

## 2.3.6 Portable Detection System

The optical detection components were enclosed inside an opaque black housing to be shielded away from environmental light, as shown in Figure 2.11. The electrical components including the data acquisition unit, which converted the measured light

intensities into digitalized signals, and the power converting units for powering the LED and the PMT modules, were all enclosed inside an aluminum case beneath the optical components housing. The whole system was built into a self-contained package with a dimension of 12 inch in length, 9 inch in width, and 5 in height.

The test samples were loaded through a silicone tubing (P625/10k.015, Instech, USA) connecting to the microfluidic chip inlet. And a mini peristaltic pump (P625, Instech, USA) was connected to the outlet of the microfluidic chip using silicone tubing. The samples were drawn through the microfluidic chip by the suction force provide by the peristaltic pump, and the test waste was collected in a plastic tube downstream.

The system was powered by the standard AC power source (110V AC, 80Hz) and the measured data was read out through a standard Universal-Serial-Port (USB) port and recorded on a laptop computer for further data analysis. Figure 2.12 shows a picture of the whole system configuration including the prototype system and a laptop computer. The operation of the prototype system was controlled by a Labview (National Instrument, USA) program running on the laptop computer.
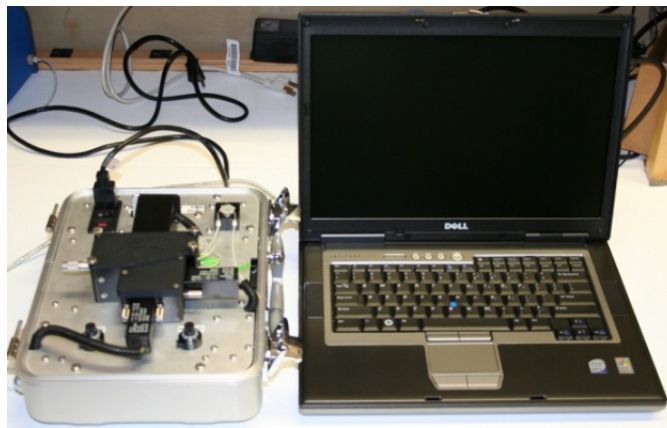


Figure 2.12. The test setup including the prototype system and a laptop computer.

## 2.4 Result and Discussion

### 2.4.1 System Evaluation with Fluorescent Beads

The overall system was first evaluated with 5μm diameter green fluorescent beads (Duke Scientific Corporations, USA) to study the optical detection performance. The beads were suspended in PBS solution to a final concentration of approximately $2\times10^3$ beads/μl as the test sample. A pumping rate of 6μl/min was used to draw the sample through the sheathless microfluidic channel for measurement, and the average flow velocity of the sample inside the interrogation area, calculated by the pumping rate divided by the cross sectional area of the fluidic channel, was about 110μm/msec. A sampling rate of 50kHz (one recorded measurement every 0.02msec) was used in the measurement, which was limited by the maximum sampling rate of the data acquisition unit used.
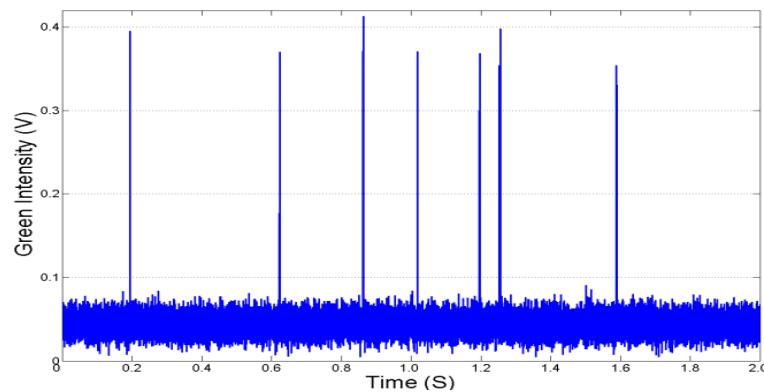


Figure 2.13. Recorded signals from the green fluorescent beads. The high peaks represent the fluorescent bead events measured.

Figure 2.13 shows the raw signal measured from the system which is the time trace of the fluorescence intensity. The fluorescent intensity was represented by the measured

voltages from the PMT sensor (green fluorescence channel). The background fluorescence had a DC level of about 0.450V and the average peak-to-DC noise amplitude was approximately 0.035V. The fluorescent peaks represented the events that fluorescent beads flowed through the interrogation area. Each peak represented one bead event counted, and the height of peak was recorded as the measured fluorescence intensity of the bead event. The average peak intensity of the recorded bead events was 0.340V. The signal-to-noise ratio (SNR) of the beads measurement is defined as:

$$SNR = 20 \cdot \log_{10} \left( \frac{V_{signal-to-DC}}{V_{noise-to-DC}} \right)$$
(3)

Given the signal intensity $V_{peak-to-DC}$ of 0.340V and the noise intensity $V_{noise-to-DC}$ of 0.035V, the SNR was calculated to be approximately 20dB.

## 2.4.2 Blood Sample Pretreatment with Fluorescent Dye Assay

Whole blood samples were then pretreated with the AO fluorescent dye assay for WBC detection, following the recipe as follow. For each experiment, 5μl whole blood was collected using a volumetric micropipette (0.5-10μl, Eppendorf Research, Inaccuracy specification: ±1.5%). The blood sample was then added to 45μl AO stock solution (10 μg/ml) and mixed well. The AO solution volume was controlled with a volumetric micropipette (10-100μl, Eppendorf Research, Inaccuracy specification: ±1.0%). The mixed sample was then incubated at room temperature for 2 minutes, being shielded away from direct light, and then loaded to the system for measurement.

| | Green band | Red band | Double band |
|---|---|---|---|
| *Lymphocyte* |  |  |  |
| *Neutrophil* |  |  |  |
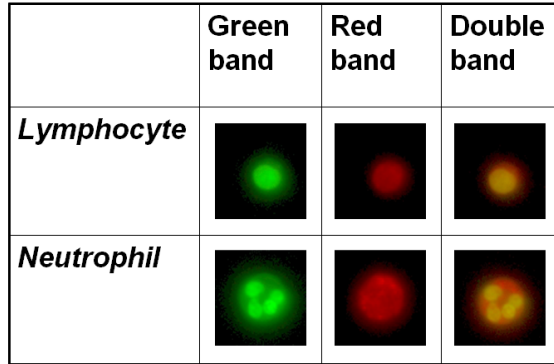
Figure 2.14. Fluorescent image of two WBCs, a lymphocyte cell and a granulocyte cell, after the AO pretreatment. The photos were taken on a fluorescence microscope (Nikon Eclipse E800) with a mercury lamp excitation. The wavelength range of the measurement band, including excitation (Ex) and emission (Em), are shown as follows. Green band: Ex 460-490nm, Em 510-560nm; red band: Ex 520-550nm, Em 590-650nm; Double band: Ex 475nm-490nm and 545-570nm, Em 510-540nm and 580-630nm.

Figure 2.14 shows the fluorescent images of two typical WBCs, lymphocyte and granulocyte, after the pretreatment. Lymphocyte and granulocyte are the two major types of WBC, and they normally account for over 90% of the total WBCs. The images were taken on a fluorescence microscope (Nikon Eclipse E800) with a mercury lamp excitation and switchable filter blocks. The nuclei of both WBCs, which were rich in DNA content, showed high green fluorescence intensity. Meanwhile, the cytoplasm, which contained RNA content, showed high red fluorescence intensity. The granulocyte had a larger size of cytoplasm than the lymphocyte, therefore, relatively higher red fluorescence intensity [87].

## 2.4.3 Blood Sample Measurement on Microfluidic Cytometer

The pretreated blood samples were then loaded to the prototype system for fluorescent measurement. While the blood sample continuously flowed through the interrogation channel, the measured fluorescence intensities were recorded. Figure 2.15 shows measured raw signal from the prototype system, without external signal processing. The measured signals showed high intensity peaks among the relatively noisy background. The green peaks were introduced by the AO binding to the nucleus of the WBCs, whereas the red peaks were introduced by the AO binding to the RNA contents in the WBC cytoplasm. The green fluorescence had relatively higher background noise than the red fluorescence. This difference was contributed to the residual AO molecules remaining in the sample, as the residual AO molecules had a green fluorescent emission (emission peak 520nm), overlapping with the green emission of AO binding to DNA.



[a]                                          [b]
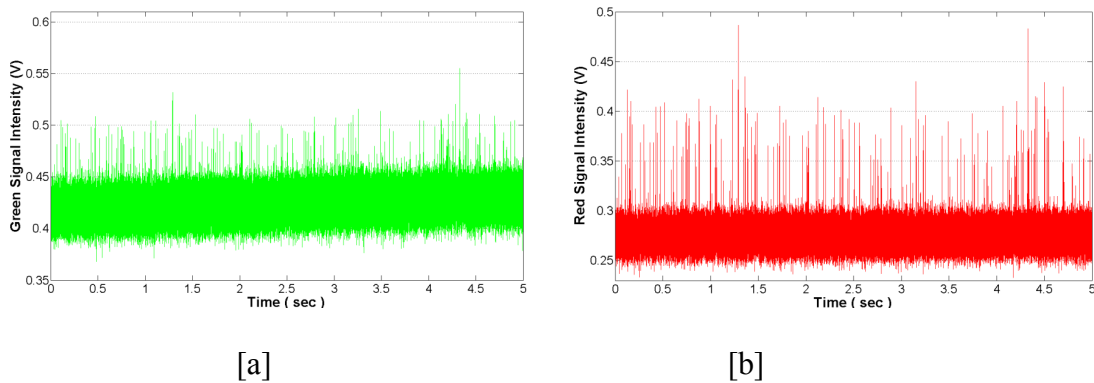
Figure 2.15. Measured fluorescence signals from the whole blood sample pretreated with the AO dye assay, (a) green fluorescence and (b) red fluorescence.

To demonstrate the feasibility of improving the SNR of the recorded data with digital signal processing, a 4-point moving average filter was used to smooth the recorded data

[88]. Figure 2.16 shows the processed results of the same data shown in Figure 2.15. The SNR of the green fluorescence, as calculated by Equation (3), increased from 5dB of the raw data to 14 dB of the processed data, whereas the SNR of the red fluorescence increased from 10 to 20dB.



[a]                                          [b]
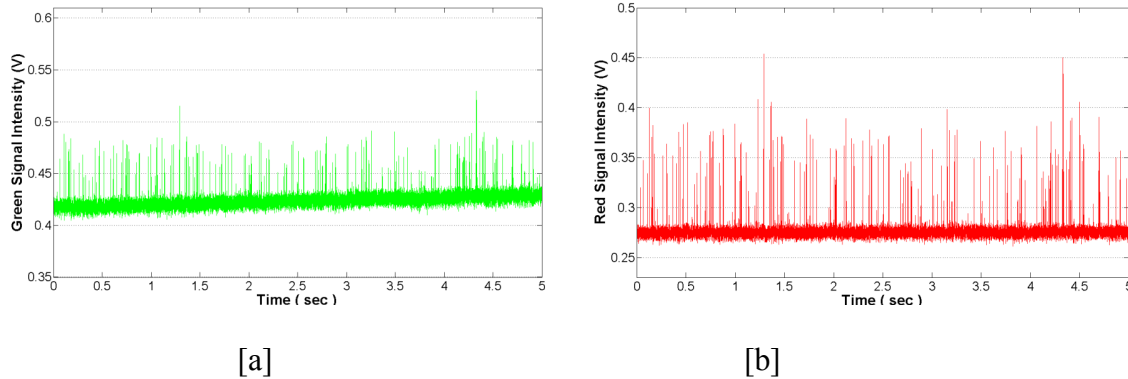
Figure 2.16. Processed fluorescence signals from the whole blood sample pretreated with the AO dye assay (after a 4-point moving average digital signal processing filter): (a) Green fluorescence and (b) Red fluorescence.

## 2.4.4 WBC Count and WBC 2-Part Differential Count

The data of the measured fluorescent intensities was first analyzed to count the number of the WBC events detected. The WBC event was defined as one high peak from the measured data, which was contributed to the AO-stained WBC flowing through the interrogation channel. For each event, the height of the green fluorescence peak and the height of the red fluorescence peak were recorded. A custom Matlab code was used to repeat this analysis on the recorded data for the whole sample. The analysis results included the total number of the detected WBC events, $N_{WBC}$, plus both the green and red fluorescence intensities associated with the WBC events. Then the results were displayed in

a scatter plot of red fluorescence intensity versus green fluorescence intensity, as shown in Figure 2.17.
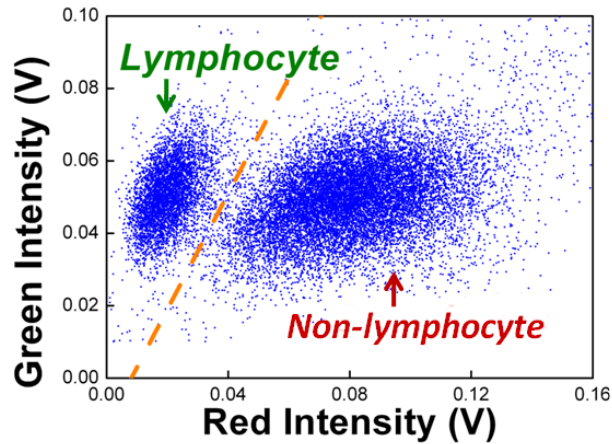


Figure 2.17. Scatter plot of the measured green fluorescent intensities versus red fluorescent intensities. Each dot represents one white blood cell event recorded.

In Figure 2.17, each dot represented one WBC event recorded, and the relative position of each dot is determined by the green and the red fluorescence intensity measured from the associated WBC event. Interestingly, the WBC events fell into two clearly separated clusters. The cluster on the left-hand side, which showed lower red fluorescence intensity, was mainly contributed to the lymphocytes among the WBCs. Lymphocytes have smaller cytoplasm than the other types of WBC and hence lower red fluorescence from the AO-RNA binding. The cluster on the right-hand side, which showed higher red fluorescence intensity, was mainly contributed to the nonlymphocyte WBCs. This observation is consistent with the AO staining pattern of WBCs previously reported [87, 89]. Afterwards, the percentages of the lymphocytes and the non-lymphocytes were determined by the number of dots in each cluster. An approximation was made to divide

these two populations, where the boundary was assigned as a straight line between the two clusters, as shown in Fig. 2.17. The number of dots in each of the two clusters, $N_{lymphocyte}$ and $N_{non-lymphocyte}$ were then recorded.

The total WBC count and a WBC 2-part differential count (lymphocyte vs. nonlymphocyte) were then obtained by the following calculation:

$$C_{WBC} = N_{WBC} / V_{sample} \tag{4}$$

$$P_{Lymphocyte} = N_{lymphocyte} / N_{WBC} \times 100\% \tag{5}$$

$$P_{Non-Lymphocyte} = N_{non-lymphocyte} / N_{WBC} \times 100\% \tag{6}$$

where $C_{WBC}$ is the WBC count and $V_{sample}$ is the total volume of blood sample tested. And we also have the following equations:

$$P_{non-Lymphocyte} = 1 - P_{Lymphocyte} \tag{7}$$

Because

$$N_{non-Lymphocyte} = N_{WBC} - N_{lymphocyte} \tag{8}$$

For the given example shown in Figure 2.17, $N_{WBC}$ = 30470 cells, $N_{lymphocyte}$ = 8227 cells, $N_{non-lymphocyte}$ = 22243 cells, and $V_{sample}$ = 5µl. Table 2.4 summarizes the results of the WBC count and the WBC 2-part differential count according to Equation (4-6).

## 2.4.5 Correlation Study with Commercial Blood Cell Counter

To verify the WBC count and the WBC 2-part differential count, tests results from the sheathless microfluidic cytometer were compared to the reference results from the commercial hematology analyzer (Beckman Coulter LH750). Five blood samples from different donors were tested and compared. For each sample, three repeated tests were

carried out on the microfluidic cytometer, and the average value was used to be compared

with results from the commercial counter.
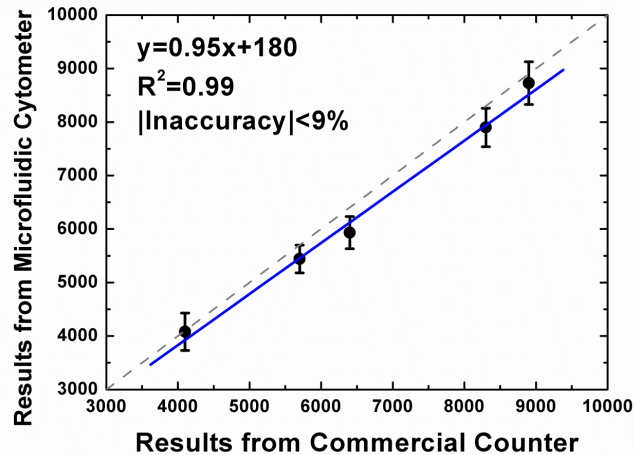


Figure 2.18. Comparison of total WBC count results from the microfluidic cytometer and

results from the commercial blood counter (Coulter LH750). Error bar shows the

variation of three measurement of the same sample on the microfluidic cytometer. The

linear relationship is obtained by linear aggression, as shown in the blue solid line (the

green dash line represents a linear relationship of y=x). The correlation coefficient ($R^2$)

and the inaccuracy as defined in Equation (10) are also shown.

Figure 2.18 shows the results of the total WBC count from the microfluidic

cytometer, $C_{WBC, MicrofluidicCytometer}$, comparing with the result from the commercial counter,

$C_{WBC, CommercialCounter}$. The measured WBC count covered a range from 4000 to 9000

WBC/μl. The measured results from the microfluidic cytometer showed good agreement

with the reference results from the commercial counter ($R^2$ correlation coefficient 0.99). In

addition, a good linearity (y=0.95x+180) was observed from the data by linear aggression.

It seems from Figure 2.18 that the WBC count results from the microfluidic cytometer are

slightly but consistently lower than the reference results. This difference was contributed to the cell loss caused by part of the WBCs adhering to the sample loading silicone tubing. Nevertheless, the maximum inaccuracy was still less than 9%, acceptable comparing to the inaccuracy tolerable range for clinical significance (10%). The measurement inaccuracy is defined as:

$$Inaccuracy = \frac{C_{WBC,MicrofluidicCytometer} - C_{WBC,CommercialCounter}}{C_{WBC,CommercialCounter}} \times 100\%$$ (9)

Figure 2.19 shows the results of the lymphocyte percentage measured from the microfluidic cytometer, $P_{lymphocyte, MicrofluidicCyometer}$, comparing with the results from the commercial counter, $P_{lymphocyte, CommercialCounter}$. The nonlymphocyte percentage, as shown in Equation (7), is determined once the lymphocyte percentage is known. The measured lymphocyte percentage covered a range from 12% to 25%. The measured results from the microfluidic cytometer showed good agreement with the reference results from the commercial counter ($R^2$ correlation coefficient 0.99). In addition, a good linearity (y=0.95x+0.64) was also observed from the comparison. The maximum inaccuracy, as defined in Equation (10), was less than 9%, and acceptable comparing to the inaccuracy tolerable range for clinical significance (10%).

$$Inaccuracy = \frac{P_{lymphocyte,MicrofluidicCytometer} - P_{lymphocyte,CommercialCounter}}{P_{lymphocyte,CommercialCounter}} \times 100\%$$ (10)
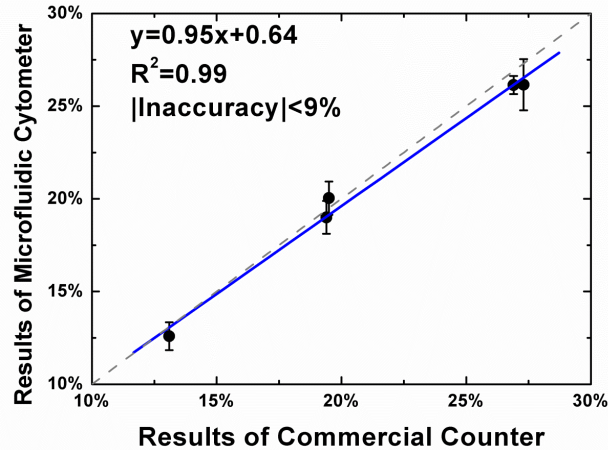
Figure 2.19. Comparison of the measured lymphocyte percentages from the microfluidic cytometer and results from the commercial blood counter (Coulter LH750). Each data point represents blood sample from a different donor. Error bar shows the variation of three measurement of the same sample on the microfluidic cytometer. The linear relationship is obtained by linear aggression, as shown in the blue solid line (the green dash line represents a linear relationship of y=x). The correlation coefficient ($R^2$) and the inaccuracy as defined in Equation (10) are also shown.

In summary, the WBC count and the WBC 2-part differential count (lymphocyte vs. nonlymphocyte) measured from the microfluidic cytometer showed close agreement with the results from the commercial blood counter.

## 2.5 Conclusion

A sheathless microfluidic cytometer was designed and fabricated for fluorescent detection of WBCs in human whole blood. The sheathless interrogation channel (cross section 32μm in width and 28μm in height) was designed to minimize the coincidence error of counting WBCs in whole blood. No sheath buffer and minimal dilution (10×) was

used for the WBC detection. The microfluidic device was fabricated with the soft lithography process of PDMS and a glass substrate.

Pretreatment of blood sample with fluorescent dye assay, AO (10 μg/ml), was used to selectively stain WBCs in whole blood. After the pretreatment, WBCs were detectable by the high fluorescence intensity introduced by the AO binding, whereas the other blood cells, RBCs and platelets, showed minimal fluorescence.

A LED-induced (central wavelength 460nm, 700mW), two-color fluorescence detection scheme was developed for the optical measurement. The measurement wavelength ranges were chosen to cover the green fluorescence (510-560nm) introduced by the AO-DNA binding, and the red fluorescence (>590nm) introduced by the AO-RNA binding. The whole system including the optical components and the supporting electronics was built into a portable-sized package (12 inch in length, 9 inch in width and 5 inch in height).

After incubated with the AO assay, blood samples were tested on the portable fluorescence detection system with the sheathless microfluidic device. The WBC events were measured to have a SNR 14dB for the green fluorescence and a SNR 20dB for the red fluorescence. The number of WBC events was counted by the number of the high intensity fluorescent peaks, and the lymphocyte and nonlymphocyte among the WBCs were identified in the scatter plot of the WBCs' green fluorescence intensity versus red fluorescence intensity. The test results of both the total WBC count and a two-part WBC differential count (lymphocyte vs. nonlymphocyte) agreed closely with the results from a commercial automatic blood counter ($R^2$ correlation coefficient 0.99, maximum error less than 10%).

# Chapter 3 : Dye Assay for WBC Differential Count

## 3.1 Introduction

In the Chapter 2, the feasibility of measuring WBCs in whole blood by the sheathless microfluidic cytometer and dye-based assay (Acridine Orange) was demonstrated. Based on this method, the WBC count and a 2-part WBC differential count (lymphocyte versus nonlymphocyte) were achieved. The results of the WBC count and the 2-part differential count are already useful in specific applications. For example, the lymphocyte count in the 2-part differential provides an important bioindicator for an astronaut's exposure to space radiation, which is needed in long-term space flight. In addition, the WBC count and the 2-part WBC differential count can be used to provide a quick screening test for discriminating viral infections against bacterial infections in physician offices.

However, a 3-part WBC differential count (lymphocyte, monocyte and neutrophil) or a more advanced 5-part WBC differential count (lymphocyte, monocyte, neutrophil, eosinophil and basophil) are more often used in clinical laboratories. Therefore, it is important to further explore the capability of using fluorescent assays and the microfluidic cytometer to deliver the 5-part WBC differential count.

### 3.1.1 Fluorescent Assays for WBC Differential in Flow Cytometer

There are two major types of fluorescent assays that are used in conventional flow cytometry for the WBC differential count. The first uses an immuno-staining assay of fluorescent-conjugated antibodies, and the second uses fluorescent dye assays. Table 3.1 briefly compares the advantages and disadvantages of these two types of assays.

Table 3.1. Comparison of the fluorescent dye assay and fluorescent-conjugated immuno-staining assay for WBC differential count.

|  | Choice of binding specificity | Shelf life | Storage | Cost |
|---|---|---|---|---|
| Immuno-staining assay | More | Short | Low (4˚C) temperature | High |
| Fluorescent dye assay | Limited | Long | Room temperature | Low |

These two types of assays stain the WBCs with different binding principles. In the immuno-staining assay, the fluorescent label is introduced by binding antibody proteins to antigens expressed in WBCs. In the fluorescent dye assays, the fluorescent label is introduced by the binding of dyes to cellular contents in WBCs (e.g., nucleic acid, protein, etc.). The performances of the two types of assays have their pros and cons in terms of the WBC differential test. For example, the antibody assay provides a wider range of staining specificity for WBC types. However, it requires a low storage temperature (normally 4˚C) and has shorter shelf life, which make it suboptimal for portable applications and long-term space flights. The fluorescent dye assays, on the other hand, have limited choice of binging specificity (e.g., nucleic acid, protein, etc.). However, the merits of fluorescent dye assays includes storage at room temperature and long shelf life, which make them suitable for the portable applications. In addition, the cost of fluorescent dye assays is much lower than the antibody assays, which is important for on-earth applications.

### 3.1.2 Dye Assay for WBC Differential

The use of dyes in the study of WBCs started since the early work of Ehrlich in 1879, and some of the dye staining methods such as the Wright's stain and the Wright-Giemsa are still widely used in manual hematology analysis for WBC differential [90]. For automated WBC analysis, Hallermann et al. started using fluorescent dye assays in conventional flow cytometer in early 1960s [16]. In the early 1970s, researchers from Bio/Physics Systems demonstrated a 3-part WBC differential with fluorescent dye Acridine Orange [16]. Later other dyes were also suggested for WBC differential, such as Oxazine dyes [91], Basic Orange 21 [92] and a Polymethine dye [93]. Shapiro et al. [94] developed an assay consisting of a three dye combination (Ethidium Bromide, Brilliant Sulfaflavine and a Stilbene Disulfonic Acid derivative), which could perform a WBC 5-part differential by using simultaneous measurements of fluorescence and light scattering. However, the detection setting (four excitation sources and six detection channels) was complicated and not optimal for portable implementations. Above all, the development of a fluorescent dye assay which not only delivers the WBC differential count but also is optimal for portable settings is still in need.

### 3.1.3 Fluorescent Dye Assays for Microfluidic Cytometer

Two fluorescent dye assays were proposed and investigated in this chapter. The first assay is a combination of two dyes, Propidium Iodide (PI) and Fluorescein Isothiocyanate (FITC). The second assay is a combination of three dyes including PI, FITC and Basic Orange 21 (BO21). Figure 3.1 shows the molecule structures of these three dyes.
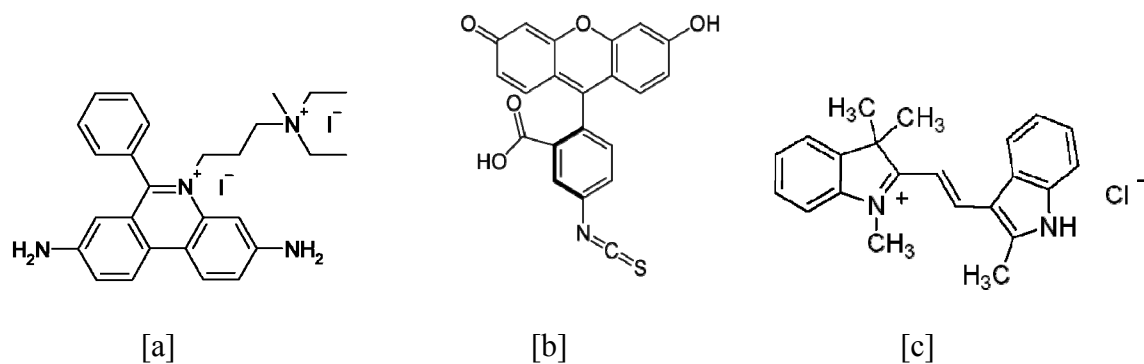
Figure 3.1. The molecule structures of the (a) Propidium Iodide (PI), (b) Fluorescein Isothiocyanate (FITC) and (c) Basic Orange 21 (BO21).

These dye candidates were chosen for their selective binding affinity toward different types of WBCs. PI is a cationic dye, which binds with high affinity to nucleic acid contents (e.g., DNA) in the WBCs. The fluorescent staining of the nucleus, as discussed in Chapter 2, can be used to detect WBCs in the whole blood sample. In addition, PI has relatively higher binding affinity to monocyte than other WBCs [95]. The difference in binding affinity was contributed to specific chromatin structure in the monocytes versus other WBCs.

FITC is an anionic dye, which binds with high affinity towards to proteins. It was previously reported that the FITC staining intensities were different among certain types of WBCs, eosinophil, neutrophil and lymphocyte [16, 96]. This difference is investigated here and used for the WBC differential test. In addition, the fluorescence wavelength of the FITC staining (emission peak 520nm) differs from the fluorescence wavelength of the PI staining (emission peak 620nm). Therefore, these two dyes can be used together and detected separately in two wavelength ranges, respectively.

The third dye, BO21, is a cationic dye, which binds with high affinity to nucleic acids when used alone. However, as shown later in this chapter, BO21 helped to improve the differential between lymphocyte and monocyte cells when used together with PI. The fluorescence emission peak wavelength of BO21 is 525nm (orthochromatic emission), which is very close to and measured together with the emission peak of FITC (520nm).

After staining blood samples with the proposed assays, the fluorescence emissions of individual WBC were detected on the microfluidic cytometer. As the fluorescence emissions were introduced by the binding of dyes to cellular contents (e.g., nucleic acid, proteins, etc.), the measured fluorescence intensities provided a quantitative evaluation of the amount of the cellular contents being stained in different cells. This information was then used to identify the WBC types.

## 3.2 Experiment and Materials

### 3.2.1 Microfluidic Device and Fluorescent Detection System

The microfluidic device used in this chapter utilized the same design and fabrication process as the one used in the Chapter 2. The fluorescence detection system, meanwhile, was upgraded from the previous prototype. The major upgrade was the replacement of the LED excitation source with a laser excitation source, which increased the excitation light intensity.

Figure 3.2 shows the laser-induced, two-color fluorescence detection scheme of the upgraded system. The excitation laser was focused on the microfluidic interrogation channel, and the fluorescence emissions from the sample were collected, passed through a

high-pass emission filter to remove the residual excitation light, and then measured simultaneously in two wavelength ranges, red and green, by the PMT sensors.
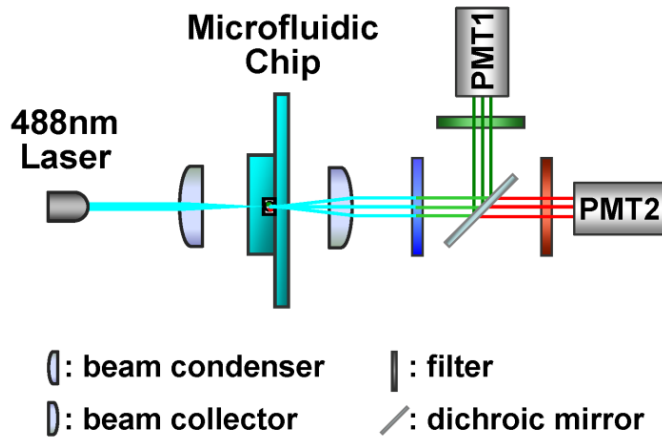


Figure 3.2. The optical configuration of the system for measuring the laser-induced, two-color fluorescence.

The prototype system, as shown in Figure 3.3, was based upon the previous LED version with the following changes. A diode-pumped solid-state (DPSS) laser (488nm, 20mW maximum power, JDSU, USA) was used as the excitation source to replace the previous LED excitation source, and the laser power was adjusted to 2mW for measurement. The laser beam had a Gaussian profile and a diameter near 1mm. It was then focused on the microfluidic interrogation channel by an optical condenser. The length of the interrogation channel, as defined by the width of the light illumination area on the microfluidic channel, was controlled by the focusing adjustment of the condenser.
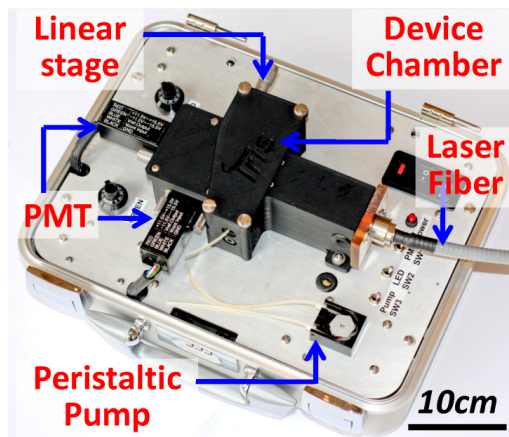
Figure 3.3. Picture of the prototype system. The microfluidic device was enclosed inside the device chamber, shielded away from environment light for the fluorescent detection.

The fluorescence emissions were collected by the second condenser, and passed through a high-pass filter (cut-off frequency 510nm) to remove the residual excitation light. The filtered light was the passed through the Dichroic mirror (Long pass, cut off wavelength 565nm), and separated into two directions based on the wavelength ranges. The portion of the collected light with a wavelength longer than 565nm was transmitted through the mirror, and measured in the red fluorescence channel. The portion with a wavelength shorter than 565nm was reflected by the mirror and measured in the green fluorescence channel. A high-pass filter (cut off wavelength 600nm) was placed in the red fluorescence channel, which mainly measures the fluorescence from the PI staining. Meanwhile, a band-pass filter (520-550nm) was placed in the green fluorescence channel, which mainly measures the fluorescence from the FITC staining and BO21 staining. The intensities of the green fluorescence and red fluorescence were finally measured by two photon-multiplier tubes (PMT, Hamamatsu H5784).

## 3.2.2 Blood Sample and Fluorescent Beads Sample

Human whole blood samples were obtained by the same procedure as described in Chapter 2. Two types of fluorescent bead were used in this chapter. First, the 5μm diameter green fluorescent beads (Duke Scientific Corporations, USA) used in Chapter 2 were tested on the enhanced system for performance comparison. Second, the PeakFlow Carmine flow cytometry reference beads (6μm diameter, Invitrogen, USA) were used for evaluating the detection variation of the optical system. Both of these beads samples were prepared by dilution with the PBS solution (Invitrogen, USA) to a final concentration around $2 \times 10^3$ beads/μl.

### 3.2.2.1 Sample of purified WBC populations

Purified WBC populations (containing only one type of WBC) were prepared using the commercial immunomagnetic isolation kit, EasySep (Stemcell Technologies, Canada), in accordance to the manufacturer's guides. The purification procedures are described briefly here. First, the WBC fraction was separation from whole blood with density gradient separation. A 5mL whole blood sample was mixed with 1mL Hetasep buffer and centrifuged at 90× g, at room temperature for 5min. Following the centrifugation, the supernatant layer containing the WBC fraction was collected, and washed twice by alternate suspending in RoboSep buffer, and pelleting by centrifugation. Second, individual types of the WBC population were purified from the WBC fraction with immunomagnetic isolation. A 400μL WBC suspension ($\sim 5 \times 10^4$ cell/μL) was incubated with the recommended amount of enrichment cocktail and magnetic particles suspension to coat the unwanted cells with magnetic particles. After incubation, the sample was brought up to a total volume of 2.5mL by addition of RoboSep buffer, and placed in the EasySep magnet

for 5min. Then the cell suspension containing the desired WBC population was poured into a new tube, whereas the unwanted cells remained bound inside the original tube. This separation step was repeated twice to ensure the purification quality. Finally, the purified WBC population was washed and resuspended in 20μL phosphate buffered saline (PBS), and the concentration of the cell suspension was enumerated using a hemacytometer, Bright-Line (Hausser Scientific, USA). The purity of the obtained WBC populations was shown to be higher than 90% with verification using Wright's Staining.

### 3.2.2.2 Recipes of fluorescent dye assay

To prepare the assay solution, first, individual stock solution of PI, FITC and BO21 were prepared. The stock solution of 150μM PI was prepared by diluting the purchased 1.5mM PI solution (Invitrogen, USA) with PBS by a 1:9 ratio. The stock solution of 100μM FTIC was prepared by first dissolving 10mg FITC powder (Invitrogen, USA) in 1mL Dimethyl Sulfoxide (Sigma Aldrich, USA), and then diluted with PBS by a 1:256 ratio. The stock solution of 250μM BO21 was prepared by first dissolving 10mg BO21 powder (Sigma Aldrich, USA) in 10ml water and then diluted with PBS by a 1:11 ratio.

The stock solution of the Assay I (PI and FITC) was then prepared by mixing the 150μM PI stock, 100μM FITC stock and the PBS solution by a volume ratio of 6:1:5. The stock solution of the Assay II was prepared by mixing the 150μM PI stock, 100μM FITC stock and 250μM BO21 stock by a volume ratio of 6:1:5. The dye stocks were kept at room temperature, and shielded away from direct light illumination.

### 3.2.2.3 Sample staining procedure

The staining of the blood sample with the fluorescent assays followed a standard protocol of PI staining cellular DNA contents with custom modifications [95].

First, a 5μL blood sample was incubated with 5μL Cal-Lyse fixation solution (Invitrogen, USA) for 8min to make the cell membrane permeable. Second, 45μL distilled water was added to the sample, mixed for 1min to lyse erythrocyte cells and then quenched by adding 6μL 10× PBS buffer (Invitrogen, USA). Finally, the sample was incubated with 12μL of the assay solution (Recipe I or Recipe II) for 7min, and 50μL of the sample was then taken for measurement. The whole staining procedure was carried out at room temperature.

The blood sample used in the staining procedure described above could be whole blood, or whole blood spiked with purified WBC populations. For the sample of purified WBC suspension in PBS, the staining followed the same procedure except that the 45μL distilled water used in the erythrocyte cells lysis step was replaced by 45μL PBS buffer.

## 3.3 Result and Discussion

### 3.3.1 System Calibration with Fluorescent Beads

First, the signal-to-noise ratio (SNR) of fluorescent detection system was evaluated by the measurement of fluorescent beads. In order to compare with the previous LED system in Chapter 2, the same batch of fluorescent beads (5μm diameter green fluorescent beads, Duke Scientific, USA) was used for evaluation, and the bead suspension ($2\times10^3$ beads/μl in PBS) was tested with the laser system at the same flow rate of 6μl/min. Figure

3.4 shows the signal measured from the system. The background noise had a DC level of about 0.2V and the average peak-to-DC amplitude 0.04V. The fluorescent peaks, which represented the events of detected fluorescent beads, showed an average peak intensity of 7.6V. The SNR of the beads measurement, as calculated by the Equation (3) of Chapter 2, is approximately 46dB. This is largely increased comparing to the SNR of 20dB measured on the previous LED system.
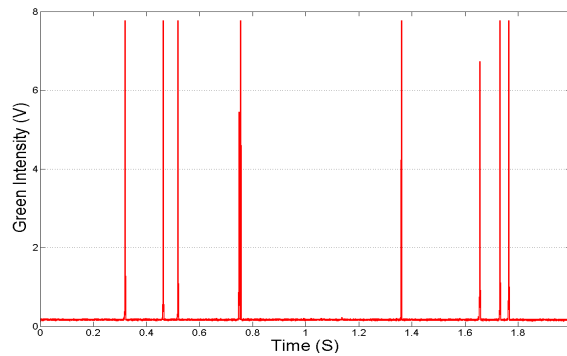


Figure 3.4. Recorded time trace of the measured fluorescence signals (intensity versus time) from the 5μm fluorescent beads.

Secondly, the detection variation caused by the sheathless microfluidic channel was evaluated. The excitation laser beam has a intensity profile of Gaussian intensity profile, which means the illumination intensity along the width of the sheathless channel is nonuniform. Therefore, when fluorescent particles (beads or cells) flowed through various positions along the channel width, the induced fluorescence intensity has variation. This variation was calibrated by using the reference fluorescent beads. PeakFlow Carmine flow cytometry reference beads (fluorescence intensity variation <1%, Invitrogen, USA) were used in this experiment for calibration. The size of the beads (6μm diameter) was chosen

here as it was close to the low end of the WBCs size (7-20μm diameter). The fluorescence emission of the beads was measured in the red channel (>600nm).



[a]                                                    [b]
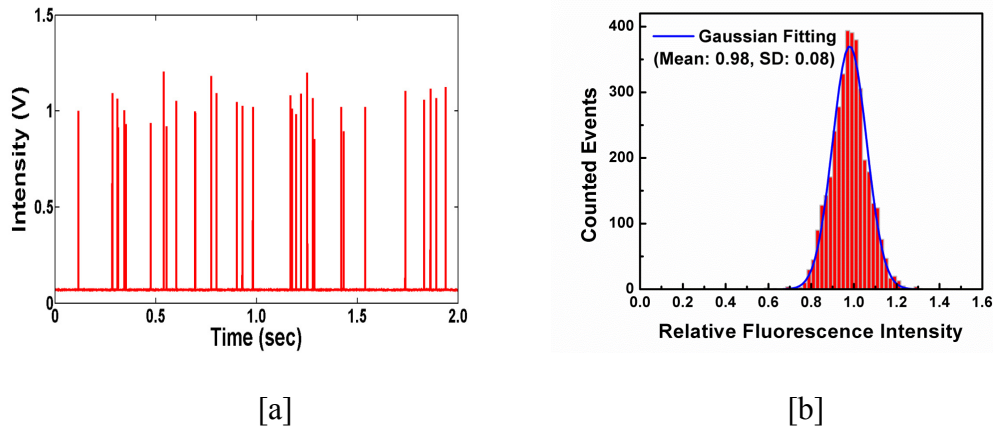
Figure 3.5. (a) Measure time trace of the calibration fluorescent beads sample. (b) The histogram analysis of the measured beads intensities. The number of counted bead events was plotted versus the measured fluorescence intensity of the beads, the data of which was fitted using a Gaussian distribution, showing a mean valve of 0.98 and a standard deviation of 0.08.

The time trace of the fluorescent signal recorded was shown in Fig. 3.5(a). The measured beads intensities showed a high SNR around 46dB. The variation of the measured beads intensities was evaluated using the histogram analysis, as shown in Fig. 3.5(b), and the results showed a coefficient of variation (CV) less than 9%.

## 3.3.2 Blood Sample Staining with Fluorescent Assays

The staining pattern of the WBC populations, i.e., lymphocyte, monocyte, neutrophil and eosinophil, were observed with a fluorescent microscope to compare their fluorescence patterns after the assay staining. The smear of the purified WBCs was prepared according

to the following procedure. First, a 5µl cell suspension of the purified WBCs was taken and stained with the dye assays. Second, 8µL of the stained sample was placed on a microscope glass slide, and spread into a thin film using a cover slide. The smear was then ready for microscope observation.

| WBC Type | Green emission | Red emission |
|---|---|---|
| Eosinophil | | |
| Neutrophil | | |
| Monocyte | | |
| Lymphocyte | | |

Figure 3.6. Fluorescent images of the WBCs after staining with the dye assay (Recipe I: PI and FITC).

Fig. 3.6 compares the fluorescent microscope pictures of the WBCs after staining with the Recipe I. The images were taken using a Nikon Eclipse E800 microscope with a 40x objective lens. The fluorescence emissions were measured in two channels, green (EM 510-550nm/EX 460-490nm) and red (EM 580-650nm/EX 530-550nm). As shown in Fig. 3.6, the WBCs showed different staining patterns by the Recipe I. The eosinophil showed highest green fluorescence intensity, the neutrophil medium green intensity, while the lymphocyte and monocyte showed lowest green intensity. The red fluorescence intensity from the PI staining of nucleus was similar among the WBCs. However, the monocyte showed a relatively larger size of nucleus.

| | Red * Emission | Green ** Emission | Red + Green |
|---|---|---|---|
| *Lymphocyte* | | | |
| *Monocyte* | | | |
| *Neutrophil* | | | |
| *Eosinophil* | | | |

**\*red emission**: >610nm. **\*\*green emission**: 515-545nm.
(excitation wavelength: 488nm.)
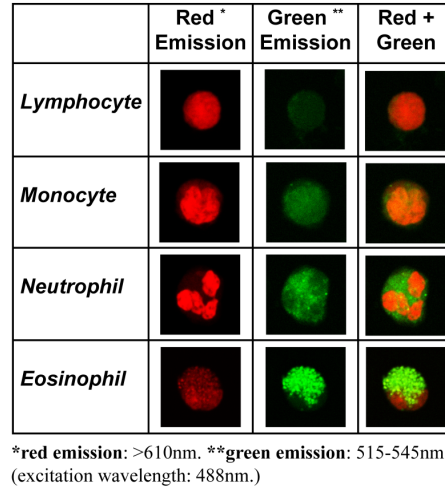
Figure 3.7. Fluorescent images of the WBCs after staining with the dye assay (Recipe II: PI, FITC and BO21).

Fig. 3.7 compares the fluorescent microscope pictures of the WBCs after staining with the Recipe II. The pictures were taken on a laser-scanning microscope, LSM510 (Zeiss, Germany) with a 100x objective lens. The fluorescent emissions were measure simultaneously in two channels, green (EX 515-545nm/EM 488nm) and red (EX >610nm/EM 488nm). The laser-scanning microscope was used here to provide a higher resolution of the imaging (100x objective lens). The fluorescence patterns of the WBCs, as shown in Fig. 3.7, are similar to the patterns observed in the Recipe I. In addition, the fluorescence intensities (red or green) of the cell images were estimated by integrating every pixel within the cells. The calculated intensities were compared in Fig. 3.8. Among the picture of the four WBC types, the eosinophil showed highest green intensity, the neutrophil showed median green intensity, whereas the lymphocyte and monocyte showed lowest green intensity. Meanwhile, the monocyte showed relative higher red intensity than the other types.
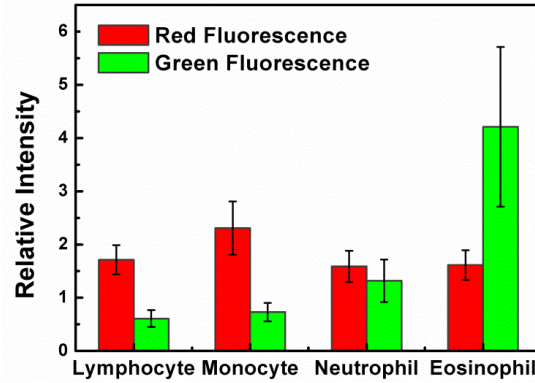
Figure 3.8. Fluorescence intensities of the WBC measured from the fluorescent microscope images. The red fluorescence (>610nm) and the green fluorescence (515-545nm) were measured simultaneously. Average value of ten cells was plotted in the bar graph for each type of the WBC, and the variations were shown in the error bar.

### 3.3.3 WBC 4-Part Differential

Whole blood samples stained with the Recipe I were then measured on the microfluidic cytometer system. Fig. 3.9 shows the typical signals measured on the system. Each peak of the red fluorescence was recorded as a WBC event. The height of the red fluorescence peak represented the amount of nucleic acid content staining by PI, and the corresponding green peak height represented the protein content staining by FITC. The heights of the peaks were then recorded and associated with each of the WBC event.
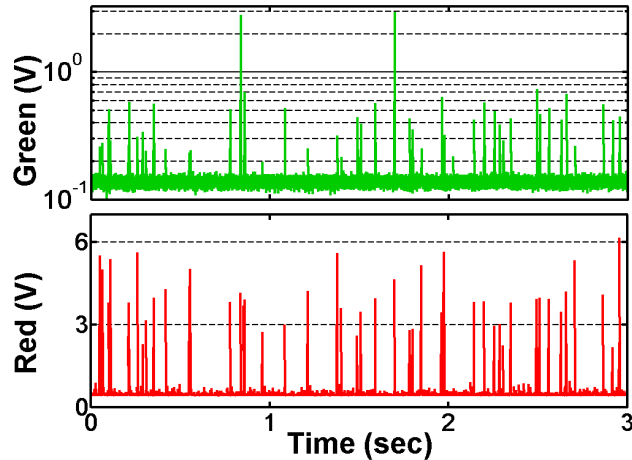
Figure 3.9. Time trace of fluorescence signal (intensity versus time) of blood sample stained with Recipe I (PI and FITC). The signals are measured on the microfluidic cytometer system. The green and red color each represents the green fluorescence signal and the red fluorescence signal being measured.

The recorded peak heights were then plotted in a scatter plot of red fluorescence versus green fluorescence, as shown in Fig. 3.10. In this example, 10,000 WBC events were displayed. The scatter plot showed four separated clusters, one with highest green fluorescence, one with medium green fluorescence and two with relatively lowest green fluorescence. The lower two were further separated by the difference in red fluorescence intensities. These four clusters were each associated to the eosinophil (highest green intensity), neutrophil (medium green intensity), lymphocyte (low green intensity and low red intensity) and monocyte (low green intensity and high red intensity) cells based on the fluorescence intensities, as shown in Fig. 3.10. This is consistent with the previous observations of fluorescence intensities of the WBCs (Fig. 3.6).
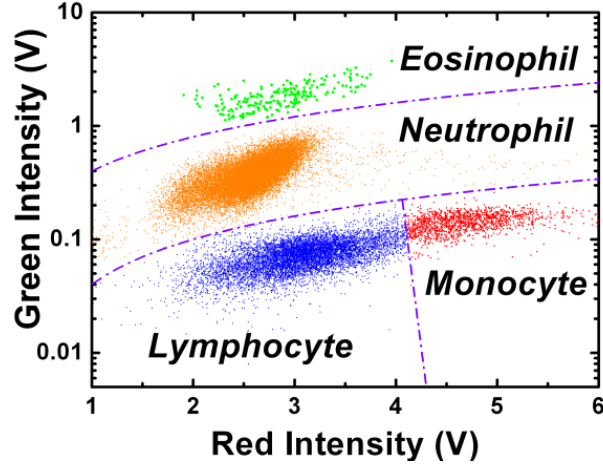
Figure 3.10. The scatter plot of the fluorescence measurement data (green fluorescence intensity versus red fluorescence intensity). Each dot represents one WBC event being recorded.

From the scatter plot, the number of cells belonging to each cluster was determined. An approximation was made to divide the clusters, where the boundaries were assigned as simple lines between the clusters. The number of dots in each cluster, $N_{lymphocyte}$, $N_{monocyte}$, $N_{neutrophil}$ and $N_{eosinophil}$ were determined. Afterwards, the total WBC count and a WBC 4-part differential count (lymphocyte, monocyte, neutrophil and eosinophil) can be obtained as following:

$$N_{WBC} = N_{lymphocyte} + N_{monocyte} + N_{neutrophil} + N_{eosinophil} \text{,} \tag{1}$$

$$C_{WBC} = N_{WBC} / V_{sample} \text{,} \tag{2}$$

$$P_{Lymphocyte} = N_{lymphocyte} / N_{WBC} \times 100\% \text{,} \tag{3}$$

$$P_{monocyte} = N_{monocyte} / N_{WBC} \times 100\% \text{,} \tag{4}$$

$$P_{neutrophil} = N_{neutrophil} / N_{WBC} \times 100\% \text{,} \tag{5}$$

$$P_{eosinophil} = N_{eosinophil} / N_{WBC} \times 100\%$$ (6)

where $V_{sample}$ is the total volume of the whole blood sample measured.

Table 3.2. Comparison of the WBC count and WBC differential results between the microfluidic cytometer system and the commercial blood counter (Beckman Coulter LH750).

|  | Microfluidic Cytometer | Commercial Counter |
|---|---|---|
| WBC Count (cell/µl) | 5,800 | 6,000 |
| WBC 4-Part Differential |  |  |
| Lymphocyte (%) | 33.2 | 34.4 |
| Monocyte (%) | 10.7 | 9.8 |
| Neutrophil (%) | 53.0 | 52.6 |
| Eosinophil (%) | 3.1 | 3.5 |

Table 3.2 summarized the count results of the sample shown in Fig. 3.10, in comparison with results from the commercial counter (Beckman Coulter LH750). The total volume of whole blood tested, $V_{sample}$, is $(5 \times 50/73)$ µl $\approx 3.43$µl as determined by the staining procedure. As shown in Table 3.2, the results from the microfluidic cytometer system matched closely with results from the commercial counter.

### 3.3.4 Correlation Study of 4-Part WBC Differential

To verify the developed 4-part differential count, the correlation studies of our method against the clinical laboratory test were carried out using whole blood samples from an anonymous donor pool. Seven samples from random donors were tested. For each sample, two vials of blood were obtained, one tested in the clinical laboratory (USC Clinical Reference Laboratory, USA) for independent full blood count analysis on a Beckman Coulter LH750 analyzer, and one tested on the microfluidic cytometer.

The differential WBC count results were compared in Fig. 3.11. The range of the WBC populations covered a significant part of the clinical range. For instance, the measured neutrophil percentages covered a range of 50%-75%, whereas the normal range is 40%-80%. In each of the four sub-figures, the x-axis was the results from the commercial counter and the y-axis was the results from the microfluidic cytometer. Liner regression was used to study the correlation between the results. Overall, close correlations were observed for the count of lymphocyte, neutrophil and eosinophil. The neutrophil count showed a linear regression slope of 0.98, the eosinophil count 1.05 and the lymphocyte count 0.9. In addition, the maximum errors of these counts, comparing to the commercial count, were less than 10%. Meanwhile, the accuracy of the monocyte count was relatively lower. The linear regression slope of the monocyte count was 0.50, and the maximum error could reach as high as 20%. This inaccuracy was mainly contributed to the overlap between the monocyte cluster and the lymphocyte cluster. The total number of monocyte, $N_{monocyte}$, was relatively low comparing to the total number of lymphocyte, and hence more vulnerable to the inaccuracy caused by the overlapping boundary.
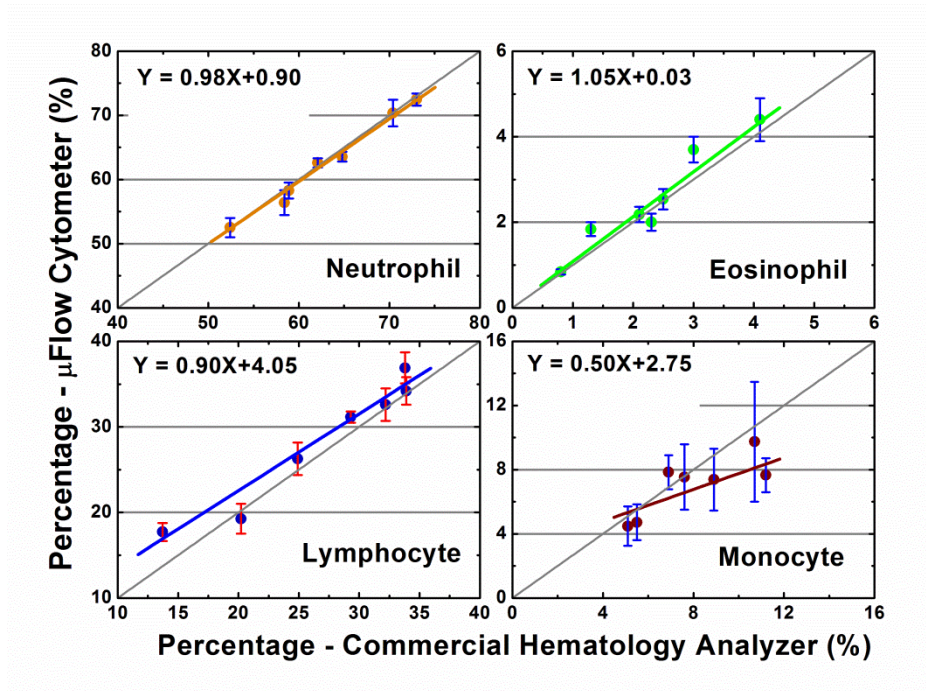
Figure 3.11. Correlation between the results from the microfluidic cytometer and commercial hematology analyzer (Beckman Coulter LH750). For each WBC type, the linear regression and correlation coefficient are calculated. Error bars show the maximum deviations from five repeated tests.

## 3.3.5 Cluster Overlap of Monocyte and Lymphocyte

As discussed above, the separation between the monocyte and the lymphocyte clusters was subjected to an ambiguous boundary. In the 4-part differential assay (Recipe I), these two clusters were separated by the PI staining fluorescence. To study the overlap between these two clusters, higher green fluorescence was introduced to the monocyte cluster, by immuno-staining assays with high affinity binding to the monocyte cells.

For comparison, two tests of the blood sample from the same donor were carried out. The control sample was stained by only PI, following a modified version of Recipe I,

where the FITC solution was replaced by PBS buffer. The experimental sample was stained with both PI and the immuno-assay (anti-CD14-FTIC, Invitrogen), following another modified version of Recipe I, where the FITC solution was replaced by the immuno-assay solution. The measurement results were compared in Fig. 3.12. From the comparison, it was clear that the monocyte cluster is distinguished from the other clusters with higher green fluorescence. In addition, two observations were made from the results. First, the monocyte cluster indeed had highest red fluorescence intensity from PI staining compared to the other WBCs. Secondly, some of the monocyte cells having relative low red fluorescence were indeed overlapping with other WBCs, most likely the large lymphocyte cells [3].



[a]                              [b]
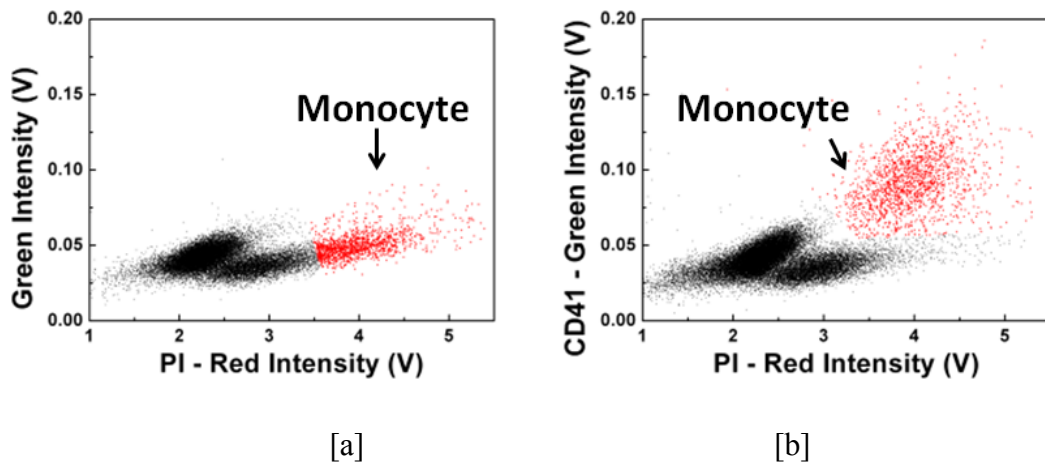
Figure 3.12. Identification of monocytes cluster. (a) The control result where monocytes (red dot) identified by PI fluorescence only. (b) The experimental result where monocytes identified by both PI fluorescence and green fluorescence from the anti-CD14 staining.

This study also suggested a way to improve the monocyte cluster separation, which is by adding another fluorescent probe that stained monocyte cells with different intensity from other WBCs. Therefore, we investigated the approach of adding a third dye to the current assay.

## 3.3.6 Improved WBC 4-Part Differential

One dye we targeted to improve the 4-part differential assay was an organic dye called Basic Orange 21 (BO21). BO21 was considered as the candidate for two reasons: first, BO21 had been shown in prior works to stain lymphocytes and monocytes with different patterns [92]; second, the fluorescence of BO21 was measurable within the current optical system (488nm excitation and 520-550nm emission).

In our experiments, it was observed that BO21 indeed stained monocyte cells differently from the lymphocyte cells. In a control sample, whole blood was stained by PI alone, whereas in an experimental sample, it was stained by a mixture of PI and BO21. The final concentrations of PI in both samples were the same as in Recipe I. The final concentration of BO21 in the experimental sample was 50μM. Then both samples were measured on the prototype system, and results were compared in Fig. 3.13.

From the comparison, it was clear that monocytes, the cells with highest red fluorescence intensity from PI staining as verified in the immuno-assay tests, distinguished further from other WBCs by the additional BO21 staining. As shown in Fig. 3.14(b), the monocyte cluster had higher green intensity, which was introduced by the BO21 staining, than the bottom cluster (most likely lymphocyte).

(a)                                              (b)
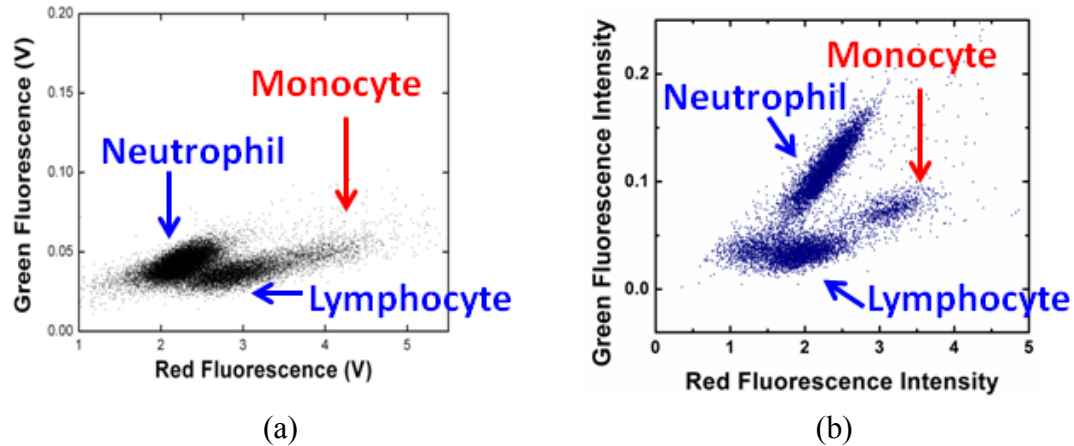
Figure 3.13. Comparison of the WBC differential pattern of blood sample staining with

(a) PI versus (b) PI and BO21.

The following experiments were then carried out to study the effect of adding BO21 to the dye assays. Fresh blood samples were stained separately by the dye assays, Recipe I and Recipe II. The stained samples were then measured on the prototype system and the results were compared, as shown in Fig. 3.14.

The sample stained with Recipe I (PI and FITC), as shown in Fig. 3.14 (a) and (b), had four clusters where the boundary between the lymphocyte and monocyte clusters was not clear due to the overlap. The sample stained with the Recipe II (PI, FITC and BO21), as shown in Fig. 3.14 (c) and (d), also showed four clusters, but the monocyte cluster was clearly distinguished from the lymphocyte cluster this time. The monocyte cluster showed both higher red fluorescence and higher green fluorescence than the lymphocyte cluster. From the comparison, it also seemed that the green fluorescence of the eosinophil cluster and the neutrophil cluster became closer after the addition of BO21. Nevertheless, the boundary between these two clusters (neutrophil and eosinophil) is still very clear and easy to separate.
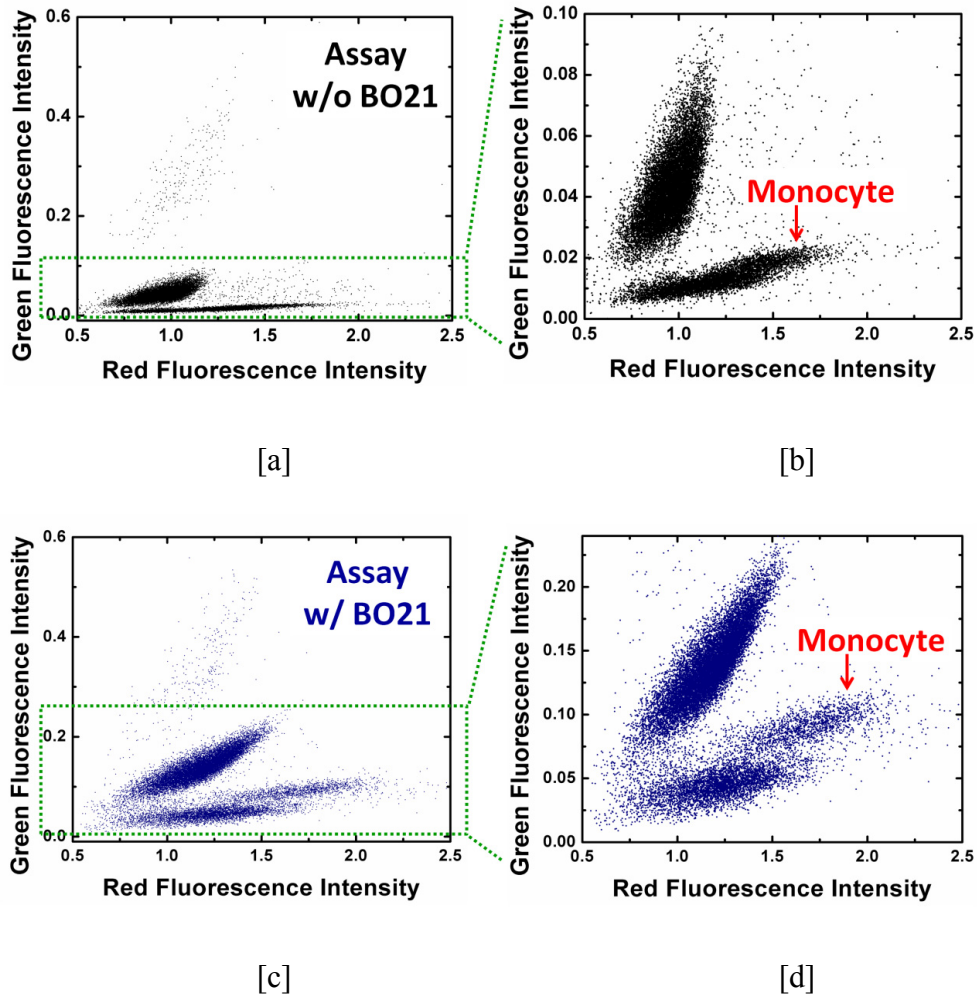
Figure 3.14. Comparison of the WBC differential pattern of blood sample staining with Recipe I (PI and FITC) versus Recipe II (PI, FITC and BO21). (a) Scatter plot of sample staining with Recipe I, and (b) zoom-in view of the scatter plot of the sample staining with Recipe I. (c) Scatter plot of sample staining with Recipe II, and (b) zoom-in view of the scatter plot of the sample staining with Recipe II.

### 3.3.7 Validation of 4-Part Differential with Purified WBC population

Spiking experiments were then carried out to validate the enhanced assay (Recipe II) for the 4-part differential. Two groups of samples were measured, where the control sample

was whole blood (3µl whole blood mixed with 2µl PBS buffer) and the experimental samples were whole blood spiked with a cell suspension of the purified WBC types (3µl whole blood spiked with 2µl of the purified cell suspension). Each of the experimental samples was spiked with only one type of the purified WBCs. The samples were then stained with the improved 4-part differential assay (Recipe II: PI, FITC and BO21), and measured on the microfluidic cytometer. Finally, the count results of the control sample and the spiked samples were compared to track the change of the target clusters.

The measured scatter plots are shown in Fig. 3.15, and the count results are summarized in Table 3.3. The amounts of spiked cells were different for experiments of each target WBC types. For instance, the neutrophil cluster initially consisted of a higher percentage (~70% of the total WBCs) than the eosinophil cluster (~2% of the total WBCs), and hence larger amount of purified neutrophil cells were needed to reach a significant change of the cluster.

The measured results, as shown in Fig. 3.15 (a-e), showed the target clusters became denser and more significant after spiking, especially the ones which were initially sparse such as the eosinophil cluster. Meanwhile, the other clusters became relatively thinner, which was most obvious in the neutrophil spiked sample. These results suggested that the spiked cells indeed correlated to the increased count of the target clusters in the measurement. The count results, as summarized in Table 3.3, supported the observed changes, showing significantly increased ratios of the target clusters. In addition, the ratios measured after spiking matched closely with the ratios expected from the amount of the purified cells spiked. This result suggested that most of the spiked cells indeed fell into the target cluster.
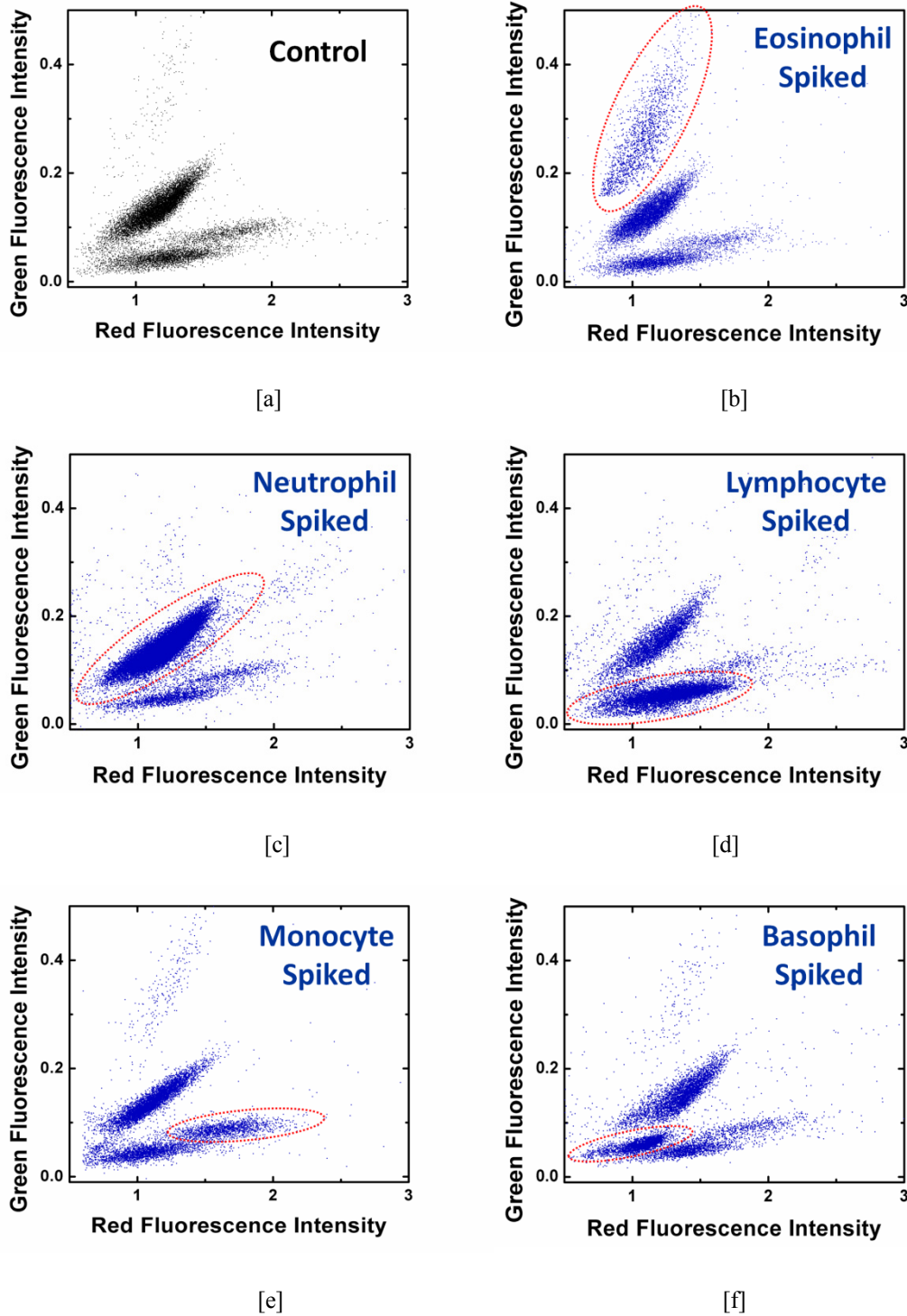
Figure 3.15. Scatter plot results of the spiking experiments, (a) the control sample, (b) eosinophil spiked sample,  (c) neutrophil spiked sample, (d) lymphocyte spiked sample, (e) monocyte spiked sample, and (f) basophil spiked sample.

Table 3.3. The count results of the spiking experiments. Test #1 to Test #5 each corresponds to the sample spiked with the purified eosinophil, neutrophil, lymphocyte, monocyte and basophil, respectively. The "Reference" data was measured in the clinical laboratory. The "Measured" data was result measured on the microfluidic cytometer. The "Expected" values of the spiked samples were calculated by assuming all the spiked cells were all counted in the target cluster. "N/A" means the count result is not available.

| | Target cluster | Before spiking | | After spiking | |
|---|---|---|---|---|---|
| | | Reference (%) | Measured (%) | Expected (%) | Measured (%) |
| 1 | Eosinophil | 2.1 | 2.1 | 14.4 | 14.0 |
| 2 | Neutrophil | 69.2 | 68.1 | 90.3 | 89.2 |
| 3 | Lymphocyte | 20.5 | 22 | 66.5 | 63.9 |
| 4 | Monocyte | 6.9 | 7.3 | 21.2 | 16.7 |
| 5 | Basophil | 0.4 | N/A | 32.0 | 29.3 |

## 3.3.8 Correlation Study of Improved 4-Part Differential

Furthermore, correlation studies of the differential results against the clinical laboratory test were carried out using whole blood samples from an anonymous donor pool. Fig. 3.16 shows a typical scatter plot obtained from a sample, where the elliptical boundaries were used to divided the clusters. The elliptical boundaries were drawn across the areas with low dot densities, where majority of the cells (>98%) located inside of the boundaries, provide sufficient statistical accuracy for the count results.
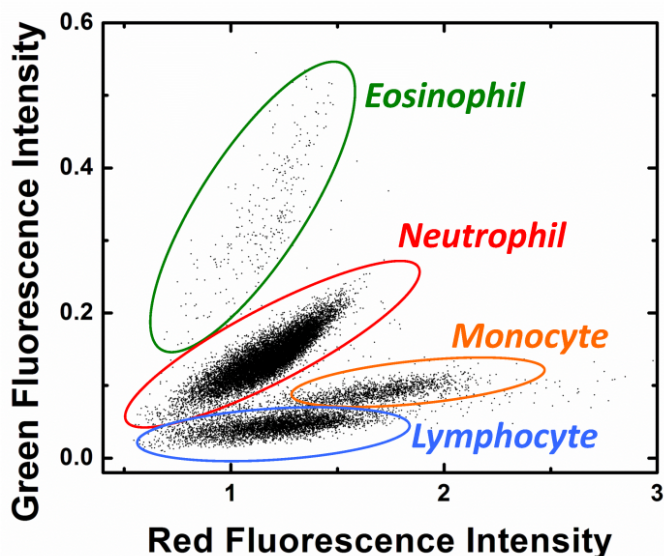
Figure 3.16. A typical 4-part differential scatter plot obtained from the blood sample for the correlation study.

Nine samples were tested (n=9). For each sample, two vials of blood were obtained, one was tested in the clinical laboratory (USC Clinical Reference Laboratory, USA) for an independent full blood count analysis on a Beckman Coulter LH750 analyzer, and one was tested on the microfluidic cytometer for three repeated measurements. The differential leukocyte count results were compared, and the correlations were studied using linear regression, as shown in Fig. 3.17.

In each plot, the x-axis corresponds to the results from the commercial count, whereas the y-axis corresponds to the results from the microfluidic cytometer. Linear regression was used to verify the correlation between the two counts, and both the linearity and the correlation coefficient $R^2$ were calculated, as shown in Fig. 3.17. The ranges of the WBC populations covered significant parts of the clinical ranges. For instance, the measured neutrophil percentages covered from 52% to 74%, whereas the normal range is

40%-80%. Overall, close correlations were observed for all four WBC types including eosinophil, neutrophil, lymphocyte and monocyte (correlation coefficients $R^2$ higher than 0.9). The correlation of the monocyte percentage was slightly weaker ($R^2$=0.9, slope=0.91) than the correlations of other WBC populations ($R^2$>0.93, and slopes close to 1), but still largely improved from the Recipe I (Fig. 3.10). Overall, the maximum inaccuracy of the differential count results was less than 10% compared with the results from the commercial counter.
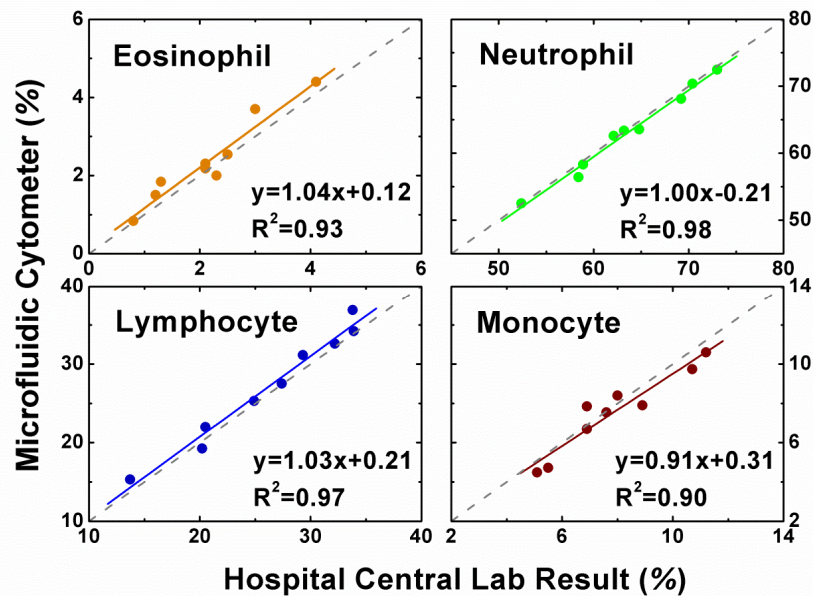


Figure 3.17. Correlation study of the WBC differential count results. Each dot compares the data measured on the microfluidic cytometer and data measured in a hospital central lab using Beckman Coulter LH750 Hematology analyzer. Nine samples were measured for each subpopulation, and the data was fitted with a linear regression (solid line). The linear correlations equation, y=Ax+B, and the correlation coefficients, $R^2$, were displayed. The grey dash lines showed a linear correlation of y=x.

### 3.3.9 WBC 5-Part Differential Feasibility

In the state-of-the-art hematology analyzers, the WBC differential results not only include the lymphocyte, monocyte, neutrophil and eosinophil, but also report the fifth WBC population, basophil. Basophil is a rare population, normally consisting of less than 1% of total WBCs. Hence the basophil population is most difficult to count and the precision is always a concern even in clinical laboratories [15]. In our method, the WBC populations are counted by the distinct clusters in the scatter plot. However, the basophil population might be too rare to form an obvious cluster.

To study the feasibility of counting basophil, a whole blood sample was spiked with purified basophil cells and measured with our method (Recipe II on the microfluidic cytometer). The experimental conditions are also summarized in Table 3.3, where the whole blood (3μl) sample was spiked with a significant amount of basophil cells (2μl purified cell suspension). Fig. 3.15 (f) shows the measured scatter plot. After spiking, a fifth cluster showed up, in addition to the four clusters observed in the control sample, as shown in Fig. 3.16 (a). The count of this cluster, as summarized in Table 3.3, matched closely with the ratio expected from the amount of the purified cells spiked, suggesting that this cluster mainly consisted of the basophil cells. This basophil cluster was very close to the lymphocyte cluster, indicating that the basophil was likely to be miscounted as the lymphocyte in samples without distinct basophil clusters. However, this error was negligible for most whole blood samples, as the basophil population (0%-1% of total WBC) was usually much lower than the lymphocyte population (20%-40% of total WBC). Table 3.4 summarizes the differential count results (lymphocyte, monocyte, neutrophil, eosinophil and basophil) of this experiment, where the measured data matched closely with

the reference data. The reference data was obtained by adjusting the results from the commercial counter with the known number of spiked basophil cells.

Table 3.4. Summary of the differential count results.  The measured results were data from the microfluidic cytometer. The reference data was result from a commercial hematology analyzer (Beckman Coulter LH750) adjusted by the known number of spiked basophil cells.

|  | Lymphocyte | Monocyte | Neutrophil | Eosinophil | Basophil |
|---|---|---|---|---|---|
| **Reference** | 19 | 5 | 44 | 2 | 30 |
| **Measured** | 18 | 6 | 46 | 2 | 28 |

The results of this experiment demonstrated the feasibility of the 5-part differential by using the developed dye assay and the microfluidic cytometer. However, a significant amount of basophil cells might be needed to form an obvious basophil cluster. Nevertheless, with the known information of the potential basophil cluster, it is feasible to flag the blood sample when high basophil population was encountered, which is useful in clinical diagnosis.

## 3.3.10 Correlation Study of Total WBC Count

Furthermore, the accuracy of the total WBC count using the improved 4-part differential assay was also verified by the correlation study with the commercial counter. Nine samples were tested (n=9). For each sample, two vials of blood were obtained, one was tested in the clinical laboratory (USC Clinical Reference Laboratory, USA) for an

independent full blood count analysis on a Beckman Coulter LH750 analyzer, and one was tested on the microfluidic cytometer for three repeated measurements. The results were compared in Fig. 3.18.
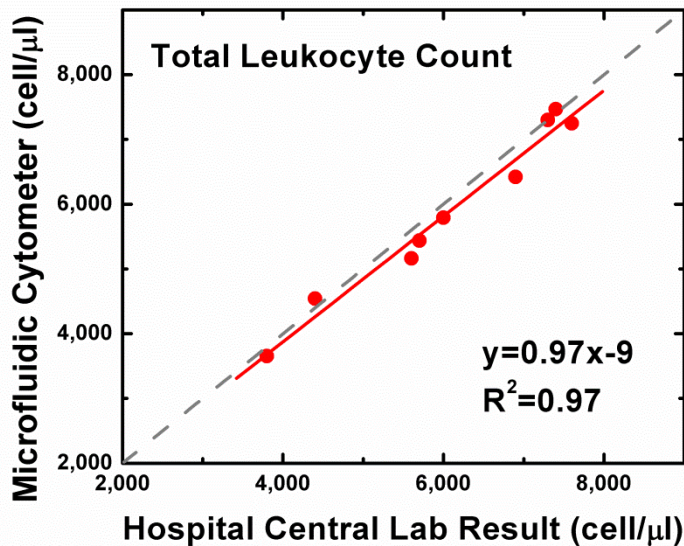


Figure 3.18. Correlation study of the absolute leukocyte count. Each dot compares the results measured on the microfluidic cytometer and the data measured in the hospital central lab using the Hematology analyzer.  Nine samples were compared, and the data was fitted with a linear regression (solid line). The linear correlations equation, y=Ax+B, and the correlation coefficients, $R^2$, were displayed. The grey dash lines showed a linear correlation of y=x.

The result showed a close match, with a correlation coefficient $R^2=0.97$ and a slope of the linear regression 0.97. It is worth noting that the obtained absolute count was slightly but consistently lower than the data from the clinical laboratory. This was mainly contributed to cell loss during the current staining protocol, particularly the RBC lysis step.

Cell loss can be reduced by optimizing the assay procedure, adding PBS buffer to prevent the unnecessary WBC lysis caused by the RBC lysis step. Nevertheless, the maximum error of the total WBC count, comparing to the commercial count, was less than 10% and considered within the tolerable range for clinical significant (10%).

## 3.4 Conclusion

In this chapter, the optical detection system of the microfluidic cytometer was upgraded with a blue laser excitation source (488nm, maximum power 20mW). Compared with the previous LED excitation prototype, the detection sensitivity of the laser-enhanced system is largely improved. The detection SNR of same fluorescent beads increased from 20 to 46dB. In addition, the detection variation associated with the sheathless microfluidic channel was evaluated with calibration beads. The measurement of the calibrated fluorescent beads (intrinsic variation <1%) in the sheathless channel showed a coefficient of variation less than 9% for fluorescence intensity measurement.

More importantly, two fluorescent dye assays have been developed to deliver the WBC 4-part differential (lymphocyte, monocyte, neutrophil and eosinophil). The developed dye assays stained the four types of WBC with different affinity, and the measured fluorescence intensities (green 520-550nm and red >600nm) on the microfluidic cytometer were able to distinguish the WBC into four separated clusters in the scatter plot (green intensity versus red intensity). The first assay (Recipe I: PI and FITC) was able to deliver the 4-part differential with a less satisfactory monocyte count. The improved assay (Recipe II: PI, FITC and BO21) was able to deliver the 4-part differential with a satisfactory monocyte count.

The associations of the differential clusters with the four types of WBCs (lymphocyte, monocyte, neutrophil and eosinophil) were verified by first the spiking experiments with purified WBC types, and then in a correlation study with the count results from a commercial blood counter (Beckman Coulter LH750). The spiking experiments confirmed that the purified WBC types indeed led to and matched with the increased count of the corresponding target cluster. The correlation study showed good match with the commercial blood count results of the WBC 4-part differential (correlation coefficients $R^2$ >0.9, maximum error<10%).

In addition, counting the fifth WBC type, basophil, was also explored by testing blood sample spiked with purified basophil cells. In the normal human whole blood, the basophil cells are rare (<1% of total WBCs) and rarely form a significant cluster. In the spiked sample, the basophil cluster became significant (~30% of total WBCs), and the measurement results showed a distinct basophil cluster in addition to the four clusters previously measured. This result demonstrated the feasibility of using the proposed method to flag the blood samples, when a significant basophil population was encountered.

# Chapter 4 : On-Chip Blood Cell Count

## 4.1 Introduction

In the last two chapters, it has been demonstrated that the WBC count and the WBC differential count can be achieved using the principles of dye-based fluorescent detection and sheathless microfluidic cytometer. However, in the prototype system, the test procedure still involves manual operations such as the collection of blood sample, incubating blood sample with staining assays, and loading samples for measurement, etc. For point-of-care applications, the end users of the instruments are often nontechnicians such as physicians or even patients. Therefore, it is necessary to integrate the whole test procedure into a cartridge chip which can minimize the manual operations required from the users. This chapter will discuss the design principle of the cartridge chip and the development of the key components of the cartridge.

### 4.1.1 Design Principle of Cartridge Chip

Fig. 4.1 illustrates the basic concept of the self-contained cartridge chip. To minimize the manual operation from end users, the following functions are proposed for the cartridge chip: blood collection, fluidic sample pumping and valving, on-chip blood staining with dye assays, microfluidic cytometer detection and waste collection. This design eliminates the fluidic connection between the cartridge chip and the external instrument, enabling a self-contained and disposable chip. When one drop of blood was applied to the cartridge inlet, the rest of the test could be carried out on the chip automatically.
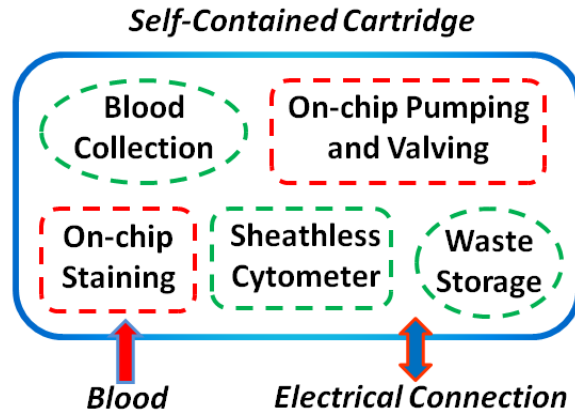
Figure 4.1. The design concept of the self-contained cartridge chip for minimizing manual operations. The interfaces of the cartridge need only blood sample input and the electrical connections for cartridge operations.

There are three major merits of using the microfluidic technology to build the disposable, self-contained cartridge. Firstly, the sizes of the microfluidic component are very small, and suitable for large scale integration of the whole test procedure on one chip. Secondly, the parallel fabrication process of the microfluidic device has the potential to largely lower the device cost, making it attractive for disposable applications. Thirdly, the microsized fluidics can reduce the consumption of the sample and reagents.

The development of microfluidic devices have been growing rapidly in last two decades [53]. The recent progress of using microfluidic devices for biomedical sensing has been discussed in detail elsewhere [62-64]. However, one major problem that still impedes many of the practical implementations of the microfluidic chips is the lack of simple, reliable microfluidic components such as microvalve, etc. [58, 61, 97, 98]. Therefore, the first and most important step in developing the disposable, self-contained cartridge is to identify and develop the key microfluidic components needed for the operation.

## 4.1.2 Key Components of Cartridge Chip

To fulfill the functions of the WBC count test, a principle design of the cartridge chip is proposed as illustrated in Fig. 4.2. Firstly, to load the sample into the chip, a microfluidic channel with hydrophilic surface is used to introduce the capillary force for collecting the blood into the sample chamber (marked red in the design). Secondly, the two loading valves (integrated microvalve) are closed, sealing the blood sample inside the chip. Thirdly, fluidic pump (integrated micropump) started to push the blood sample and stored assay for mixing and incubation in the meander channel. Finally, the fluorescent detection is carried out in the sheathless cytometer channel, and the tested sample is collected into the waste storage chamber.
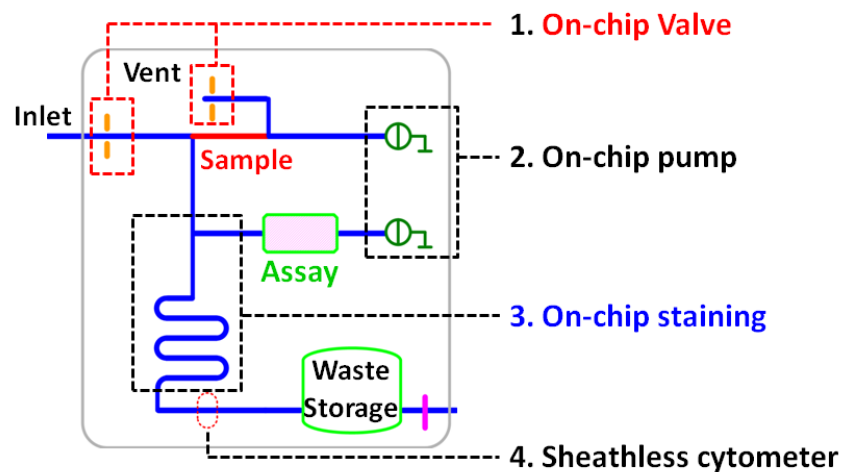


Figure 4.2. The design principle of the cartridge chip. The chip includes components of microvalve, micropump, on-chip mixing, sheathless cytometer and waste storage chamber. The assay is stored in the storage chamber (green). Blood is collected by capillary force into the sample collection chamber (red). The microvalve is used to seal the loading channels of blood sample, and ensure the micropump can deliver the sample for downstream mixing and cytometer analysis.

Four major components were identified for this design, including the integrated microvalve, the micropump, the on-chip mixing, and the sheathless cytometer channel. The design and implementation of the sheathless cytometer channel has been discussed extensively in Chapter 2. For the integrated pump, electrolysis micro pump is employed for the merits of the simplicity and the capability to provide a large volume expansion, which have been investigated extensively in previous reports [97, 99].

Two key components, including the micro valve and the on-chip mixing channel, are investigated here to demonstrate the feasibility of the cartridge chip. Various types of microvalves have been reported previously [98], including active valves controlled by mechanical actuations (magnetic, electrostatic, piezoelectric, thermal, pneumatic, etc.), or nonmechanical actuations (electrochemical phase change, rheological, etc.). The mechanical valves normally require complicated valve structures and fabrication processes [98], and hence not optimal for disposable chip applications. Non-mechanical valves such as the ones utilizing phase-change materials [100] or rheological materials [101] normally have simpler structures. However, special valve materials (phase change or rheological materials) are needed for valve actuation, complicating the fabrication processes. Above all, the lack of a reliable, simple structure micro valve is still considered an important factor limiting the practical implementations of microfluidic devices. Therefore, it is of great interest to develop a reliable valve that has very simple fabrication process and actuation principle, and suitable for disposable chips. In the proposed cartridge design, the minimal requirement of the valve function is a one-time use, open-to-close valve.

The study of mixing two fluidic samples in the microfluidic channel itself is still an interesting problem attracting extensive attentions. There are two major types of micro

mixers including the active mixer and passive mixer [102]. The passive mixers are more popular for disposable applications because of the merits of simple structure and fabrication process. The mixing process in the passive mixer relies mainly on the diffusion due to the laminar nature of the microfluidics. However, there have also been approaches to introduce chaotic advection to improve the mixing efficiency [102]. For this particular cartridge application, the main design focus of the mixer is to demonstrate the feasibility of the on-chip staining of blood sample with the dye assay.

# 4.2 Blood Clogging Micro-Valve

## 4.2.1 Principle

### 4.2.1.1 Thermal coagulation of blood

Blood thermal coagulation is a natural property of the blood. Thermal heating converts the liquid blood into solid coagulum by biochemical reactions. This thermal coagulation process is a complex phenomenon which includes deformation and rupture of erythrocytes, protein denaturation, aggregation, and gelation [103].

Normally, the human whole blood is in a liquid form, comprising the plasma fluid (55% weight) and the cellular components (45% weight). There are three major sources of proteins in the whole blood, including the albumin (45g/L) and globulin (25g/L) in plasma, and also the hemoglobin in RBCs (140-160g/L of whole blood) [103].

Upon the thermal heating, firstly, the morphology changes happen to the blood cells. The normally biconcave RBCs start to assume biconvex shapes, and then form spherocytes (starting around 45°C). Partial membrane fragmentation of RBCs occurs (starting around 60°C), resulting in the release of hemoglobin (60°C). Eventually the RBC cellular

membrane disintegrates into globules, which aggregate to form a mesh, and the release of hemoglobin is completed [103]. Meanwhile, the protein contents in the blood go through a continuous physical transition due to the thermal heating. The denaturation of the protein contents cause the blood to form initially a jellylike structure and finally a solid coagulum [104].

**4.2.1.2 Blood thermal coagulation as microvalve**

The thermal coagulation of blood provides a natural valving mechanism that has not been well explored in the microfluidics previously. Fig. 4-3 illustrates the basic principle of the valve mechanism. The fluidic channel is normally open, allowing the blood sample to flow through freely. To close the valve, the blood sample inside the valve zone is converted from a liquid form into a solid coagulum by the thermal heating actuation. The formed coagulum physically stems the fluidic channel and closes the valve.
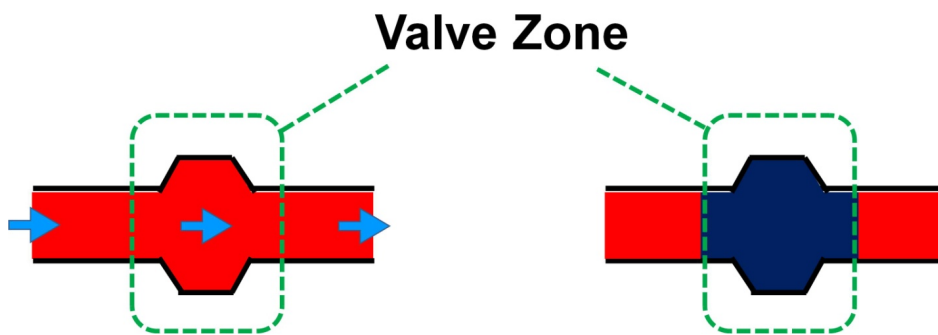


Figure 4.3. The operation principle of the micro valve using blood thermal coagulation. The fluidic channel is normally open, allowing the blood sample to flow through freely. Upon actuation, the blood sample inside the valve zone is subjected to thermal heating, and converted from liquid form into solid coagulum. The blood coagulum stems the fluidic channel as a closed valve.

This valve mechanism provides a one-time use, open-to-closed valve, which enjoys a very simple valve structure and easy actuation. The valve needs no extra fluidic design other than the fluidic channel itself. In addition, the blood sample for valve actuation is readily available for devices targeting at the blood analysis. To introduce thermal coagulation inside the valve area, the localized heating by various methods such as laser or micro-heater can be explored, avoiding excessive heating to other parts of the microfluidic chip.

### 4.2.1.3 Laser induced thermal clogging of blood

Focused laser beam was investigated in this study to introduce the localized blood clogging. Laser has been previously used in medical surgery to repair the leaking blood vessel by locally introducing blood thermal coagulation. This procedure is normally referred as laser photocoagulation. The basic principle of the laser photocoagulation is that the hemoglobin in RBCs absorbs the light (e.g., 400~600nm), the energy of which is converted into heat and raises the temperature of the blood sample to introduce the thermal coagulation process.
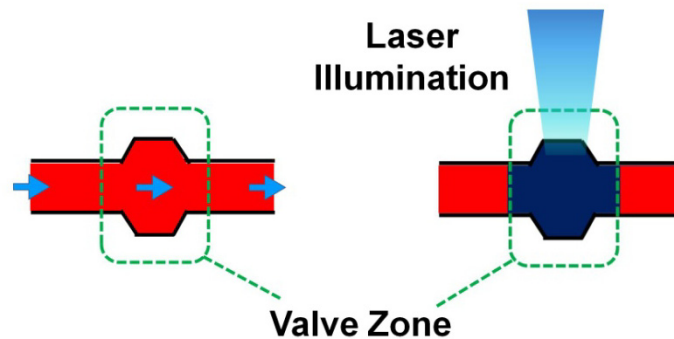


Figure 4.4. The operation principle of the laser induced blood clogging.

Focused laser beam in the visible spectrum (e.g., 488nm) is used in this study to introduce the localized heating, as shown in Fig. 4.4. By focusing the laser illumination on the valve zone, the thermal heating can be introduced to the blood sample inside the valve zone and unnecessary heating to the blood sample outside the valve zone can be minimized. In addition, this actuation method can operate the valve without any physical or electrical interconnection, which largely simplifies the valve structure design.

## 4.2.2 Material and Experiment

### 4.2.2.1 Blood samples

Fresh whole blood samples from healthy human donors were used for the following experiments. The venous blood were purchased from Hemacare Corp. (CA, USA) and tested within 48 hours after the blood drawing. The samples were kept in the standard 5 ml purple tubes with Ethylenediaminetetraacetic acid (EDTA) coating and stored in 4°C refrigerator before experiments.

### 4.2.2.2 Thermal coagulation of blood

To study the blood thermal coagulation as the valve mechanism, the heating parameters (heating temperature and heating time duration) required to form solid coagulum were investigated.

Blood samples were tested in glass capillary tubes (0.38 mm in diameter, 10 μl Accu-Fill Micropet) to form the coagulum. For each test, 2μl whole blood was first loaded into the capillary tubes, forming a continuous portion of blood slot (18mm length). Secondly, the capillary tubes were immersed into a heated water bath to introduce the blood thermal coagulation. The open ends of the capillary tubes were sealed by a thin layer of plastic film

to prevent water reaching the blood slot. The temperature of the water bath was monitored by a mercury thermometer (-10°C to +150°C reading, 0.5°C accuracy), and the heating time duration was monitored by a digital timer (VWR, 1 second reading accuracy). The capillary tubes were cooled down immediately after heating by immersing into another water bath keeping at room temperature. A wide range of heating temperatures (60°C, 65°C, 70°C, 75°C, 80°C, 85°C, 90°C) and variable heating times (0, 1/6, 1/2, 1, 2, 3, 5 and 10 min) were evaluated. Any heating time duration higher than 10min was considered too long for practical valve application and thus not considered here.

Afterwards, the capillary tubes containing the formed clog were tested by the configuration shown in Fig. 4.5, measuring the maximum back pressure that the clog can withstand before breaking.
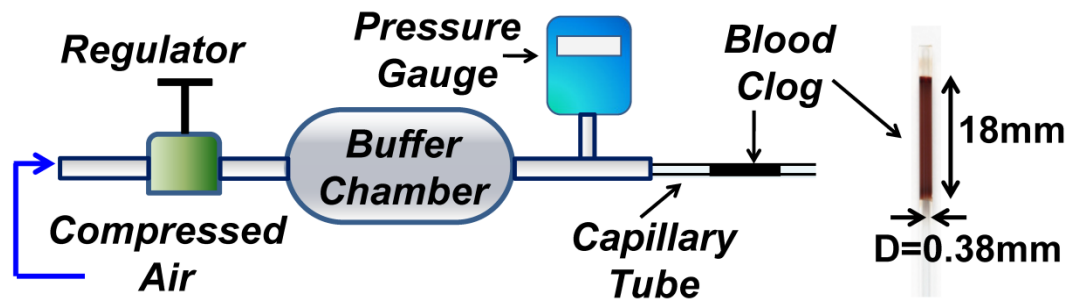


Figure 4.5. The test configuration of the back pressure measurement (left) and (right) a picture of a capillary tube with blood clog formed inside.

The test pressure was imposed by applying compressed air at one end of the capillary tube. The pressure range was adjusted by a pressure regulator (0-100 psig continuously) and monitored by a pressure gauge (Omega PLC100-1K). For each measurement, the applied pressure started at 0 psig and increased with a ramping rate of 1psig/5sec. The

maximum back pressure was recorded as the pressure before either the clog burst or air leakage observed (bubble forms at the other end of the tube, which was sealed by a water drop).

### 4.2.2.3 Thermal coagulation of blood in microfluidic channel

The feasibility of thermally introducing blood coagulum inside a microfluidic channel was then investigated by using PMDS devices. The PDMS devices were fabricated using the same procedure as described in Chapter 2, where the fluidic channel was formed between a PDMS piece and a glass substrate. The fluidic design, as shown Fig. 4.6, consisted of a main valve zone and four fluidic ports. The valve zone of the device was first fulfilled with blood sample by loading through two fluidic ports on the opposite sides of the valve zone. Then the whole device was heated up in a water bath with the glass side immersing in the water.



[a]                                                              [b]
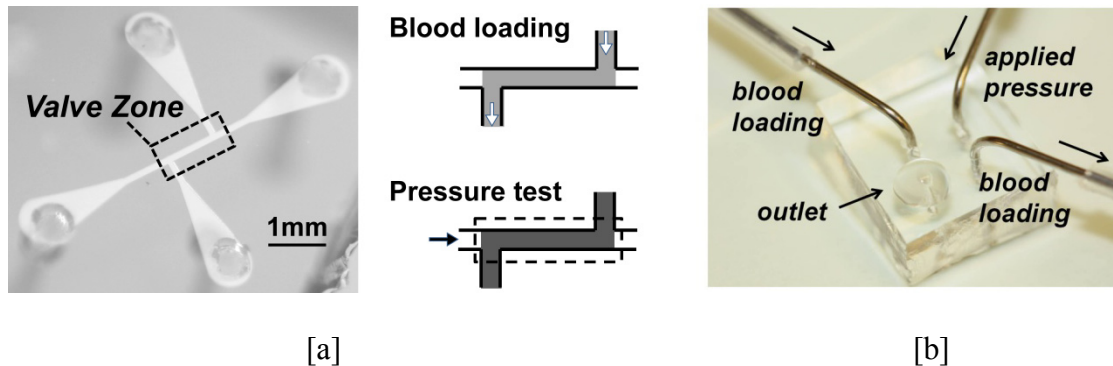
Figure 4.6. (a) Design and test principle of the microfluidic device for introducing thermal coagulum. (b) The port connection used for blood loading and pressure testing.

Finally, the maximum back pressure the coagulum could withstand was measured under the same setting of Fig. 4.5. Two valve zone designs were compared here (Design

100 µm in width, 50 µm in height, 800 µm in length; Design II: 100 µm in width, 50 µm in height, 1600 µm in length).

### 4.2.2.4 Laser induced thermal clogging

To investigate the feasibility of using focused laser beam to locally introduce thermal blood clogging, a test platform was setup as shown in Fig. 4.7 (a). The test platform was based on an optical microscope (Axioskop 50, Zeiss) with two major modifications. Firstly, a solid-state blue laser (488nm, maximum 20mW, JDSU) was used to replace the mounted camera, and the laser beam was introduced by the original camera optical pathway for sample illumination. Secondly, an eye-piece USB camera was used to replace one of the two eyepiece lens, enabling the real-time observation.

Fig. 4.7 (b) illustrates the optical pathways of the test platform. The laser beam (1 mm diameter) was passed through a beam splitter (70% transmission) and focused by a 20× objective lens on the sample stage (light spot approximately 50 µm in diameter). The beam splitter controlled two operation modes of the test platform. When the splitter pushed in, the laser was shielded and only the bright field image was captured by the eyepiece camera. When the splitter pulled out, the laser was used for illumination, and the bright field image was captured simultaneously by the camera as well. A high-pass filter (stop band 488nm) was used before the camera, reducing the reflected laser entering the camera. The microfluidic device was mounted on the microscope sample stage. The stage provides the z-axis focusing, and the x-axis and y-axis tuning of the device position. The alignment between the device and the laser illumination was monitored through the video camera. The PDMS devices with microfluidic channels of 36 µm in width and 30 µm in height were used for the laser induced blood clogging tests.
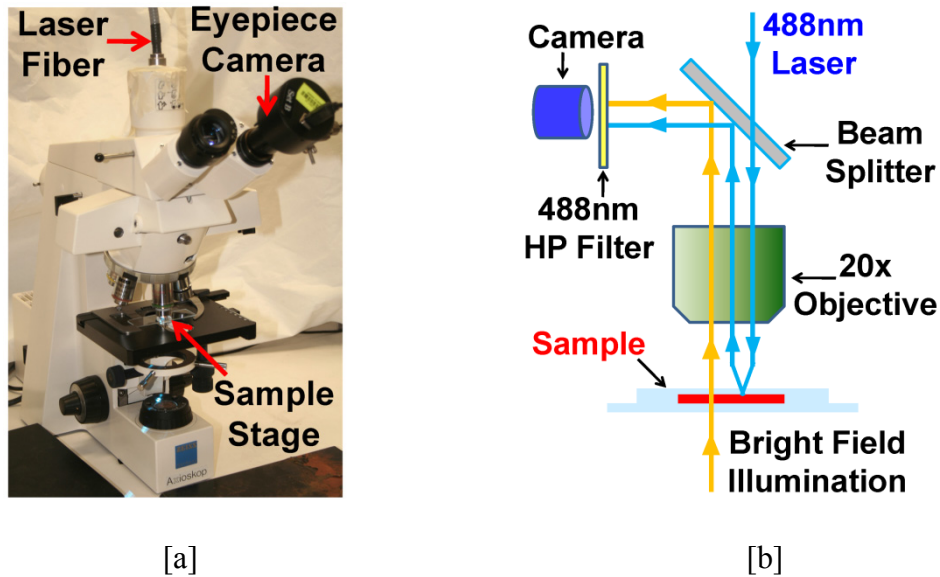
Figure 4.7. (a) The laser test platform modified from a Zeiss Axioskop 50 microscope, and (b) the basic optical configuration.

## 4.2.3 Results and Discussions

### 4.2.3.1 Thermal coagulation of blood

Fig. 4.8 compared the pictures of blood clog formed in the glass capillary tubes, which were heated for 3min under different temperature (fresh blood versus heating at 55°C, 60°C, 65°C, 70°C, 75°C, 80°C, 85°C, 90°C). As seen from the pictures, the blood samples heated at temperatures higher than 70°C were totally solidified (also a darker color from visual observation), the sample heated at temperature 65°C was partially solidified, and the samples heated at temperature lower than 60°C remained liquid form.
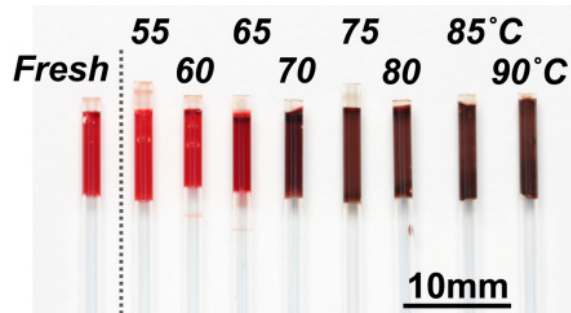
Figure 4.8. Blood coagulum formed at different heating temperatures (heating time 3min) in capillary tubes (1.4mm in diameter). The samples heated at temperatures ≥70˚C were solidified and the ones heated at ≤ 60˚C remained liquid form. The one heated at 65˚C was partially solidified.

Fig. 4.9 summarizes the measurement results of maximum back pressure the blood clog (in capillary tubes) withstanding (pressure versus heating time under different heating temperatures). In general, higher heating temperatures took shorter heating time duration to reach the thermal coagulation. For example, for a heating temperature of 60˚C, the blood remained liquid form after a 5min heating period. On the other hand, for a heating temperature of 80˚C, 30sec heating duration was sufficient to convert the blood into solid coagulum which could withstand a high back pressure (>40 pisg). This tendency was as expected because the thermal coagulation was temperature dependent due to the nature of the protein denaturation process.
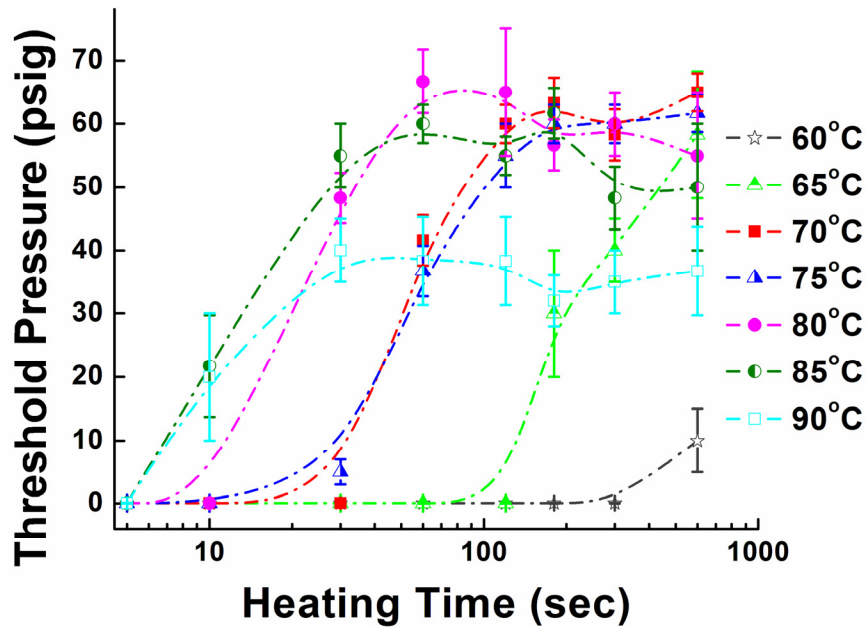
Figure 4.9. Measured maximum back pressure of the blood coagulum formed in capillary tubes vs. heating time with respect to different heating temperatures.

For the same heating temperature, meanwhile, increasing heating time first led to a higher back pressure the clog could withstand, and then reached a relatively stable range (50-70 psig for heating temperature of 65°C to 85°C , 30-40psig for heating temperature of 90°C), after which longer heating time could only lead to a similar back pressure. The blood was considered fully coagulated after reaching these stable ranges. For 90°C, the stable range (30-40psig) is lower than the ones of lower temperatures (50-70psig for 65°C-85°C). This difference was contributed to the excessive dehydration of the sample due to heating at a temperature as high as 90°C.

To investigate the minimal amount of heating needed to initiate the coagulation, the heating time needed for the sample to be partially solidified (defined here as being able to withstand a back pressure of 10psig) was recorded and plotted against the heating

temperature, as shown in Fig. 4.10. It was straightforward to conclude from the results that higher heating temperatures needed shorter heating duration. A heating time longer than 10min was considered here as too slow for valve operation, and hence any heating temperature lower than 60˚C was not suitable for this application.
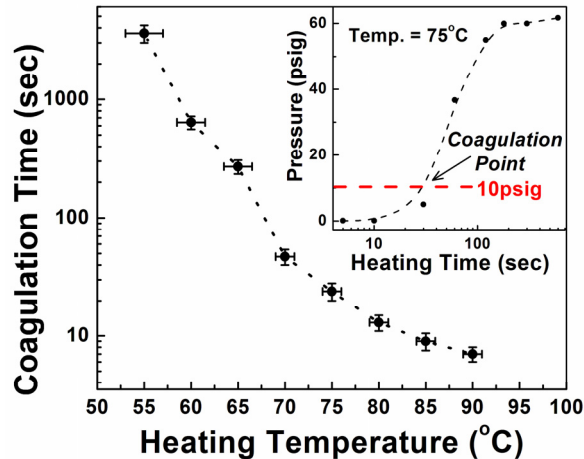


Figure 4.10. The measured minimal heating time needed to initiate the coagulation versus heating temperatures. The threshold coagulation point was defined as the coagulum could withstand a back pressure of 30psig.

In addition, the measured maximum back pressures were compared against the heating temperature (60˚C to 90˚C) under given heating times, as shown in Fig. 4.11. Three heating time length were compared including 2, 5 and 10min. For these three given heating time duration, as shown in Fig. 4.11, the maximum pressure the clog withstood first increased with the increase of heating temperature (from 60˚C to 70˚C). At the temperature range of 70˚C to 80˚C, the maximum back pressure was relatively constant. For temperatures of even higher, such as 85˚C and 90˚C, the maximum back pressure decreased with the further increase of the heating temperature. In addition, as the heating

temperature reached or became higher than 95˚C, the samples were vulnerable to bubbles formed inside the clog and thus not used in this study. Therefore, it was not helpful to use a temperature higher than 85˚C to operate the valve, considering the heating duration used in this study (2, 5 and 10min).
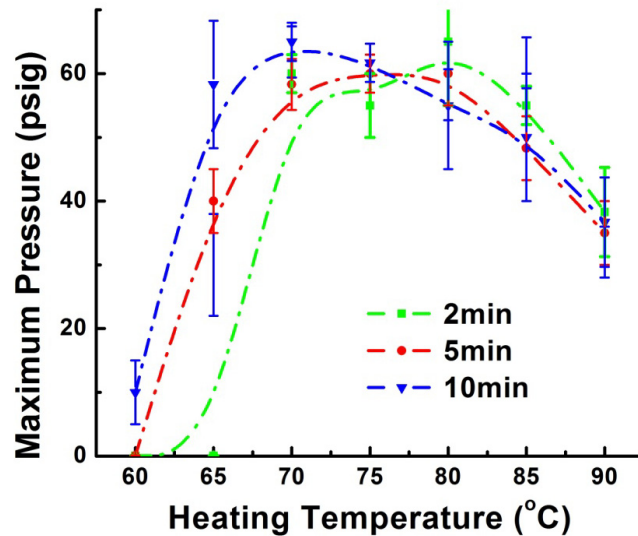


Figure 4.11. Measured maximum back pressure of the blood coagulum formed in capillary tubes vs. heating temperature. Different heating duration (2min, 5min and 10min) were compared.

Above all, a 70˚C-90˚C, 1-3 min heating was able to introduce a blog coagulum that could withstand a back pressure of 30 psig or higher, and considered sufficient for the valve actuation.

Furthermore, experiments were carried out to investigate the difference between fresh blood and stored blood. In practical use, blood sample might need storage for transportation or other reasons before being analyzed, and it is important the stored blood

can still be used to operate the valve. For comparison, one tube of fresh blood was first tested, and then stored in 4°C refrigerator for 48 hours before being tested again. Same heating parameters were used (heating temperature 78°C, heating duration 30, 120, 180, 300sec). The measured back pressures were compared in Fig. 4.12. After the storage, the blood sample could still form the clog that withstands a maximum back pressure close to 40psig. The pressure range (40 psig) was slightly lower comparing to the range of the freshly drawn blood (60psig), but still more than sufficient for valve operation.
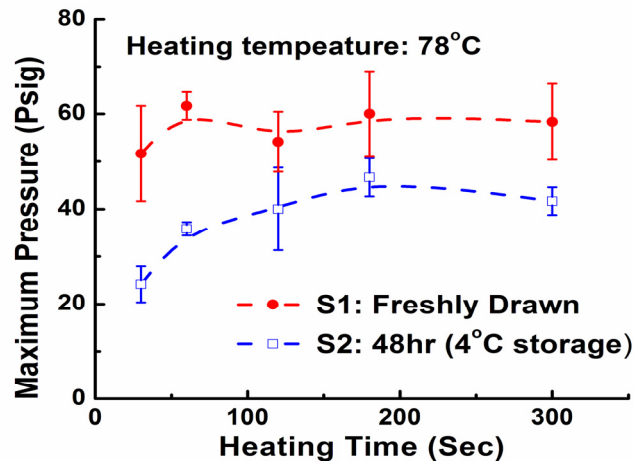


Figure 4.12. Comparison of coagulum formed with fresh blood (S1) versus stored blood (S2).

## 4.2.3.2 Thermal coagulation of blood in microfluidic channel

Fig. 4.13 compares the microscope pictures of the microfluidic channel before and after blood coagulation was introduced. The fresh blood in the channel, as shown in Fig. 4.13(a), was still in liquid form, and the individual RBCs were still distinct from the surrounding plasma. After heating at 80°C for 3 min, as shown in Fig. 4.13(b), a solid coagulum was formed, which showed a uniform color. The coagulum blocked the whole cross section of the fluidic channel.

[a]                                    [b]
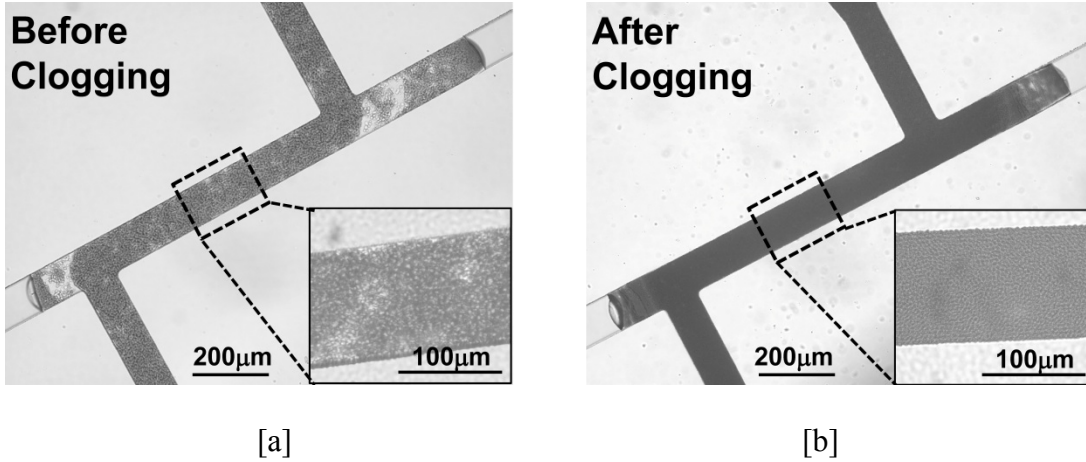
Figure 4.13.  Microscope pictures of the blood in a PDMS channel (100μm channel height) (a) before and (b) after thermal coagulation. The inset shows the zoom-in picture of the outlined area.

Table 4.1. Measured maximum back pressure of the blood clogs. Two geometry designs (W: width, H: height, L: length) are compared, and the results show the average valve from three tests.

| Design | Dimension (μm)<br><br>W × H × L | Pressure (psig) |
|--------|----------------------------------|-----------------|
| *A* | 100 x 50 x 800 | 35 ± 8 |
| *B* | 100 x 50 x 1600 | >50, PDMS delaminated |

The maximum back pressure this clog could withstand was then measured, and the results were summarized in Table 4.1. Two valve designs were tested. The results showed that the clog indeed sealed the channel, and could withstand a high back pressure. The

design A withstood a pressure as high as 35 psig, and the design B held a pressure up to 50 psig until the point that the PDMS channel delaminated from the glass substrate and the experiment was disrupted.

### 4.2.3.3 Laser induced thermal clogging

For the experiments to investigate laser induced thermal clogging, fresh blood sample was loaded into a microfluidic channel (PDMS/glass bond devices, cross section 36 μm in width and 30 μm in height). The device was then fixed on the sample stage of the microscope platform test (Fig. 4.7). The laser spot, with a 50μm diameter, was aligned with the center of the microfluidic channel, and the blood sample was illuminated for 1min before the laser beam was shuttered off by the beam splitter. The measured optical intensity of the laser spot was approximately 7mW.

Fig. 4.14 compares the blood samples in the microfluidic before and after the laser illumination (7mW, 1min illumination). Before illumination, the blood sample was in the liquid form. After illumination, the portion of the blood sample that was underneath the laser spot was solidified and turned into a darker color. As the diameter of the laser spot (~50 μm) was slightly larger than the width of the channel (36 μm), the whole cross section of the channel was sealed by the clog. These two samples were then tested and compared for maximum back pressure they could hold by the setting of Fig. 4.5.
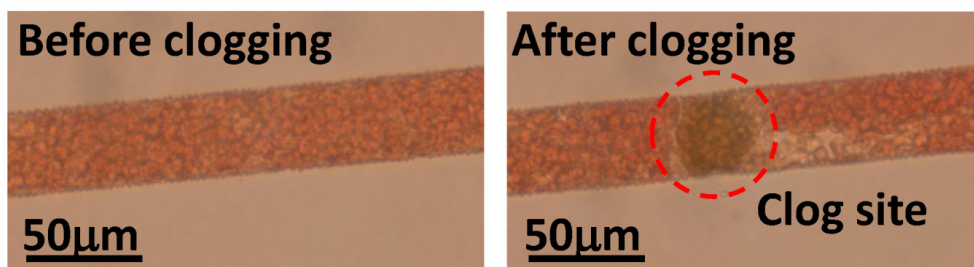
Figure 4.14. Microscope pictures of the blood in a PDMS channel (a) before and (b) after laser-induced clogging. The outline of the clog site is determined by the size of the laser spot (around 50 μm diameter), which is slightly wider than the fluidic channel (36 μm width).

The blood sample without laser illumination was easily pushed out of the channel by an applied back pressure less than 0.1psig. On the other hand, the blood sample after laser illumination withstood a back pressure of 26 psig before the sample was pushed out. These results demonstrated that the laser illumination indeed introduced the thermal clogging of the blood sample, and the clog was sufficient to be used as a closed valve in the microfluidic channel. After the blood sample was pushed out, the microfluidic channels were observed under the optical microscope to be intact, which verified there was no channel melting.

Two different geometry designs of the valve zone (as shown in Fig. 4.15) were tested for the laser induced clogging. Same amount of laser illumination was used (7mW, 1min illumination). The measure results (average of three measurements) showed that Design A could withstand a back pressure of 25 psig and design B could withstand a back pressure of 28 psig.

**Design A:**          **Design B:**
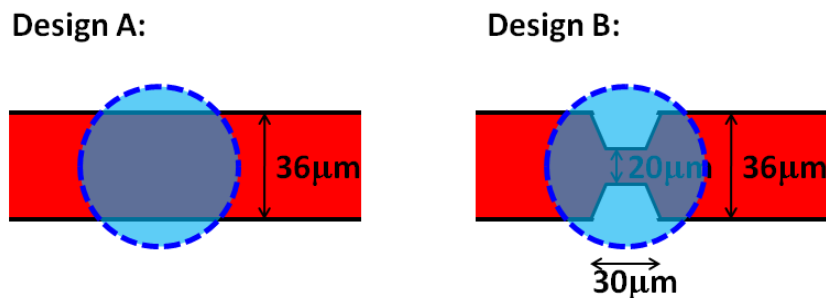


Figure 4.15. Geometry designs of the laser-induced clogging valve. The blood circles
illustrate the illumination from the focused laser beam (diameter approximately 50μm).

Finally, the feasibility of using the laser clogging valve for controlling the delivery of
blood sample in microfluidic was investigated. The design principle of the test PDMS chip
was illustrated in Fig. 4.16. The microfluidic chip consisted of mainly a sample chamber,
the volume of which measured the amount of blood sample for downstream analysis. Four
fluidic ports were connected to the sample chamber. One was connected to an upstream
pump (the top one) for sample delivery and another one (the bottom one) was connected to
a downstream detection channel. The other two ports (the left-hand side and the right-hand
side) were used as loading channels to fill up the sample chamber with blood.

As shown in Fig. 4.16(I), the sample chamber was first fulfilled with blood through
the two loading channels. Afterwards, as shown in Fig. 4.16(II), the loading channels were
closed by the laser-induced clogging valves, isolating the blood chamber from the external
ports. In this way, as shown in Fig. 4.16(III), the upstream pump could start delivering the
blood sample to the downstream cytometer channel, where the fluorescent detection was
carried out. Upon emptying the sample chamber, as shown in Fig. 4.16(IV), a fixed amount
of blood sample was delivered, the volume of which was equal to the volume of the sample
chamber.
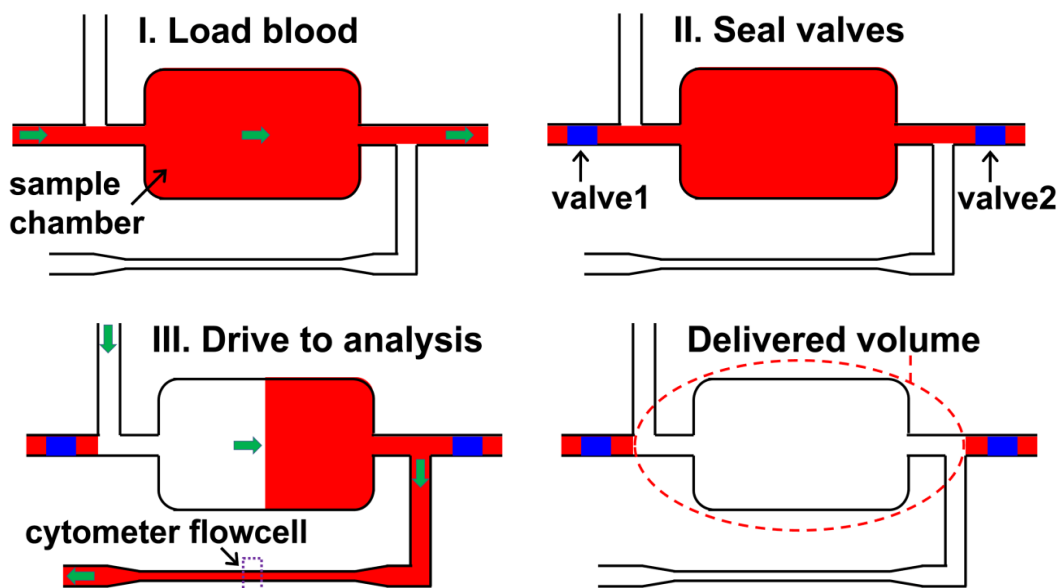
Figure 4.16. Illustration of the design principle of a fixed volume, sample delivery scheme, where the laser-induced clogging valves are used for fluidic control.

A PDMS device was designed and tested to demonstrate this operation, as shown in Fig. 4.17. External pumps (syringes) were used here. One syringe was used to load the sample chamber with blood sample. The loading channels, after the chamber was fulfilled with whole blood sample, were sealed by the laser-induced clogging (7mW, 1min illumination), as shown in Fig. 4.17(a). Then the second syringe (acting as the upstream pump) started to apply pressure. As the clogging valves sealed the loading channels, the sample in the chamber was hence pushed toward the downstream analysis channel. After the chamber was emptied, as shown in Fig. 4.17(b), the clogging valves were still holding in the place, and a fixed volume of blood (0.1 ml designed by the volume of the sample chamber) was successfully delivered for downstream analysis.
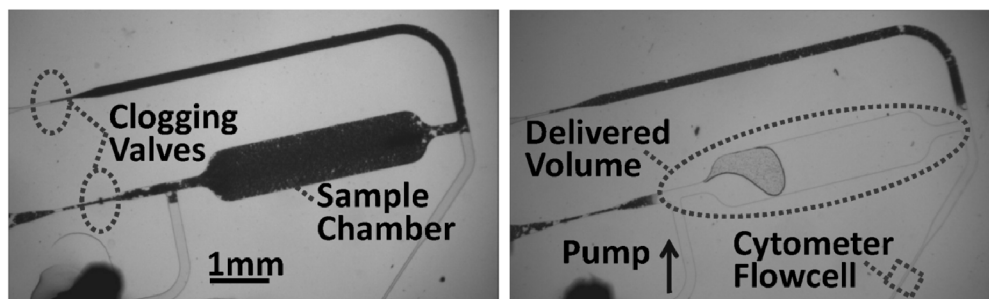
Figure 4.17. Microscope pictures of the PDMS device which uses the laser-induced clogging valve in the delivery of a fixed volume of blood sample. (Left) Blood was loaded into the sample chamber and sealed inside by two clogging valves. (Right) The sample was pushed out by an upstream syringe and directed towards the downstream cytometry channel for measurement.

## 4.2.4 Conclusion

This study demonstrated the feasibility of using blood thermal clogging as a valve mechanism for microfluidics. The thermal coagulation of human whole blood was investigated, and results showed that thermal heating at 70˚C-90˚C for 1-3 min converts liquid blood into solid coagulum, which could sustain a high back pressure in capillary tubes (>40psig).

In addition, it was also demonstrated that focused laser illumination (488nm blue laser) introduced localized blood clogging in microfluidic channel. The laser-induced clogging stemmed the normally open microfluidic channel as a one time, open-to-close valve. The clog formed in microfluidic channels (PDMS/glass bond devices), could withstand a back pressure of 22psig.

# 4.3 On-Chip Blood Staining with Fluorescent Dye Assay

## 4.3.1 Mixing in Microfluidics

At a macro-scale level, mixing is conventionally achieved by a turbulent flow, which makes possible the segregation of the fluid in small domains, thereby leading to an increase in the contact surface and decrease in the mixing path. In the microfluidic systems, the Reynolds number of the flow is usually small, and therefore the flows cannot be turbulent. Owing to this limitation, mixing in the microfluidic is generally achieved by taking advantage of the relevant small length, using fluidic designs that dramatically decrease the mixing path and increase the mixing contact surface area.

Various types of microfluidic mixer have been previously developed including passive mixer and active mixer [102, 105]. Active micro-mixers use external energy inputs to introduce time-dependent perturbation that stirs the fluidic for accelerating the mixing process. Generally, active mixers have higher mixing efficiency, however, the requirement of the external energy input leads to mixer structures that more complicate and more expansive. Meanwhile, passive mixing devices rely entirely on fluidic pumping energy and use special design to restructure the flow in a way that reduces the diffusion length and maximizes the contact surface area. The device structures of the passive mixers are simpler than the structure of the passive mixers and suitable for integrated microfluidic chips.

Therefore, passive mixer was used here to investigate the on-chip staining of the blood sample with the dye assays. The reduction of mixing time in the passive mixers can be achieved by methods such as splitting the fluid stream using serial or parallel lamination, hydrodynamic focusing, enhancing chaotic advection using ribs and grooves designed on the channel wall, etc. [102]. Particularly, a mixing scheme of hydrodynamic

focusing is chosen here because of the merits of simple mixer structure and short diffusion path [106], which is suitable for on-chip integration.

## 4.3.2 Theory of Passive Hydrodynamic Focusing Mixer

Fig. 4.18 shows the basic structure of the hydrodynamic focusing mixer. The mixer has three inlet streams: one sample stream sandwiched between two identical sheath streams. The three inlet streams enter into the mixing channel, where a rectangular shaped channel is considered here. The flow direction of the mixing channel is in x-axis, and the cross section of the channel lies in the y-z plane. The channel width is in y-axis and the channel height is in the z-axis.
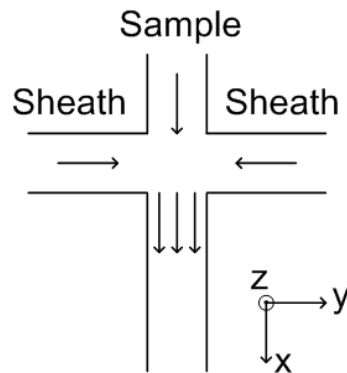


Figure 4.18. The illustration of the hydrodynamic focusing mixer design.

This micro-mixer can be used in the laminar flow regimes, which is characterized by the Reynolds number (*Re*):

$$\text{Re} = \frac{\rho u D_h}{\mu} = \frac{u D_h}{\eta},$$

(1)

where $\rho$ and $\mu$ are the fluidic density and dynamic viscosity, respectively; $\eta$ is the kinematic viscosity; $u$ is the velocity of the fluid and $D_h$ is the hydraulic diameter of the channel. For a rectangular channel, $D_h$ is represented by:

$$D_h = \frac{2 \cdot W \cdot H}{W + H},$$

(2)

where $W$ and $H$ are channel width and height respectively.

## 4.3.2 Velocity Distribution in Hydrodynamic Focusing Mixer

For incompressible, immiscible fluids, a 2D model has been developed by *Wu et al.* to describe the velocity field in the microchannel [106], as shown in Fig. 4.19.
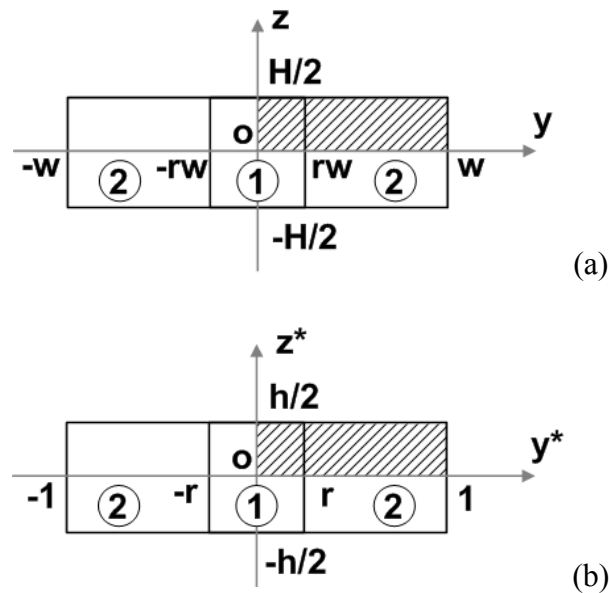


Figure 4.19. Analytical model of the hydrodynamic focusing mixer: (a) actual geometry, and (b) the dimensionless model.

In this model, the velocity distribution $u_1$ and $u_2$ in the channel is described by the Navies-Stokes equations:

$$\frac{\partial^2 u_1}{\partial y^2} + \frac{\partial^2 u_1}{\partial z^2} = \frac{1}{\eta_1} \cdot \frac{\partial p}{\partial x},$$ (3)

$$\frac{\partial^2 u_2}{\partial y^2} + \frac{\partial^2 u_2}{\partial z^2} = \frac{1}{\eta_2} \cdot \frac{\partial p}{\partial x},$$ (4)

where indices 1 and 2 describes the sample flow and the sheath flow, respectively.

Nondimensionalizing the velocity by a reference velocity $u_0$ and the coordinates by $W$ leads to the dimensionless model:

$$\frac{\partial^2 u_1^*}{\partial y^{*2}} + \frac{\partial^2 u_1^*}{\partial z^{*2}} = \frac{W}{\eta_1 u_0} \cdot \frac{\partial p}{\partial x^*},$$ (5)

$$\frac{\partial^2 u_2^*}{\partial y^{*2}} + \frac{\partial^2 u_2^*}{\partial z^{*2}} = \frac{W}{\eta_2 u_0} \cdot \frac{\partial p}{\partial x^*}.$$ (6)

The solutions of the equation (5) and (6) have the form ($0<y^*<1$, $0<z^*<h/2$):

$$u_1^*\left(y^*, z^*\right) = P'\left[\frac{z^{*2} - h^2/4}{2} + \sum_{n=1}^{\infty} \cos \theta z^* \left(A_{n1} \cosh \theta y^* + B_{n1} \sinh \theta y^*\right)\right],$$ (7)

$$u_2^*\left(y^*, z^*\right) = \frac{P'}{\beta}\left[\frac{z^{*2} - h^2/4}{2} + \sum_{n=1}^{\infty} \cos \theta z^* \left(A_{n2} \cosh \theta y^* + B_{n2} \sinh \theta y^*\right)\right],$$ (8)

Where:

$$P' = \frac{W}{n_1 u_0} \cdot \frac{\partial p}{\partial x^*}, \quad \beta = \eta_1/\eta_2, \quad h = H/W \text{ and } \theta = (2n-1)\pi/h.$$

The coefficient of $A_{n1}$, $B_{n1}$, $A_{n2}$, $B_{n2}$, are determined by the following boundary conditions [106]:

$$u_2^*(1, z^*) = 0,$$ (7)

$$\left.\frac{\partial u_1^*}{\partial y^*}\right|_{y^*=0} = 0 \tag{8}$$

$$u_2^*(r, z^*) = u_1^*(r, z^*) \tag{9}$$

$$\left.\frac{\partial u_1^*}{\partial y^*}\right|_{y^*=r} = \beta \cdot \left.\frac{\partial u_2^*}{\partial y^*}\right|_{y^*=r} \tag{10}$$

And the position of the stream interface can be estimated as (h<<1):

$$r = \frac{1}{1+2\beta k} \tag{11}$$

where k is the flow rate ratio between the one sheath stream and the sample stream.

$$k = \frac{Q_2}{Q_1} \tag{12}$$

### 4.3.3 Diffusion Analysis in Hydrodynamic Focusing Channel

The diffusion between the sheath stream and the sample stream in the mixing channel is a convective/diffusive dispersion process, which is characterized by the Peclet number:

$$Pe = \frac{UW}{D} \tag{13}$$

where $U$, $W$ and $D$ are the uniform velocity, the channel width and the diffusion coefficient, respectively.

Following the previous velocity distribution model, a 2D analytical model has also been developed by Wu et al. [106] to describe the diffusion in the hydrodynamic focusing channel (along x-y plane). In this model, the flow velocity across the microchannel is assumed to be uniform, $U$, which is a simplified assumption. Nevertheless, this model can still predict the concentration profile in the sample stream, particularly for the case of

diffusion from the sheath streams to the sample stream, with shows close agreement with the numerical model (which consider the velocity distribution discussed in the previous session) [106]. In addition, the priority of this study is to demonstrate the experimental feasibility of using on-chip staining to introduce fluorescent labels to the blood sample. Therefore, this analytical model is adopted here to guide the design of the mixing channel.



(a)



(b)
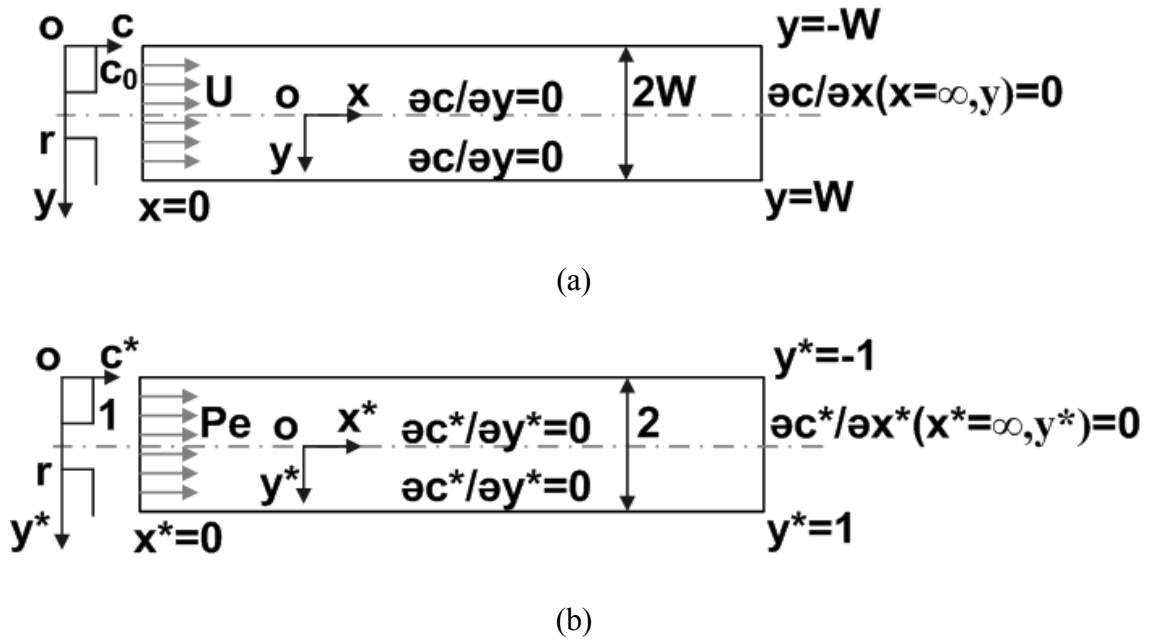
Figure 4.20. Analytical model for convective-diffusive mixing in the mixing channel: (a) the physical geometry, and (b) the dimensionless model.

Fig. 4.20 shows this simplified 2D model (h<<1, and no diffusion along z-axis). Because of the symmetry condition, only half of the channel is considered. The mass conservation including both diffusion and convection can be formulated as:

$$U \frac{\partial c}{\partial x} = D \left( \frac{\partial^2 c}{\partial x^2} + \frac{\partial^2 c}{\partial y^2} \right)$$

$$\qquad (14)$$

By introducing the dimensionless variables for the coordinates system x*=x/W, y*=y/W, the dimensionless concentration c*=c/c₀, the equation (14) can be transformed into:

$$Pe\frac{\partial c^*}{\partial x^*} = \frac{\partial^2 c^*}{\partial x^{*2}} + \frac{\partial^2 c^*}{\partial y^{*2}},$$
(15)

where $c_0$ is the original dye concentration in the sheath stream. Considering the following boundary conditions:

$$c^*\big|_{(x^*=0,0\leq y^*<r)} = 0, \quad c^*\big|_{(x^*=0,y^*=r)} = r \quad \text{and} \quad c^*\big|_{(x^*=0,r<y^*\leq 1)} = 1,$$

$$\frac{\partial c^*}{\partial x^*}\bigg|_{(x^*=\infty,0\leq y^*\leq 1)} = 0 \quad \text{and} \quad \frac{\partial c^*}{\partial y^*}\bigg|_{y^*=0,1)} = 0.$$

The solution of equation (14) is:

$$c^*\left(x^*,y^*\right) = \frac{2}{\pi}\sum_{n=1}^{\infty}\frac{\sin\left[n(1-r)\pi\right]}{n}\cos\left[n\pi(1-y^*)\right]$$
$$\times \exp\left[\left(Pe - \sqrt{Pe^2 + 4n^2\pi^2}\right)x^*\middle/2\right] + 1 - r$$
(16)

## 4.3.4 Design of Hydrodynamic Focusing Channel

Dye Acridine Orange (AO) dye is used here to demonstrate the on-chip staining of the blood sample, because of the merits of quick binding (binding time in ms range) of AO molecule to the DNA contents [107]. The diffusion coefficient of AO in the bulk water is $4.2\times10^{-10}m^2/s$ [108]. Considering the viscosity of blood (3.6mPa•s, hematocrit 45%) [109] is four times higher than the viscosity of water (0.9mPa•s) at room temperature (25°C), the diffusion coefficient of AO in the blood (D) is then approximately $1.05\times10^{-10}m^2/s$, which is close to the observation of Sethu et al. [110].

A design of the mixing channel with 100μm width (2W) and 30μm height (H) is used here. The channel height was chosen to be consistent with the sheathless cytometer channel (30μm height), hence simplifying the fabrication process. The channel width was chosen to be wide enough for the passing of blood cells (maximum 20μm diameter), and meanwhile narrow enough to decrease the diffusion path.

The pumping rate of the streams used here is dye solution : blood : dye solution = 0.2μl/min:0.05μl/min:0.2μl/min. From equation (12), the ratio of the stream flow rate (considering the symmetry):

$$k = Q_2 \Big/ Q_1 = \frac{0.2}{0.05/2} = 8$$

Therefore, the position of the boundary between the blood stream and sheath dye stream can be estimated by equation (11):

$$r = \frac{1}{1+2\beta k} = \frac{1}{1+2\times\left(0.9mPa\cdot s\Big/3.6mPa\cdot s\right)\times 8} = \frac{1}{5}$$

Therefore, the width of the blood stream will be 100μm/5=20μm, and the width of each sheath stream will be (100μm−20μm)/2=40μm.

The uniform velocity $U$ used in the 2D model of equation (14), which describes the diffusion process, is approximated by the total flow rate (blood and dye sheath) divided by the total cross section area of the channel. Therefore,

$$U = \frac{0.2ul/\min + 0.05ul/\min + 0.2ul/\min}{100um \times 30um} = 2500um/s$$

The Peclet number is then given by:

$$Pe = \frac{UW}{D} = \frac{2500um/s \times (100um/2)}{1.05\times 10^{-10} m^2/s} \approx 1190$$

Therefore, according to equation (16), the dye concentration distribution along the flow streams can be calculated, and the results are shown in Fig. 4.21. At the mixing inlet, the dye concentration in the sheath stream (($r<y^*\leq1$) is $c^*=1$, and the concentration in the sample stream ($0\leq y^*<r$) is $c^*=0$. As the streams flow along the mixing channel, the dye molecules start to diffuse into the sample stream, leading to an increasing concentration in the sample stream and a decreasing concentration in the sheath streams along the channel length. At the point $x_1^*=600$, which corresponds to a channel length $x=30mm$, the dye concentrations along the channel width has become nearly uniform ($c^*=0.82$).
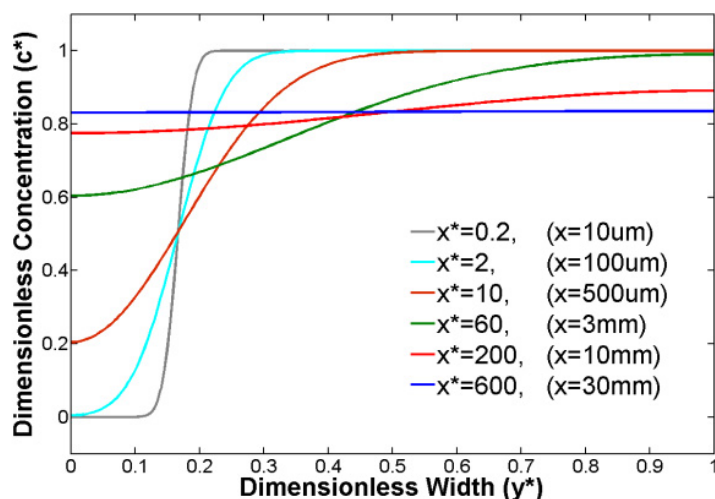


Figure 4.21. The simulation result of the dye concentration profile in the mixing channel.

## 4.3.5 Material and Experiment

The micro-mixer chip was made by the standard PDMS/glass bonding process as described in Chapter 2. Fig. 4.22 shows the fabricated device of the hydrodynamic focusing mixer. The width of the three inlet channels and the mixing channel are all 100μm. The mixing channel following the mixing joint had a meander shape, and a total length of

60mm. At the end of the mixing channel, a sheathless cytometer channel (30μm width) was used for the fluorescent measurement of the sample. The heights of the channels were all 30μm.

For all experiments, the blood sample was pumped into the inlet channel in the middle, and the dye solutions were pumped into the other two inlet channels to form the sandwiched flow pattern. External syringe pumps (PicoPlus, Harvard Apparatus) were used for the sample delivery, and the syringes used are 50μl glass syringe (Gas Tight, Hamilton). The two sheath streams were delivered by the same syringe pump with two separate syringes, assuring the consistent flow rates between the two sheath streams. The sample stream was delivered by a second syringe pump, enabling the independent adjustment of the flow rate.
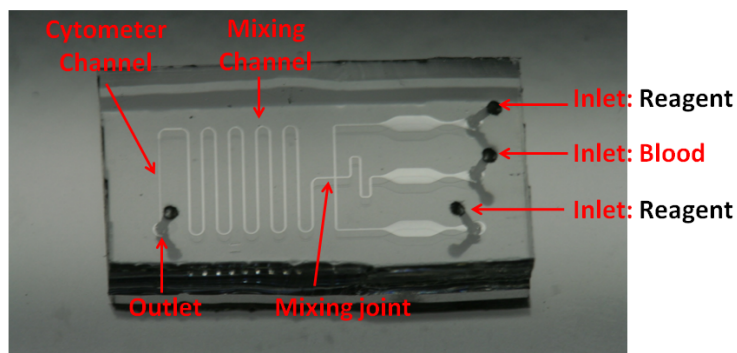


Figure 4.22. The fabricated PDMS device of the hydrodynamic focusing mixer.

A pumping rate of sheath stream: sample stream: sheath stream = 0.2μl/min: 0.05μl/min: 0.2μl/min was used for the experiment. According to the analytical model discussed above, as shown in Fig. 4.21, the dye concentration across the mixing channel

width could reach a uniform profile after a mixing channel length of 30mm. A total 60mm length of mixing channel was used in this device to ensure the proper staining of the blood samples. Considering the average flow velocity of 2500μl/s, the samples had a total incubation time approximately 24sec in the 60mm length mixing channel.

Blood samples (fresh human venous blood with EDTA as anticoagulant) were purchased from HemaCare (USA), and tested within 48 hours after blood drawing. The samples were kept in 4°C refrigerator before experiment. The AO dye stock used here had a concentration of 20μg/ml in PBS solution. The mixing process was first observed under a fluorescent microscope, to measure the sample stream width in the mixing channel, and the change of fluorescent intensities of the streams along the channel length. The fluorescent intensities measured was used to demonstrate the dye concentration profile in the streams across the channel width. Afterwards, the devices were loaded to the optical system shown in Fig. 3.2 to carry out the cytometer detection of the WBCs.

## 4.3.6 Result and Discussion

### 4.3.6.1 Stream ratio in mixer channel

First, the micro-mixer device was observed under a optical microscope (Nikon Eclipse E800 microscope) with a 20x objective lens to study the mixing boundary between the sheath streams and the blood sample stream. Bright field, white-light images were taken at the mixer inlet. Three different combinations of the pumping rates were compared, including combination I= sheath : blood sample : sheath = 0.2μl/min: 0.4μl/min: 0.2μl/min, combination II= sheath : blood sample : sheath = 0.2μl/min: 0.1μl/min: 0.2μl/min, and

combination III= sheath : blood sample : sheath = 0.2μl/min: 0.05μl/min: 0.2μl/min. The

images of the streams were compared in Fig. 4.23.
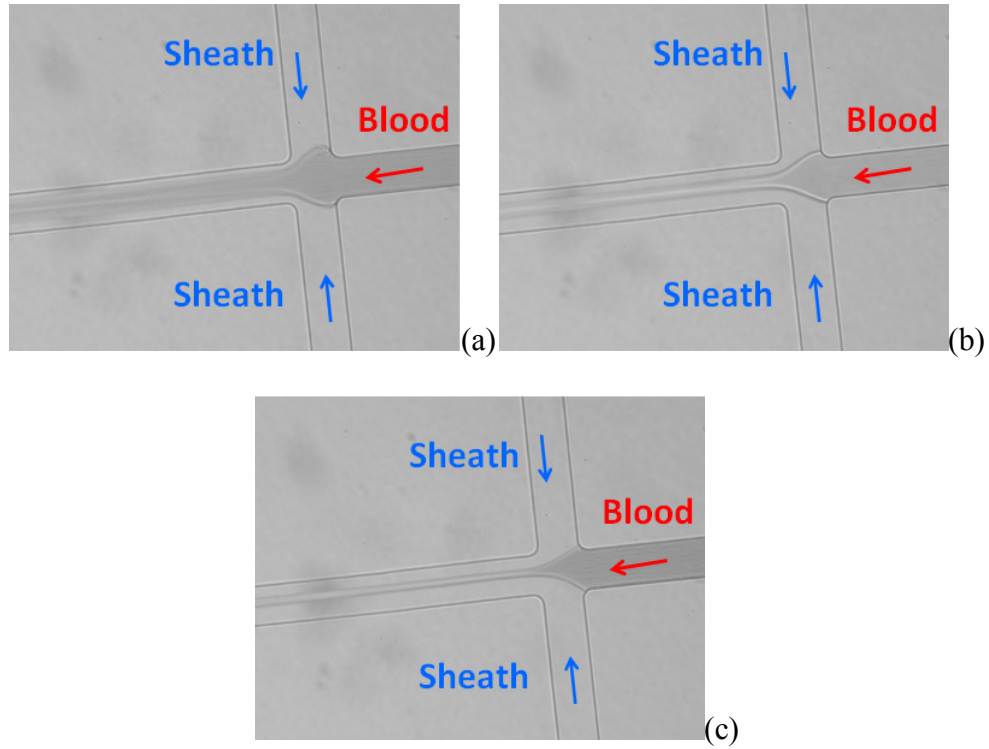


Figure 4.23. Microscope images of the flow streams at the mixer inlet. (a) Flow rate

sheath : blood sample : sheath = 0.2μl/min: 0.4μl/min: 0.2μl/min, (b) sheath : blood

sample : sheath = 0.2μl/min: 0.1μl/min: 0.2μl/min, and (c) sheath : blood sample : sheath

= 0.2μl/min: 0.05μl/min: 0.2μl/min. The mixer channels were 100μm in width.

As seen from Fig. 4.23(a) of the combination I (sheath : blood sample : sheath =

0.2μl/min:0.4μl/min:0.2μl/min, $k$=1), the blood sample stream covered more than half of

the channel width (boundary position r≈0.65). This was due to the higher viscosity of the

blood (3.6mPa•s) than the dye solution (0.9mPa•s). By reducing the flow rate of the blood

sample (combination II sheath : blood sample : sheath = 0.2μl/min: 0.1μl/min: 0.2μl/min, $k$=4), the width of the blood sample stream was reduced correspondingly (boundary position r≈0.34), as shown in Fig. 4.23(b). For the designed flow rate combination (Combination III sheath : blood sample : sheath = 0.2μl/min: 0.05μl/min: 0.2μl/min, $k$=8), as shown in Fig. 4.23(c), the width of the blood sample stream was approximately 20μm at the mixing channel inlet (boundary position r≈0.2). A narrower width of the blood sample stream reduces the diffusion path, hence increasing the mixing efficiency. Therefore, the combination III was used in the following experiments.

### 4.3.6.2 Fluorescence intensity measurement of mixing streams

Second, the fluorescence intensity along the mixing channel was observed under the fluorescent microscope (Nikon Eclipse E800 microscope) with a 10x objective lens, and the filter block used was to measure green fluorescence (EM 510-550nm/EX 460-490nm) from the dye Acridine Orange (AO). The pumping rates used were sheath : blood sample : sheath = 0.2μl/min: 0.05μl/min: 0.2μl/min, where the sheath stream was the AO dye solution (20μg/ml). Fluorescence images of the mixing streams were taken at different positions along the channel length (e.g., x=100μm, 500μm, 3mm, 30mm, etc.). Afterwards, the intensity profiles of the green fluorescence across the stream width were calculated from the images by using the software tool ImageJ.

Fig. 4.24 compares the fluorescence images and the fluorescence intensity profiles of the streams at different position along channel length (x=100μm, 500μm, 3mm, 30mm). Then the intensity profiles across the streams were quantitatively compared by calculating the green intensities from the images. The intensity profiles were calculated by the RGB Profile Plot function of ImageJ.
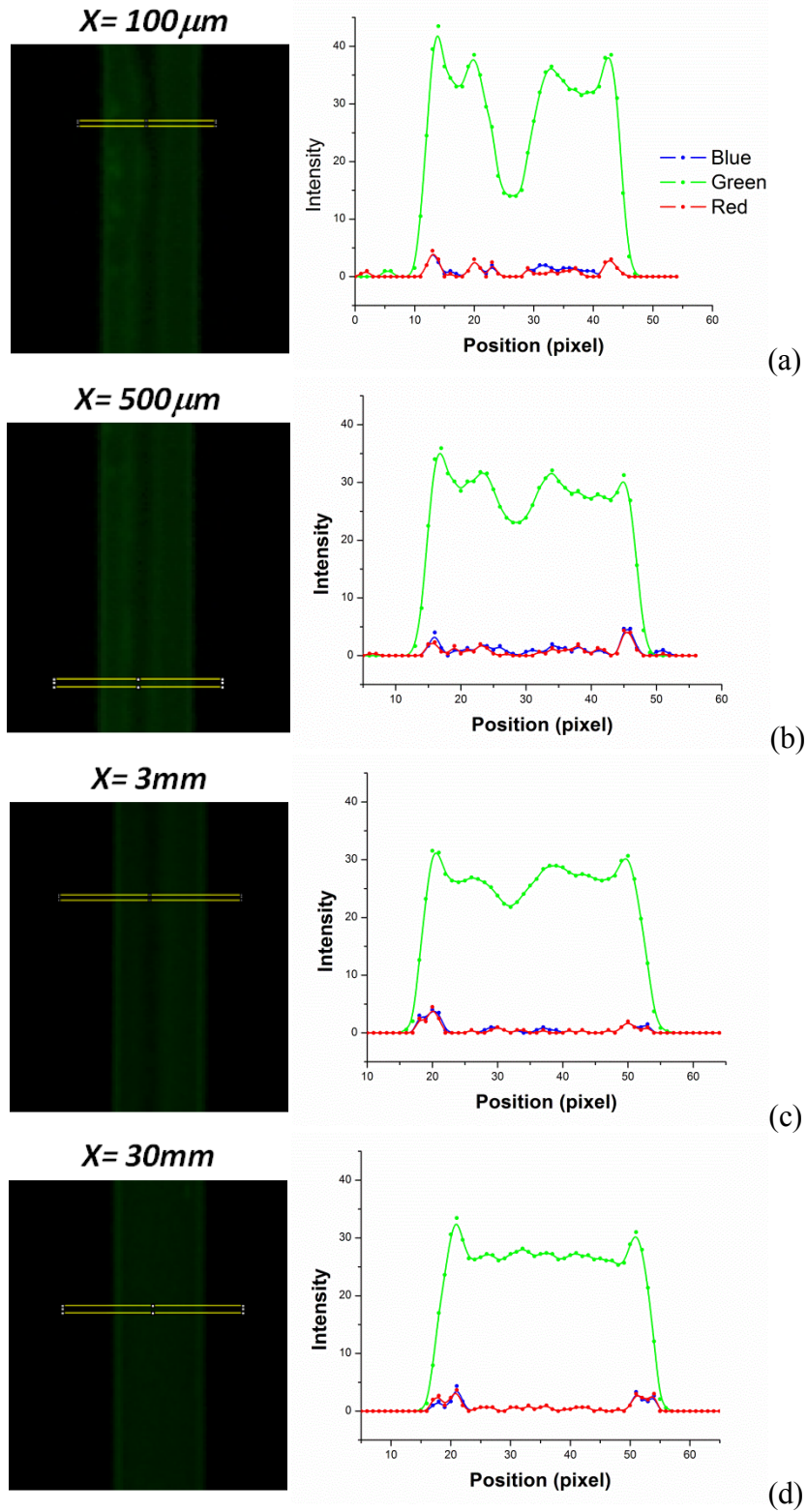
Figure 4.24. Fluorescence images and the quantitative readings of the green intensity across the mixing channel, at (a) length x=100μm, (b) x=500μm, (c) x=5m, (b) x=5mm.

At the first three locations ($x=100\mu m$, $500\mu m$, 3mm), Fig. 23 (a-c), the blood sample stream was still distinguishable from the sheath streams by the lower fluorescence intensity. At the location of $x=30mm$, the three streams showed uniform fluorescence intensities and not visibly distinct anymore. The yellow rectangular boarders shown in the fluorescence images indicated the areas where the RGB intensity profiles were measured. From the quantitative profiles measured at the first three locations ($x=100\mu m$, $500\mu m$, 3mm), Fig. 23 (a-c), it seemed the fluorescence intensities of the sample stream were indeed lower than the intensities of the sheath streams. In addition, the intensity of the sample stream increased along the channel length, which was contributed to the continuous diffusion of dye molecules from the sheath streams.

The mixing efficiency from the experiment results, as shown in Fig. 4.23, however, seemed to be higher than the results predicted by the 2D analytical model, as shown in Fig. 4.21. For example, at the channel length $x=3mm$, the intensity the sample stream (in the middle) had already been close to the intensity of the sheath streams (at both sides). But from the analytical model, at $x=3mm$, the concentration of the dye in the sheath streams should still be 1.6 times higher than the concentration in the sample stream.

This increased mixing efficiency was contributed to the lateral diffusion of the blood cells. In the analytical model, the flow streams were assumed to have a uniform viscosity along the channel length. However, as the streams moved along the mixing channel, not only dye molecules diffused from the sheath streams into the sample stream, but also the blood cells diffused from the sample stream into the sheath streams. This lateral diffusion caused a continuously decreasing of the cell concentration in the sample stream, hence a decreasing viscosity [109]. The diffusion coefficient of the dye molecule increased with the

decreased viscosity, and hence the mixing efficiency of the dye molecule from the sheath stream to the sample stream was improved.

Above all, it was demonstrated that the dye concentration in the sample stream could reach as high as in the sheath streams at the 30mm channel length.

### 4.3.6.3 Fluorescent detection of WBCs

The fluorescent detection of WBCs from the sample was then carried out using the optical system of the microfluidic cytometer. The previous measurement had showed that a nearly uniform dye concentration across the streams could be reached at the mixing channel length of 30mm. This dye concentration was estimated to be 18μg/ml assuming a fully mixed sample, based on the flow rate of the streams. In addition, the total length of the mixing channel of the micro-mixer was 60mm. The blood sample would be continuously exposed to this dye concentration in the following 30mm length mixing channel. As calculated above, the average velocity of the sample was 2500μm/sec. Therefore, the ample would be further incubated with the dye solution for another 12sec before reaching the cytometer channel, where the fluorescent detection of the sample was carried out using the optical system shown in Fig. 3.2.

Fig. 4.24 showed the fluorescent intensities (green 520-550nm and red >600nm) measured from the cytometer system. The measured signals show clear fluorescent peaks measured as the WBCs flowing through the detection channel. The measured high green peaks had an average SNR≈17dB, and the measured red peaks had an average SNR≈15dB. Each high peak of the green fluorescence intensity, introduced by the WBC nucleus stained by the dye AO, was recorded as one WBC event being detected. The total number of the

WBC events was recorded, as well as the corresponding fluorescence intensities of each WBC event, for further analysis.
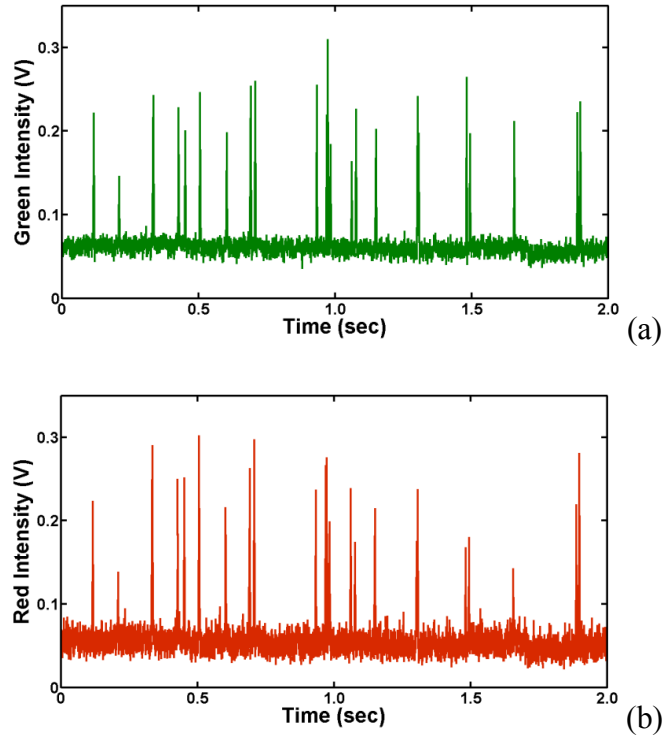


Figure 4.25. Measured fluorescence intensities from the cytometer channel at the downstream of the mixer channel: (a) green fluorescence, and (b) red fluorescence.

The rate of cell recovery from the WBC detections was then calculated from the measured number of WBC events. The total detected WBC events from a continuous 5 minutes measurement was recorded. Given the fixed flow rate of blood sample stream (0.05μl/min), and the known WBC concentration in per volume blood (7,500WBCs/μl), the average number of WBC flowing through the channel in the 5 minute time could be estimated (1,875 WBCs). The WBC concentration was measured form the same batch of blood sample using a commercial blood counter Coulter LH 750 (Beckman Coulter, USA)

before the experiments. Then the recovery rate of the detection could be calculated by dividing the measured amount of WBCs with the expected average amount. Table 4.2 shows the recovery rates measured from five tests. An average recovery rate of 90.1% was obtained from the tests. The results showed that mostly of the WBCs in the blood sample were stained by the dye assay and detected by the cytometer. The cell loss rate (9,9%) was tolerable for clinical significance (tolerance range 10%).

Table 4.2. The recovery rate of WBCs detection measured from five tests.

|  | Test1 | Test2 | Test3 | Test4 | Test5 | Average |
|---|---|---|---|---|---|---|
| **Expected (cells)** | 1,875 | 1,875 | 1,875 | 1,875 | 1,875 | 1,875 |
| **Detected (cells)** | 1,690 | 1,610 | 1,840 | 1,750 | 1,630 | 1,704 |
| **Recover Rate (%)** | 90.1 | 85.9 | 98.1 | 93.3 | 86.9 | 90.1 |

Furthermore, the recorded fluorescent intensities (green versus red) were display in a scatter plot, as shown in Fig. 4.26. In the scatter plot, each point represented one WBC event being measured. The scatter plot showed a WBC differential pattern similar to the one obtained with the manual sample preparation, as shown in Fig. 2.17, where two clusters were formed each relating to the lymphocyte and the non-lymphocyte, respectively. However, the separation of the two clusters was not as clear as the separation

obtained in the manual sample preparation. This was mainly contributed to the shorter incubation time used in this mixer design (24sec in total). In the manual preparation experiment, the total incubation time was 2 minutes. The separation of the nonlymphocyte from the lymphocyte depended on the red fluorescence intensity (AO binding to RNA), which shifted and improved separation with increased incubation time [30]. An extra incubation channel can be used following the mixing channel to provide longer incubation time, and hence better separation between the two clusters if needed in the future.
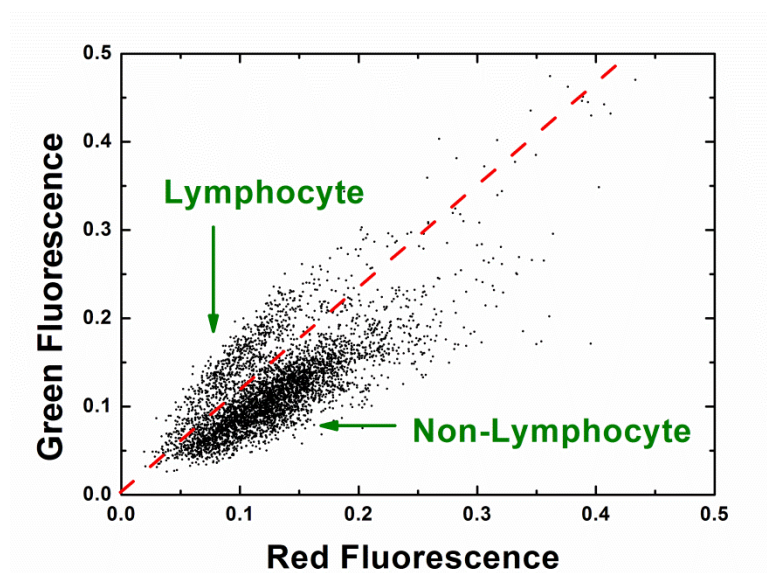


Figure 4.26. Scatter plot of the WBC detection results measured from the cytometer channel with the on-chip mixer.

### 4.3.4 Conclusion

On-chip staining of the blood sample with the dye assay (Acridine Orange) was demonstrated here using a hydrodynamic focusing mixer. The mixer channel had a dimension of 100μm in width, 30μm in height and 60mm in length. The pumping rates of

the fluid streams were sheath: blood sample : sheath = 0.2μl/min:0.05μl/min:0.2μl/min. The blood sample stream had a width of approximately 20μm entering the mixing channel, sandwiched between the two sheath streams of dye solutions. At the channel length 30mm, the fluorescence intensity of the sample stream had reached the same intensities of the sheath streams, indicating a relatively uniform dye concentration reached by the mixer.

In addition, the fluorescent detection of the WBCs was carried out in the cytometer channel (30μm in width, 30μm in height) following the mixer, and the two-color fluorescence signals (green 520-550nm and red >600nm) measured from the sample showed high SNR for the WBC detection (SNR of green peaks ~17dB, SNR of red peaks ~15dB). A recovery rate of 90% was achieved from the fluorescent detection, which indicated that most of the WBCs entering the mixer were stained with the assay and detected by the cytometer channel, demonstrating the feasibility using this mixer for on-chip blood staining.

# Chapter 5 : Microfluidic Cytometer for Biosensing of Microalgae

## 5.1 Introduction

The last three chapters investigated the feasibility of using the sheathless microfluidic cytometer and the fluorescent dye assays for the portable blood cell analysis. The study of this chapter, on the other hand, investigated the implementation of the microfluidic cytometer for other biosensing measurement, and one example demonstrated here is the biosensing of microalgae cells in waters.

### 5.1.1 Microalgae and Harmful Algal Bloom

Microalgae, a.k.a. phytoplankton, are unicellular plant species typically found in both freshwater and marine system. The size of the microalgae cells can range from a few micrometers to a few hundreds of micrometers depending on the species. The biodiversity of microalgae is enormous. It has been estimated that about 200,000-800,000 species exist of which about 35,000 species are described. Microalgae are important for sustaining life on earth because of their ability to perform photosynthesis. In total they produce approximately half of the oxygen and consume simultaneously half the carbon dioxide in the earth atmosphere. Meanwhile, the photosynthesis of microalgae also provides approximately 95% of the supply for the food chain of the ocean ecosystem.

Despite their importance, the temporal overgrowth of the microalgae population, which is known as algal bloom, can be very harmful to the aquatic system. An algal bloom is natural phenomena of rapid proliferation of one or just a few species of microalgae, where the concentrations of the microalgae cell can reach as high as millions of cells per

milliliter water volume. Any species of the phytoplankton may cause the algal bloom, but the main species are typically dinoflagellates, raphidophytes, crptophytes, diatoms and cyanobacteria. The algal bloom has a series of negative impacts on the aquatic systems, such as toxin production and mortality of larger aquatic organisms (fish, shellfish, sea-grasses, etc.). In the past decade, the onset of such harmful algal blooms has increased both in frequency and extent, causing significant environmental loss and economical loss worldwide.

However, the factors driving the selective proliferations of microalgae are still poorly understood. Part of the reason for this lack of knowledge is the time- and labor-intensive nature of the analysis for specific bloom-causing organisms in water samples. Flow cytometer is widely used for this analysis in ocean-observing systems nowadays. However, the conventional flow cytometers are limited to use in central laboratories because of their bulky system size, complicated operation procedure, and high cost. In order to better understand the causes and the rapid progress of the algal bloom, higher monitoring frequency for both temporal and spatial distribution of the microalgae populations are important, necessitating the development of portable, low-cost sensors.

Therefore, this chapter explored the feasibility of using the microfluidic cytometer for the monitoring tests of microalgae samples. The portable cytometer system developed in this study is suitable for on-field use of sensing microalgae population in waters, the capability of which is needed in the algal bloom research. In addition, the feasibility of using this cytometer system for other microalgae-based biosensing assays, for example, the algal bioassays for assessing the toxicity of natural waters, was also investigated here.

## 5.1.2 Microalgae Sensing by Microfluidic Cytometer

One important feature that distinguishes microalgae from other nonphotosynthesis particles in waters is their cellular content of chlorophyll pigment. Chlorophyll is a vital element of the photosynthesis process, allowing microalgae to absorb energy from light. The Chlorophyll pigment absorbs most strongly the blue light in the visible light spectrum (e.g., Chlorophyll-α absorbance maximum at 430nm, Chlorophyll-β absorbance maximum at 453nm). Meanwhile, it emits fluorescence at red light spectrum (e.g., Chlorophyll-α, fluorescence maximum at 673nm). The fluorrescent measurement of the Chlorophyll content in microalgae is regulary carried out on conventianl flow cytometers [111, 112], as central laboratory analysis of microalgae concentraion in the colleted water samples [113].

The microfluidic cytometer we developed was considered suitable for the fluorescence measurement of the microalgae, providing a portable alternative of traditional flow cytometer for on-field assessment. To acommodate the measurement of microalgae samples, two sets of optical configuration were investigated here, as shown in the Fig. 5.1.

The first set of the optical configuration investigated here is the same as the laser-induced, two-color fluorescence detection system used in Chapter 3, as reillustrated in Fig. 5.1(a). In this setting, the red fluorescence (wavelength >600nm) channel can be used to measure the Chlorophyll fluorescence from the microalgae cells, and the green fluorescence (wavelength 520-550nm) channel is used for additional fluorescence measurement. This configuration was investigated in the algal bioassay for assessing the toxicity of water samples.
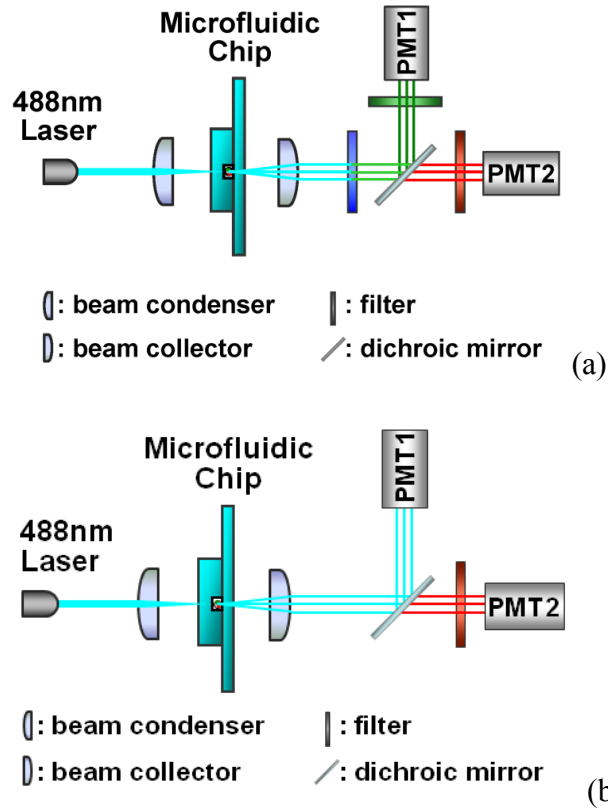
Figure 5.1. Optical configuration of the system for microalgae detection. (a) The system measuring two-color fluorescence (green 520-550nm, red>590nm). (b) The system measuring red fluorescence (>590nm) and light extinction.

The second set of configuration, as shown in Fig. 5.1(b), is a modified version of the first one. In this newly proposed setting, the red fluorescence channel (wavelength >600nm) is still used for the Chlorophyll measurement. But the second detection channel is modified (by taking out the 488nm high-pass filter and the 520-550nm band-pass filter from the first set) to measure the light extinction signal. This channel measures the total light loss (light absorption, scattering, etc.) caused by cells flowing through the sensing area of the cytomter, which is also regarded as a measurment of the cell size [16]. This configurtion was investigated for monitoring microalgae populations in water samples.

The microfluidic device used in this chapter for investigating the microalgae detection had the same design as the one described in Chapter 2 (Fig. 2.9). The sheathless channel had a rectangular cross section measuring 32μm in width and 28μm in height. This dimension allowed the detection of the microalgae species with relatively small size (e.g., diameter 1-20um), which could demonstrate the detection sensitivity. The dimension of the cytometer channel could be further optimized to accommodate microalgae species with larger size in future studies. The size of the whole system, as shown in Fig. 5.2, was suitable for on-field use.



Figure 5.2. The test platform configuration of the microfluidic cytometer. (a) The optical system was used together with a laptop computer, and (b) the system was packaged into a suitcase for being carried around.

## 5.1.3 Microalgae Population Monitoring and Algal Bioassay

For the application of monitoring microalgae population, two important functions need to be verified. First, the microfluidic cytometer was able to provide sufficient signal integrity (e.g., SNR) for the measurement of the Chlorophyll fluorescence from microalgae cells. Second, the Chlorophyll fluorescence measurement and the light extinction

measurement obtained from the microfluidic cytometer were able to discriminate between different types of the microalgae cells. Even on conventional flow cytometers, it is still not feasible to discriminate all types of microalgae cells (considering the over 200,000 microalgae species) by the measurement of Chlorophyll fluorescence and the light extinction signal alone. But it could demonstrate the feasibility of using the microfluidic cytometer for microalgae population monitoring by discriminating certain types of the microalgae cells.

For the application of the algal bioassay, it is important to demonstrate that the microfluidic cytometer was able to measure simultaneously the Chlorophyll fluorescence from the microalgae cells, and additional fluorescence from cells' response to the assay condition.

The algal bioassay for assessing the toxicity of water samples has been previously demonstrated on the conventional flow cytometer [114]. In this bioassay, microalgae cells are first cultured in the water sample. Afterward, the microalgae samples are stained with a fluorescent probe, Fluorescein Diacetate (FDA), and the fluorescence from this staining is measured as a quantitative indicator of the water toxicity level [115]. Fig. 5.3 shows the molecule structure of the fluorescent probe, FDA, and the basic principle of the staining process. FDA molecule is nonfluorescent itself. However, upon entering the microalgae cells, the FDA molecule would be converted into Fluorescein by the nonspecific esterase in the cytoplasm. The fluorescence intensity of the generated Fluorescein is then measured as an indicator of the esterase activity level of the microalgae cells. The fluorescence of the Fluorescein (emission peak 521nm) can be measured in the green channel of the microfluidic cytometer.
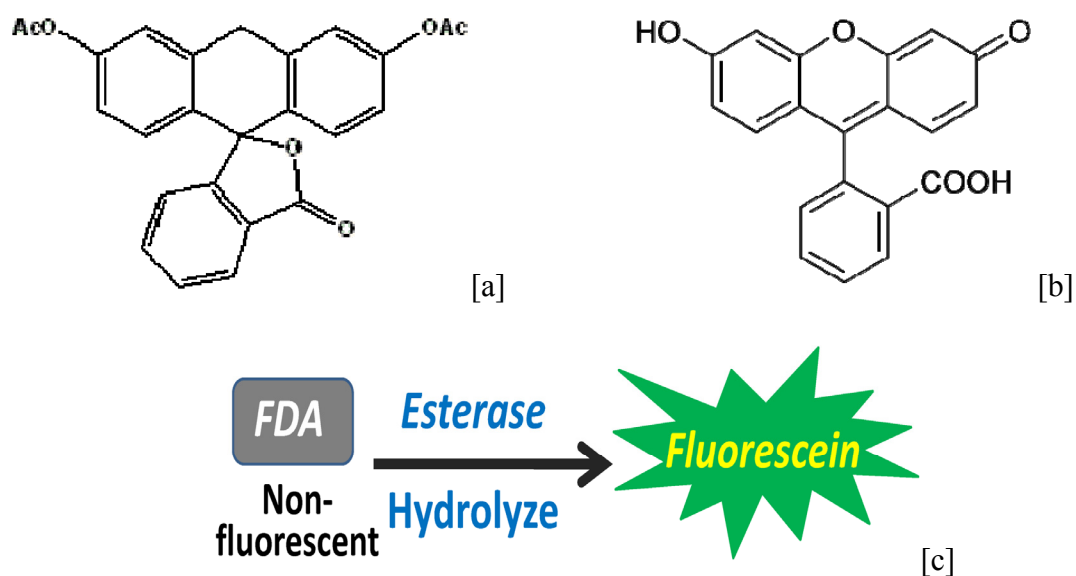
Figure 5.3. The molecule structures of (a) Fluorescein Diacetate (FDA) and (b) Fluorescein, and the basic principle of the hydrolysis process. The non-fluorescent FDA was converted into Fluorescein by the nonspecific esterase inside the microalgae cytoplasm.

## 5.2 Material and Experiment

Microalgae samples, Ostreococcus, Phaeocystis and Dunaliella, were generous gifts from Dr. David Caron of Biology Science Department of University of Southern California. The samples were cultured in the standard f/2-Si medium (UTEX, USA), in a chamber of constant temperature range (15˚C -20˚C), under lighting condition simulating the natural light cycle (dark/light cycle of 12 hour/12 hour, white fluorescent bulb, 580 lumens, 10 watts, 4100K), as shown in Fig. 5.4.

(a)                                                    (b)
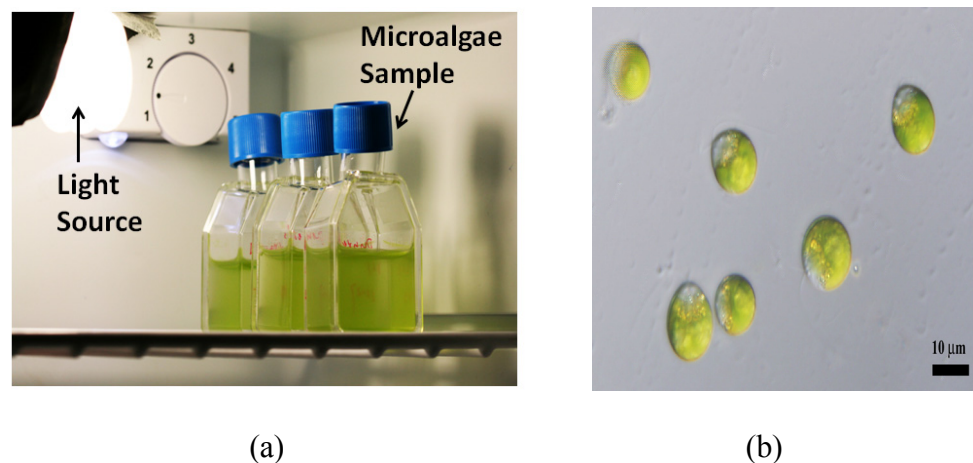
Figure 5.4. (a) The picture of the culture setup for microalgae samples, and (b) the

microscope picture of the microalgae, Dunaliella, cells.

The microalgae samples of Ostreococcus (1-2µm in diameter), Phaeocystis (6-10µm

in diameter) was used for studying the microalgae population monitoring. The

Ostreococcus was one of the smallest types of microalgae, hence suitable to be used to

investigate the measurement sensitivity of the microfluidic cytometer. The Phaeocysis was

used in comparison with the Ostreococcus to investigate the feasibility of species

discrimination by the Chlorophyll fluorescence and the light extinction measurement.

The microalgae Dunaliella (6-10µm) was used in the algal bioassay for assessing the

toxicity of water sample. The heavy metal toxicant $Cu^{2+}$ previously studied in algal

bioassays was used here to introduce toxicity in water samples [115]. To compare the

microalgae's responses to the toxicant, the control sample was cultured in a standard

medium (f/2-Si culture medium, diluted 5× by water), whereas the experimental sample

was cultured in the same standard medium with additional $Cu^{2+}$ spiking. The $Cu^{2+}$ spiking

was introduced by adding copper sulfate solution (4% weight/volume in water) in the

medium, and two final concentrations (low:13ppm, high:32ppm) were investigated. The

microalgae samples were cultured in the same environment as described above (15˚C-20˚C, dark/light cycle of 12 hour/12 hour) before experiments. For measuring the esterase activity of the microalgae cells, the FDA staining of the samples was carried out by the following recipe: 30μl microalgae suspension was incubated with 6μl FDA stock solution (1μg/ml) for 5 minutes (shielded away from environment light). The samples were then loaded onto the microfluidic cytometer for measurement.

## 5.3 Result and Discussion

First, microalgae samples of Phaeocystis and Ostreococcus were loaded to the microfluidic cytometer, using the optical configuration of Fig. 5.1(b) for measuring the Chlorophyll fluorescence and light extinction signal. Fig. 5.5 shows the measured time trace of the signal intensities from the sample of Phaeocystis. Distinct peaks with high intensities were clearly distinguished from the background signal, which was introduced by the microalgae cells flowing through the cytometer channel. The red fluorescence signal, introduced by the Chlorophyll fluorescence, showed high intensity peaks with an average SNR near 40dB. This was due to the factor that Chlorophyll pigment was contained inside the microalgae cells, but rarely in the water sample. The light extinction signal showed the measurement of the light loss due to microalgae cells flowing through the cytometer channel, hence showing negative peaks. The measured signal had an average SNR near 15dB.
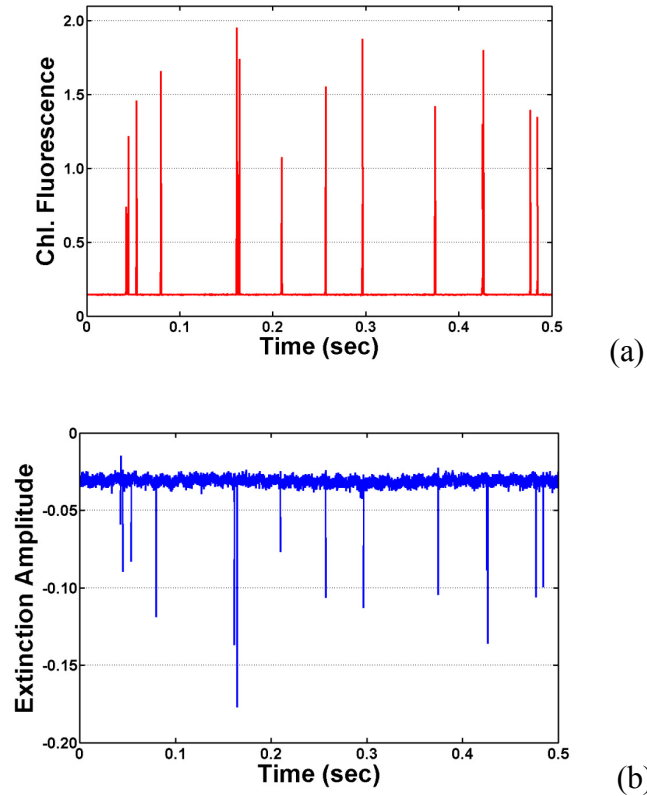
Figure 5.5. The measured time trace of the (a) red fluorescence signal and the (b) light extinction signal (intensity versus time) from the microalgae, Phaeocystis. The light extinction signal measures the light loss due to the cell passing through the detection area (including light absorption, scattering, etc.), hence shows as negative peaks in the time trace.

The recorded peak heights of the measured signals (Chlorophyll fluorescence versus light extinction) were then plotted in the scatter plot, as shown in Fig. 5.6. Each dot represented one microalgae event being detected. Fig. 5.6(a) was the scatter plot from the sample containing only Phaeocystis cell, and Fig. 5.6(b) was the scatter plot from the sample containing both Phaeocystis and Ostreococcus cells. By comparison, it showed clearly that only one cluster was formed in the first sample, and two distinct clusters were

formed in the second sample. The cluster with both higher Chlorophyll fluorescence and higher light extinction signal was associated with the Phaseocystis population, and the other cluster was associated with the Ostreococcus population. The difference was due to the factor that the Phaseocystis cells (6-8μm) had larger cell size and more Chlorophyll pigment than the Ostreococcus cells (1-2 μm).
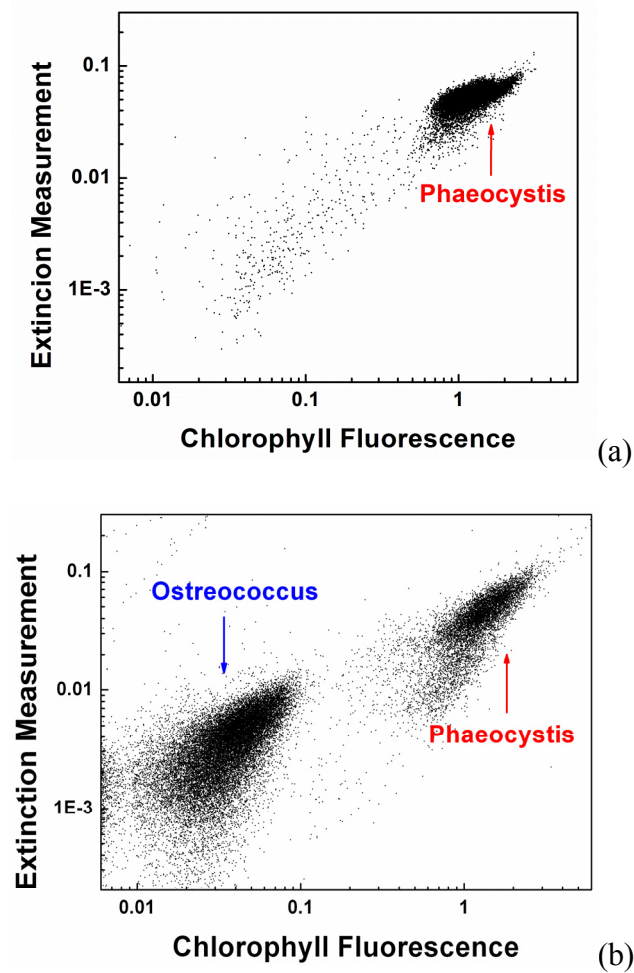


Figure 5.6. The scatter plots of the recorded data from (a) the sample with one type of microalgae, Phaeocystis, (b) the sample with two types of microalgae, Ostreococcus.

These results demonstrated that the microfluidic cytometer was capable of measuring the Chlorophyll fluorescence and light exaction signals from microalgae types as small as the Ostreococcus. In addition, the measured signals showed good SNR, and were able to discriminate the microalgae species, in this case, Phaseocystis and Ostreococcus.

Second, the algal bioassay was evaluated with the optical configuration of Fig5.1(a). Fig. 5.7 showed the measured two-color fluorescence intensities from the microalgae sample, Dunaliella. This sample was cultured as the control sample without exposure to the toxicant, and stained by the FDA fluorescent probes before measurement. The measured Chlorophyll fluorescence showed high SNR (near 40dB) similar to the signal measured in the previous optical configuration. The measured green fluorescence of the FDA staining showed a SNR near 30dB. The FDA fluorescence was due to the esterase activity in the microalgae cells.



(a)          (b)
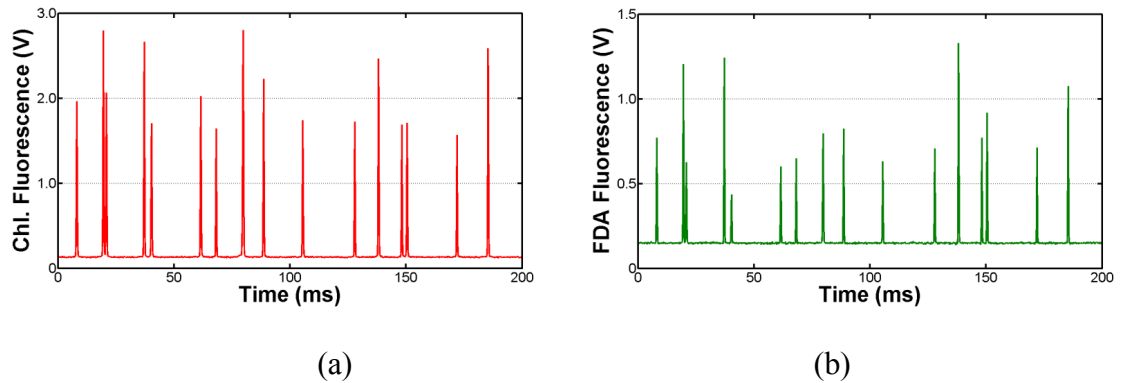
Figure 5.7. The measured time trace of the two-color fluorescence signals from the bioassay experiments. (a) The red fluorescence of the Chlorophyll content, and (b) the green fluorescence from the FDA staining.

In the algal bioassay, the esterase activity level of the microalgae cells (in terms of the FDA fluorescence intensity) was used to evaluate the toxicity of the water sample. The FDA fluorescence intensities of cells from two different samples, the experimental sample with exposure to toxicant (32ppm $Cu^{2+}$, 8 hour exposure) and the control sample (0ppm $Cu^{2+}$, 8 hour exposure), were compared in Fig. 5.8. The cells from the control sample, Fig. 5.8(a), had brighter green fluorescence from the FDA staining, whereas the cells from the experimental sample, Fig. 5.8(b), shower much dimmer green fluorescence. The difference was consistent with the previous observation that the exposure to the toxicant $Cu^{2+}$ led to a lower esterase activity in the microalgae cell, and hence a dimmer FDA fluorescence [115]. This difference was then quantitatively measured on the microfluidic cytometer system.
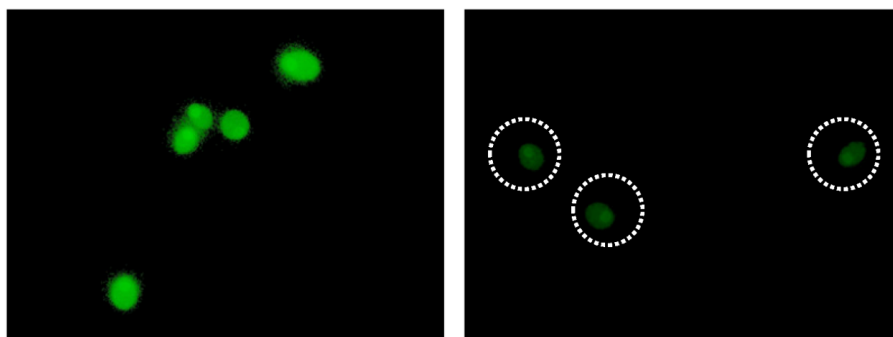


Figure 5.8. The fluorescence microscope pictures of the microalgae sample. Dunaliella, after cultured in the medium (a) containing with 0ppm $Cu^{2+}$ as the control and (b) containing with 32ppm $Cu^{2+}$ as the experimental sample, for 8 hours. The cells with inhibited esterase activity were marked with white circles for visualization.
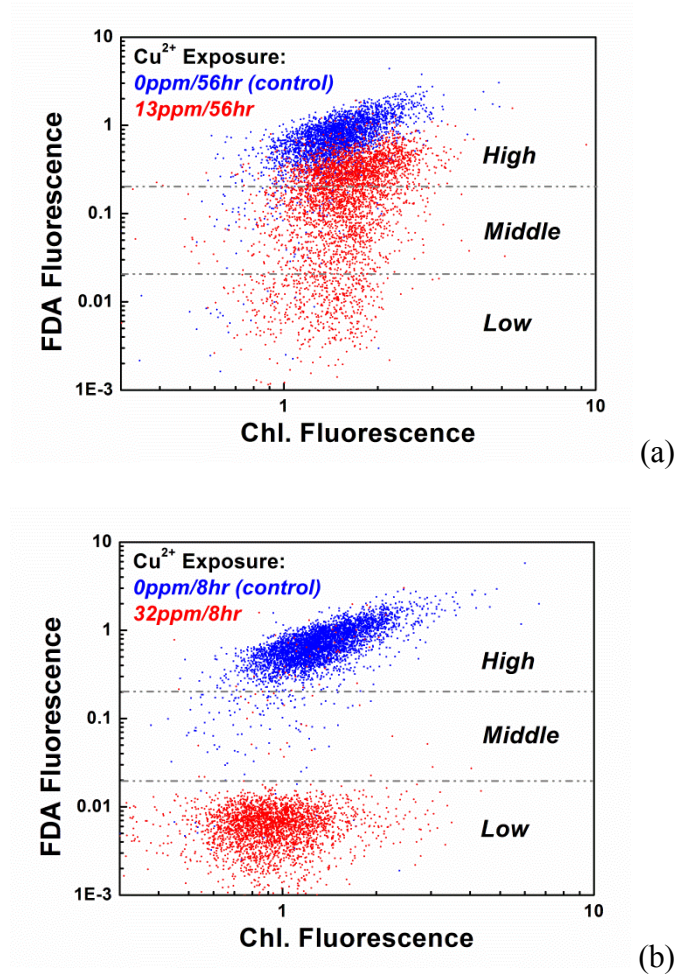
Figure 5.9. Scatter plots of the two-color fluorescence measurement results from the bioassays. (a) The comparison between the control sample (0ppm $Cu^{2+}$) and the experimental sample (13ppm $Cu^{2+}$) after 56 hour toxicant exposure. (b) The comparison between the control sample (0ppm $Cu^{2+}$) and the experimental sample (32ppm $Cu^{2+}$) after 8hour toxicant exposure. The control samples were plotted as blue dots and the experimental samples were plotted as red dots. The level of the esterase activity was defined according to the green fluorescence intensity from the FDA staining.

Fig. 5.9 showed the scatter plots of the measured signals (Chlorophyll red fluorescence vs. FDA green fluorescence) from two different bioassay trials. Fig. 5.9(a)

compared the data from a experimental sample (13ppm $Cu^{2+}$, 56 hour exposure) and a control sample (0ppm $Cu^{2+}$, 56 hour exposure) in the same plot. The microalgae cells showed similar level of Chlorophyll fluorescence with and without the toxicity exposure. However, the difference of the FDA fluorescence was significant. The cells from the control sample mostly had strong FDA fluorescence. On the other hand, the cells from the experimental sample showed wide distribution in terms of the FDA fluorescence, with part of the population showing high FDA fluorescence and the rest part medium even low FDA fluorescence.

On average, it was clear that the experimental sample had lower FDA fluorescence than the control sample. This difference was mainly attributed to the inhibition of the esterase activity by the toxicant exposure. In addition, the cells in the experiment sample showed various level of inhibition, which suggested that it would be more accurate to measure the response from a large population of cells rather than from individual cell.

The microalgae cells' response to the toxicity exposure was even more significant in the example shown in Fig. 5.9(b). Fig. 5.9(b) compared the data from another experimental sample (32ppm $Cu^{2+}$, 8 hour exposure) with the corresponding control sample (0ppm $Cu^{2+}$, 8 hour exposure). The major cell population in the control sample had high FDA fluorescence, whereas the major cell population in the experimental sample showed low FDA fluorescence, forming two distinct clusters. In addition, the average Chlorophyll fluorescence of the experimental sample was also lower than the control sample. Comparing the results from Fig. 5.9(a) and (b), the microalgae bioassay showed distinguishable levels of responses (measured in terms of FDA fluorescence) to the different toxicity level (13ppm $Cu^{2+}$ versus 32ppm $Cu^{2+}$).

Fig. 5.10 showed one example for quantitative evaluation of the toxicity level by measuring the bioassay responses. After the two-color fluorescence signals were measured from the samples, the percentage of microalgae cells with low FDA fluorescence among the total microalgae population was recorded. The threshold of the low FDA fluorescence was defined as 10% of the average valve from the control sample (cell with FDA fluorescence lower than the threshold was considered close to dead). The recorded percentages were then plotted versus the exposure time and results from different toxicant levels were compared, as shown in the example of Fig. 5.10. For the 32ppm $Cu^{2+}$ toxicity level, this percentage reached over 95% after an 8 hour exposure time. On the other hand, for the 13ppm $Cu^{2+}$ toxicity level, this percentage was less than 1% after the same 8 hour exposure time, and remained lower than 20% after 56 hour exposure time. For the control sample (0ppm $Cu^{2+}$), this percentage was lower than 1% after 124 hour exposure time.
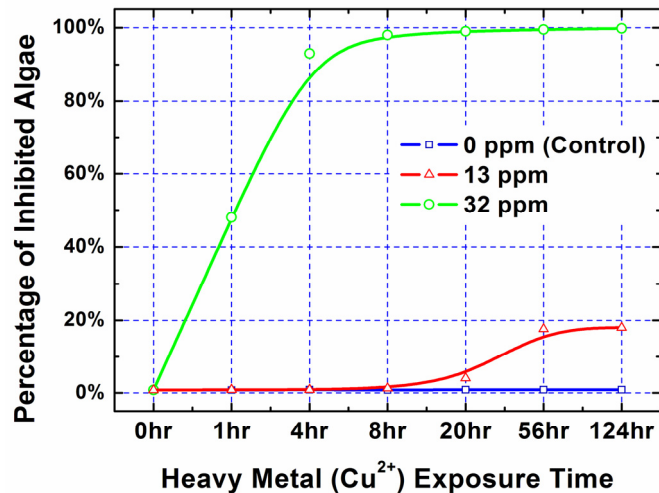


Figure 5.10. Comparison of the measured percentages of the inhibited microalgae cells versus culture time for three culture conditions (toxicant $Cu2^{+}$ concentration of 0, 13 or 32ppm).

These results demonstrated the feasibility of using the microfluidic cytometer for measuring both the Chlorophyll fluorescence and the FDA fluorescence in the algal bioassay. The measured data showed good SNR. In addition, the measured results of the FDA fluorescence could be used to evaluate the microalgae cells' response to different level of toxicities (0, 13 and 32ppm $Cu^{2+}$) in the water sample.

## 5.4 Conclusion

This chapter demonstrated the feasibility of using the microfluidic cytometer for the sensing of the microalgae samples. Two optical configurations were developed, one measuring the two-color fluorescence (red >600nm, green 520-550nm), while the other measuring the fluorescence (red >600nm) and the light extinction signal.

The measurement results confirmed that the microfluidic cytometer was able to detect the Chlorophyll fluorescence and the light extinction signal from the microalgae cells. The data from the microalgae, Phaseocystis, showed good SNR for the measurement (40dB for Chlorophyll fluorescence and 15dB for the light extinction). In addition, the measured data was able to discriminate between the two microalgae species, Phaseocystis and Ostreococcus. The detection of the Ostreococcus (1-2μm diameter) also demonstrated the feasibility of using the microfluidic cytometer for measuring the one of the smallest microalgae cell types.

Besides, the implementation of the microfluidic cytometer in an algal bioassay was also demonstrated. The simultaneous measurement of the Chlorophyll fluorescence and the Fluorescein Diacetate (FDA) fluorescence was used to evaluate the microalgae's (Dunaliella) responses to the level of the toxicant $Cu^{2+}$ in water samples. The measured signal showed good SNR (40dB for Chlorophyll fluorescence and 30dB for the FDA

fluorescence) from the sample stained with the fluorescent probe FDA (1μg/ml). In addition, the measured data was able to discriminate the microalgae's response (in terms of FDA fluorescence) to different levels of the toxicant (0, 13 and 32ppm $Cu^{2+}$) in water samples.

# Chapter 6 : Conclusion

White blood cell (WBC) count remains one of the most frequently used clinical tests in hospitals. In addition, the need for WBC counting has been rapidly growing, from central hospitals to near-patient sites. For example, in NASA human spaceflight missions, WBC count is required during the flight to monitor astronaut's health-status in outer space. In addition, for on-earth telemedicine systems, WBC count is needed at patients' home or at community centers, so that proper diagnosis can still be made without visits to clinical laboratories. A portable, easy-to-use WBC count test is required to meet all these emerging needs.

However, there is a gap between the need for a portable WBC test and the currently existing technologies. The portable tests require the use of a small-sized instrument and minimal volume of samples. But the existing WBC count technologies are optimized for use in centralized hospitals, normally need a large-sized instrument and large volume of reagents. To bridge this gap, therefore, it is necessary to develop new WBC count technologies optimized for portable use.

This study developed such a portable WBC count test based on microfluidic technologies. A microfluidic cytometer was used here as the test platform for counting WBCs in blood samples. A sheathless, fluorescent detection scheme was developed to minimize the volumes of both blood sample (5μl) and test reagents (50μl). In addition, dye assays were used to enable the fluorescent detection of WBCs in blood samples.

Based on this technology, a portable instrument (12"× 9"× 5") was built for WBC count test. The instrument detected two-color fluorescence emissions (e.g., green 520-550nm, red >600nm), and the measured fluorescence intensities were able to selectively count WBCs in blood samples. The test of the total WBC count was successfully demonstrated on this prototype system. A count accuracy with maximum error less than 10%, was achieved for a WBC concentration range from 4,000 WBCs/µl to 9,000 WBCs/µl.

In addition to the total WBC count, the test of WBC differential count was also investigated here. There are five major types of WBCs in human blood, including lymphocytes, monocytes, neutrophils, eosinophils and basophils. A WBC differential count is used to measure the percentages of each WBC type. In this study, dye assays were developed for the WBC differential test, and a 4-part differential (lymphocyte, monocyte, neutrophil and eosinophil) was successfully demonstrated with the portable technology. A differential count accuracy of maximum error less than 10% was achieved. Meanwhile, the feasibility of counting basophil cells was also demonstrated.

Furthermore, this study also explored two key components for future integrating the portable technology into a self-contained chip. First, a micro-valve actuated by blood thermal coagulation was developed. Blood thermal coagulation was investigated here as an alternative valve mechanism for microfluidics. A one-time-use, open-to-closed valve was demonstrated using laser-induced coagulation, and the closed valve withstood a back pressure of up to 20psi. Second, on-chip staining of blood with dye assays was demonstrated. The staining was introduced using a passive micro-mixer. The mixing of

blood sample with dye assays, and the following fluorescent detection of WBCs were successfully demonstrated.

In addition, the sensing platform (sheathless microfluidic cytometer) developed here for WBC count can also find implementations in other cell-detecting applications. One example demonstrated in this study was detection of microalgae cells in water samples. The feasibility of detecting microalgae cells and measuring cells' response to water toxicity were demonstrated. The portable sensing platform is suitable for on-field test.

Above all, the WBC count technology developed in this study is suitable for portable applications. It requires only a small amount of sample and can be built into small-sized instrument. This technology is promising to meet the increasing demands of WBC count test in the near-patient setting.

# REFERENCES

1.  McKenzie, S.B., *Textbook of hematology*. 1988, Philadelphia: Lea & Febiger. xiv, 507 pages,.

2.  Brown, B.A., *Hematology: principles and procedures*. 5th ed. 1988, Philadelphia: Lea & Febiger. xii, 461 pages.

3.  Bain, B.J., *Blood cells: a practical guide*. 4th ed. 2006, Malden, Mass.: Blackwell.

4.  Miale, J.B., *Laboratory medicine: hematology*. 2nd ed. 1962, Saint Louis,: C.V. Mosby Co. 918 pages.

5.  Williams, W.J., *Hematology*. 3rd ed. 1983, New York: McGraw-Hill. xxvi, 1728 pages.

6.  Zheng, S., et al., *On-chip blood count*. Ph.D. thesis. 2007, Pasadena, California: California Institute of Technology, 186 pages.

7.  George-Gay, B. and K. Parker, *Understanding the complete blood count with differential.* J Perianesth Nurs, 2003. **18**(2): p. 96-114.

8.  McKenzie, S.B., *Clinical laboratory hematology*. 2nd ed. 2009: Pearson.

9.  Dixon, L.R., *The complete blood count: physiologic basis and clinical usage.* J Perinat Neonatal Nurs, 1997. **11**(3): p. 1-18.

10. Sandhaus, L.M. and P. Meyer, *How useful are CBC and reticulocyte reports to clinicians?* Am J Clin Pathol, 2002. **118**(5): p. 787-793.

11. Andersohn, F., C. Konzen, and E. Garbe, *Systematic review: agranulocytosis induced by nonchemotherapy drugs.* Ann Intern Med, 2007. **146**(9): p. 657-665.

12. Crawford, J., et al., *Risk and timing of neutropenic events in adult cancer patients receiving chemotherapy: the results of a prospective nationwide study of oncology practice.* J Natl Compr Canc Netw, 2008. **6**(2): p. 109-118.

13. Crawford, J., D.C. Dale, and G.H. Lyman, *Chemotherapy-induced neutropenia: risks, consequences, and new directions for its management.* Cancer, 2004. **100**(2): p. 228-237.

14. Tesfa, D., M. Keisu, and J. Palmblad, *Idiosyncratic drug-induced agranulocytosis: possible mechanisms and management.* Am J Hematol, 2009. **84**(7): p. 428-434.

15. Buttarello, M. and M. Plebani, *Automated blood cell counts: state of the art.* Am J Clin Pathol, 2008. **130**(1): p. 104-116.

16. Shapiro, H.M., *Practical flow cytometry.* 4th ed. 2003, New York: Wiley-Liss. l, 681 p.

17. Matsuno, K. and S. Ishizuka, *New technology of automated blood cell differential counting.* Rinsho Byori, 1998. **46**(4): p. 361-366.

18. George, T.C., et al., *Distinguishing modes of cell death using the ImageStream multispectral imaging flow cytometer.* Cytometry A, 2004. **59**(2): p. 237-245.

19. Ortyn, W.E., et al., *Sensitivity measurement and compensation in spectral imaging.* Cytometry A, 2006. **69**(8): p. 852-862.

20. Rogers, S., *Comparison of the AcT 5 diff autoloader hematology analyzer to the Abbott Cell-Dyn 3200 analyzer at Charlevoix area hospital.* Lab Hematol, 2003. **9**(3): p. 160-166.

21.     Bhuta, U.M. and H. Ulstein, *Evaluation of the Beckman Coulter AcT 5 diff AL hematology analyzer in a hospital setting.* Lab Hematol, 2003. **9**(3): p. 167-174.

22.     Bagdasaryan, R., et al., *Neutrophil VCS parameters are superior indicators for acute infection.* Lab Hematol, 2007. **13**(1): p. 12-16.

23.     Kaplan, S.S., et al., *Performance characteristics of the Coulter LH 500 hematology analyzer.* Lab Hematol, 2004. **10**(2): p. 76-87.

24.     Brown, W., et al., *Validation of body fluid analysis on the Coulter LH 750.* Lab Hematol, 2003. **9**(3): p. 155-159.

25.     Aulesa, C., et al., *Validation of the Coulter LH 750 in a hospital reference laboratory.* Lab Hematol, 2003. **9**(1): p. 15-28.

26.     Brown, M. and C. Wittwer, *Flow cytometry: principles and clinical applications in hematology.* Clin Chem, 2000. **46**(8 Pt 2): p. 1221-1229.

27.     McCurley, T.L. and R. Larson, *Clinical applications of flow cytometry in hematology and immunology.* Clin Lab Sci, 1996. **9**(6): p. 358-362.

28.     Melamed, M.R., T. Lindmo, and M.L. Mendelsohn, *Flow cytometry and sorting.* 2nd ed. 1990, New York: Wiley-Liss. xii, 824 p.

29.     Orfao, A., et al., *Flow cytometry: its applications in hematology.* Haematologica, 1995. **80**(1): p. 69-81.

30.     Shmarov, D.A., et al., *Flow cytometry in hematology. Methods and technique of flow cytometric analysis.* Klin Lab Diagn, 1997(8): p. 3-9.

31.     Fernandes, B. and Y. Hamaguchi, *Performance characteristics of the Sysmex XT-2000i hematology analyzer.* Lab Hematol, 2003. **9**(4): p. 189-197.

32.  Grimaldi, E., et al., *Evaluation of the monocyte counting by two automated haematology analysers compared with flow cytometry.* Clin Lab Haematol, 2005. **27**(2): p. 91-97.

33.  Grimaldi, E. and F. Scopacasa, *Evaluation of the Abbott CELL-DYN 4000 hematology analyzer.* Am J Clin Pathol, 2000. **113**(4): p. 497-505.

34.  Harris, N., et al., *Performance evaluation of the ADVIA 2120 hematology analyzer: an international multicenter clinical trial.* Lab Hematol, 2005. **11**(1): p. 62-70.

35.  Harris, N., J. Kunicka, and A. Kratz, *The ADVIA 2120 hematology system: flow cytometry-based analysis of blood and body fluids in the routine hematology laboratory.* Lab Hematol, 2005. **11**(1): p. 47-61.

36.  Kendall, R., et al., *Performance evaluation of the Abbott Cell-Dyn 1800 automated hematology analyzer.* Lab Hematol, 2003. **9**(3): p. 143-152.

37.  Langford, K., et al., *Performance evaluation of the Sysmex XT-2000i automated hematology analyzer.* Lab Hematol, 2003. **9**(1): p. 29-37.

38.  Suh, I.B., et al., *Evaluation of the Abbott Cell-Dyn 4000 hematology analyzer for detection and therapeutic monitoring of Plasmodium vivax in the Republic of Korea.* Trop Med Int Health, 2003. **8**(12): p. 1074-1081.

39.  Chung, T.D. and H.C. Kim, *Recent advances in miniaturized microfluidic flow cytometry for clinical use.* Electrophoresis, 2007. **28**(24): p. 4511-4520.

40.  Heikali, D. and D. Di Carlo, *A Niche for microfluidics in portable hematology analyzers.* Jala, 2010. **15**(4): p. 319-328.

41. Toner, M. and D. Irimia, *Blood-on-a-chip.* Annu Rev Biomed Eng, 2005. **7**: p. 77-103.

42. Institute of Medicine (U.S.). Committee on Creating a Vision for Space Medicine during Travel Beyond Earth Orbit., J. Ball, and C.H. Evans, *Safe passage : astronaut care for exploration missions.* 2001, Washington, D.C.: National Academy Press. xxiii, 291 pages.

43. Epelman, S. and D.R. Hamilton, *Medical mitigation strategies for acute radiation exposure during spaceflight.* Aviat Space Environ Med, 2006. **77**(2): p. 130-139.

44. Iniewski, K., *CMOS bio-microsystems : where electronics meets biology.* 2011, Hoboken, New Jersey: Wiley. xi, 502pages.

45. Rotstein, R., et al., *The usefulness of telemedicine for the detection of infection/inflammation at the point of care.* Telemed J E Health, 2001. **7**(4): p. 317-323.

46. Urbach, J., et al., *Telemedicine-based application for the detection of inflammation in pediatrics.* Telemed J E Health, 2003. **9**(3): p. 241-245.

47. Briggs, C., et al., *ICSH Guideline for worldwide point-of-care testing in haematology with special reference to the complete blood count.* Int J Lab Hematol, 2008. **30**(2): p. 105-116.

48. Junker, R., H. Schlebusch, and P.B. Luppa, *Point-of-care testing in hospitals and primary care.* Dtsch Arztebl Int, 2010. **107**(33): p. 561-567.

49. Rao, L.V., et al., *Evaluation of a new point of care automated complete blood count (CBC) analyzer in various clinical settings.* Clin Chim Acta, 2008. **389**(1-2): p. 120-125.

50.     Briggs, C., et al., *Performance evaluation of a new compact hematology analyzer, the Sysmex pocH-100i.* Lab Hematol, 2003. **9**(4): p. 225-233.

51.     Whisler, S. and C. Dahlgren, *Performance evaluation of the Sysmex pocH-100i automated hematology analyzer.* Lab Hematol, 2005. **11**(2): p. 107-117.

52.     Osei-Bimpong, A., et al., *Point-of-care method for total white cell count: an evaluation of the HemoCue WBC device.* Int J Lab Hematol, 2009. **31**(6): p. 657-664.

53.     Whitesides, G.M., *The origins and the future of microfluidics.* Nature, 2006. **442**(7101): p. 368-373.

54.     Saliterman, S., *Fundamentals of bioMEMS and medical microdevices.* 2006, Hoboken, NJ: Wiley-Interscience ;. xxvii, 610 p.

55.     Terry, S.C., J.H. Jerman, and J.B. Angell, *Gas-chromatographic air analyzer fabricated on a silicon-wafer.* IEEE Transactions on Electron Devices, 1979. **26**(12): p. 1880-1886.

56.     Haber, C., *Microfluidics in commercial applications; an industry perspective.* Lab Chip, 2006. **6**(9): p. 1118-1121.

57.     De Jong, J., R.G.H. Lammertink, and M. Wessling, *Membranes and microfluidics: a review.* Lab Chip, 2006. **6**(9): p. 1125-1139.

58.     Erickson, D. and D.Q. Li, *Integrated microfluidic devices.* Anal Chim Acta, 2004. **507**(1): p. 11-26.

59.     Sandmaier, H., *Special Issue on Microfluidics - Introduction.* Journal of Micromechanics and Microengineering, 1994. **4**(4): p. U157-U157.

60. Squires, T.M. and S.R. Quake, *Microfluidics: fluid physics at the nanoliter scale.* Reviews of Modern Physics, 2005. **77**(3): p. 977-1026.

61. Liu, M., *Integrated microfluidic devices for cell culture and assay*, Ph.D. Thesis, in *Division of Engineering and Applied Science.,*2010, California Institute of Technology: Pasadena, Califfornia.

62. Godin, J., et al., *Microfluidics and photonics for bio-system-on-a-chip: a review of advancements in technology towards a microfluidic flow cytometry chip.* J Biophotonics, 2008. **1**(5): p. 355-376.

63. Kuswandi, B., et al., *Optical sensing systems for microfluidic devices: a review.* Anal Chim Acta, 2007. **601**(2): p. 141-155.

64. Mairhofer, J., K. Roppert, and P. Ertl, *Microfluidic systems for pathogen sensing: a review.* Sensors (Basel), 2009. **9**(6): p. 4804-4823.

65. Prot, J.M., et al., *A cocktail of metabolic probes demonstrates the relevance of primary human hepatocyte cultures in a microfluidic biochip for pharmaceutical drug screening.* International Journal of Pharmaceutics, 2011. **408**(1-2): p. 67-75.

66. Carr, J.A., et al., *A microfluidic platform for high-sensitivity, real-time drug screening on C. elegans and parasitic nematodes.* Lab Chip, 2011. **11**(14): p. 2385-2396.

67. Karlsson, M., et al., *Microfluidic chip solutions for patch-clamp-based ion channel drug screening and characterization.* Journal of Neurochemistry, 2005. **94**: p. 112-112.

68. Ateya, D.A., F. Sachs, and S.Z. Hua, *Microfluidic cell volume biosensor for high throughput drug screening.* Nanoscale Materials Science in Biology and Medicine, 2005. **845**: p. 261-266.

69. Kim, P., et al., *Soft lithography for microfluidics: a review.* Biochip Journal, 2008. **2**(1): p. 1-11.

70. Rivet, C., et al., *Microfluidics for medical diagnostics and biosensors.* Chemical Engineering Science, 2011. **66**(7): p. 1490-1507.

71. Kraus, M.S., et al., *Characterization of cardiac troponin I as an indicator of cardiac damage in horses utilizing an iSTAT (R) 1 analyzer.* Journal of Veterinary Internal Medicine, 2007. **21**(3): p. 604-605.

72. Pipper, J., et al., *Catching bird flu in a droplet.* Nat Med, 2007. **13**(10): p. 1259-1263.

73. Lee, W.G., et al., *Nano/Microfluidics for diagnosis of infectious diseases in developing countries.* Adv Drug Deliv Rev, 2010. **62**(4-5): p. 449-457.

74. Altendorf, E., et al., *Differential blood cell counts obtained using a microchannel based flow cytometer.* Transducers 97 - 1997 International Conference on Solid-State Sensors and Actuators, Digest of Technical Papers, Vols 1 and 2, 1997: p. 531-534.

75. Kummrow, A., et al., *Microfluidic structures for flow cytometric analysis of hydrodynamically focussed blood cells fabricated by ultraprecision micromachining.* Lab Chip, 2009. **9**(7): p. 972-981.

76. van Berkel, C., et al., *Integrated systems for rapid point of care (PoC) blood cell analysis.* Lab Chip, 2011. **11**(7): p. 1249-1255.

77. Holmes, D., et al., *Leukocyte analysis and differentiation using high speed microfluidic single cell impedance cytometry.* Lab Chip, 2009. **9**(20): p. 2881-2889.

78. Seo, S., et al., *High-throughput lens-free blood analysis on a chip.* Analytical Chemistry, 2010. **82**(11): p. 4621-4627.

79. Chan, S.D.H., et al., *Cytometric analysis of protein expression and apoptosis in human primary cells with a novel microfluidic chip-based system.* Cytometry Part A, 2003. **55A**(2): p. 119-125.

80. Wang, J.H., et al., *An integrated microfluidic system for counting of CD4(+)/CD8(+) T lymphocytes.* Microfluidics and Nanofluidics, 2011. **10**(3): p. 531-541.

81. Yun, H., et al., *Simultaneous counting of two subsets of leukocytes using fluorescent silica nanoparticles in a sheathless microchip flow cytometer.* Lab Chip, 2010. **10**(23): p. 3243-3254.

82. Frankowski, M., et al., *A microflow cytometer exploited for the immunological differentiation of leukocytes.* Cytometry Part A, 2011. **79A**(8): p. 613-624.

83. Terstappen, L.W., et al., *Four-parameter white blood cell differential counting based on light scattering measurements.* Cytometry, 1988. **9**(1): p. 39-43.

84. Huh, D., et al., *Use of air-liquid two-phase flow in hydrophobic microfluidic channels for disposable flow cytometers.* Biomedical Microdevices, 2002. **4**(2): p. 141-149.

85. Irimia, D., *Cutting edge: Electronic counting of white blood cells.* Lab Chip, 2009. **9**(20): p. 2875-2876.

86.    Mercer, W.B., *Calibration of coulter counters for particles -1 Mu in diameter.* Review of Scientific Instruments, 1966. **37**(11): p. 1515.

87.    Zheng, S.Y., et al., *Fluorescent labeling, sensing, and differentiation of leukocytes from undiluted whole blood samples.* Sensors and Actuators B-Chemical, 2008. **132**(2): p. 558-567.

88.    Smith, S.W., *The scientist and engineer's guide to digital signal processing.* 1st ed. 1997, San Diego, Calif.: California Technical Pub. xiv, 626 p.

89.    Adams, L.R. and Kamentsk.La, *Machine characterization of human leukocytes by acridine orange fluorescence.* Acta Cytologica, 1971. **15**(3): p. 289.

90.    Gurr, E., *Staining: practical and theoretical.* 1962, Baltimore,: Williams and Wilkins. 631 p.

91.    Tibbe, A.G., et al., *Optical tracking and detection of immunomagnetically selected and aligned cells.* Nat Biotechnol, 1999. **17**(12): p. 1210-1213.

92.    Kass, L., *Metachromatic dye sorption means for differential determination of leukocytes*, 1983.

93.    Kass, L., *Identification of lymphocyte subpopulations with a polymethine dye.* J Histochem Cytochem, 1988. **36**(7): p. 711-715.

94.    Shapiro, H.M., et al., *Combined blood cell counting and classification with fluorochrome stains and flow instrumentation.* J Histochem Cytochem, 1976. **24**(1): p. 396-401.

95.    Darzynkiewicz, Z. and X. Huang, *Analysis of cellular DNA content by flow cytometry.* Curr Protoc Immunol, 2004. **Chapter 5**: p. Unit 5 7.

96.     Bedner, E., et al., *High affinity binding of fluorescein isothiocyanate to eosinophils detected by laser scanning cytometry: a potential source of error in analysis of blood samples utilizing fluorescein-conjugated reagents in flow cytometry.* Cytometry, 1999. **36**(1): p. 77-82.

97.     Laser, D.J. and J.G. Santiago, *A review of micropumps.* Journal of Micromechanics and Microengineering, 2004. **14**(6): p. R35-R64.

98.     Oh, K.W. and C.H. Ahn, *A review of microvalves.* Journal of Micromechanics and Microengineering, 2006. **16**(5): p. R13-R39.

99.     Shih, J., *Microfabricated high-performance liquid chromatography (HPLC) system with closed-Loop flow control*, Ph.D. Thesis, in *Electrical Engineering*2008, California Institute of Technology.

100.    Beebe, D.J., et al., *Functional hydrogel structures for autonomous flow control inside microfluidic channels.* Nature, 2000. **404**(6778): p. 588.

101.    Yoshida, K., et al., *Fabrication of micro electro-rheological valves (ER valves) by micromachining and experiments.* Sensors and Actuators a-Physical, 2002. **95**(2-3): p. 227-233.

102.    Nguyen, N.T. and Z.G. Wu, *Micromixers - a review.* Journal of Micromechanics and Microengineering, 2005. **15**(2): p. R1-R16.

103.    Pfefer, T.J., et al., *Pulsed laser-induced thermal damage in whole blood.* J Biomech Eng, 2000. **122**(2): p. 196-202.

104.    Glass, G.B., *The thermal coagulation point of blood serum.* Am J Med, 1950. **8**(6): p. 745-754.

105. Lee, C.Y., et al., *Microfluidic mixing: a review.* Int J Mol Sci, 2011. **12**(5): p. 3263-3287.

106. Wu, Z.G. and N.T. Nguyen, *Hydrodynamic focusing in microchannels under consideration of diffusive dispersion: theories and experiments.* Sensors and Actuators B-Chemical, 2005. **107**(2): p. 965-974.

107. Geacintov, N.E., et al., *Dynamics of the Binding of Acridine-Dyes to DNA Investigated by Triplet Excited-State Probe Techniques.* Journal of Physical Chemistry, 1981. **85**(24): p. 3608-3613.

108. Zulli, S.L., et al., *Lateral Diffusion of an Adsorbate at a Chromatographic C-18 Water Interface.* Analytical Chemistry, 1994. **66**(10): p. 1708-1712.

109. Kundu, P.K. and I.M. Cohen, *Fluid mechanics.* 4th ed. 2008, Amsterdam ; Boston: Academic Press. xxviii, 872 p.

110. Sethu, P., et al., *Continuous flow microfluidic device for rapid erythrocyte lysis.* Analytical Chemistry, 2004. **76**(21): p. 6247-6253.

111. Maxwell, K. and G.N. Johnson, *Chlorophyll fluorescence - a practical guide.* Journal of Experimental Botany, 2000. **51**(345): p. 659-668.

112. Sugahara, K., N. Murata, and A. Takamiya, *Fluorescence of Chlorophyll in Brown Algae and Diatoms.* Plant and Cell Physiology, 1971. **12**(3): p. 377.

113. Premazzi, G., G. Buonaccorsi, and P. Zilio, *Flow-Cytometry for Algal Studies.* Water Research, 1989. **23**(4): p. 431-442.

114. Franklin, N.M., J.L. Stauber, and R.P. Lim, *Development of flow cytometry-based algal bioassays for assessing toxicity of copper in natural waters.* Environmental Toxicology and Chemistry, 2001. **20**(1): p. 160-170.

115. Franklin, N.M., et al., *Development of an improved rapid enzyme inhibition bioassay with marine and freshwater microalgae using flow cytometry.* Archives of Environmental Contamination and Toxicology, 2001. **40**(4): p. 469-480.